

# Light and Shape-Memory Polymers: Characterization, Preparation, Stimulation, and Application

Liang Fang,\* Wan Yan, Shunping Chen, Qiong Duan, Madhubhashitha Herath, Jayantha Epaarachchi, Yue Liu,\* and Chunhua Lu

Shape-memory polymers (SMPs) are smart materials that change shape when exposed to stimuli and have various applications in different fields due to their unique properties. Light, as a kind of electromagnetic radiation, plays an important role in understanding the structure-property relations of SMPs, preparing original shapes, using them as non-contact stimuli sources, and tuning the optical properties of SMPs. This review provides a comprehensive review of the involvement of light in structure-preparation-stimuli-application of SMPs. The review is divided into four sections. First, applications of optical/spectroscopic approaches that provide information for understanding structure-property relations in SMPs, especially during programming and recovery. Second, describes how to build SMPs with light, including different photochemical reactions and 3D photocuring technologies. Third, discusses how light is used to trigger the shape change of SMPs through both photochemical and photothermal mechanisms. Last, focuses on how to take advantage of the shape-memory effect to tune the optical characteristics of polymers, including various structures of SMP color-changing materials and their synthetic strategies. Future research could focus on developing efficient photothermal fillers, new 3D printing techniques for SMPs, exploring their use in biomedical and wearable devices, and optimizing SMPs for industrial applications.

## 1. Introduction

Light is a kind of electromagnetic radiation, including radio waves, microwaves, infrared (IR) light, near-IR (NIR) light, vis-UV light, as well as X-rays, determined by their wavelength or frequency. When a substance interacts with an incident light beam, either absorption, transmittance/refraction or scattering/reflection of the radiation happens. Light beams with different wavelengths present various behaviors with substances. As far as polymeric materials are concerned, UV light with short wavelengths usually takes charge of photo-induced reactions to break covalent bonds with low energy for polymerization, crosslinking, chain scission, etc.<sup>[1–4]</sup> Besides, UV aging is one important issue for outdoor-use polymer products.<sup>[4,5]</sup> The transparency or opaque properties of polymers with visible light determine their application fields, which are controlled by both aggregate structures or micro-/nanostructures on polymer surfaces.<sup>[6,7]</sup> NIR laser beams can be used to cut, weld,

L. Fang, Q. Duan, C. Lu  
State Key Laboratory of Materials-Oriented Chemical Engineering,  
College of Materials Science and Engineering  
Nanjing Tech University  
Nanjing 210009, P. R. China  
E-mail: lfang@njtech.edu.cn


L. Fang, Q. Duan, C. Lu  
Jiangsu Collaborative Innovation Center for Advanced Inorganic Function  
Composites  
Nanjing Tech University  
Nanjing 210009, P. R. China

L. Fang, Q. Duan, C. Lu  
Jiangsu National Synergetic Innovation Center for Advanced Materials  
(SICAM)  
Nanjing Tech University  
Nanjing 210009, P. R. China

W. Yan, Y. Liu  
Institute of Active Polymers  
Helmholtz-Zentrum Hereon  
Kantstr. 55, 14513 Teltow, Germany  
E-mail: yue.liu@hereon.de

S. Chen  
State Key Laboratory of Molecular Engineering of Polymers, Department of  
Macromolecular Science  
Fudan University  
Shanghai 200438, P. R. China

M. Herath, J. Epaarachchi  
Centre for Future Materials & Institute of Advanced Engineering and Space  
Sciences  
University of Southern Queensland  
Toowoomba, QLD 4350, Australia

 The ORCID identification number(s) for the author(s) of this article can be found under <https://doi.org/10.1002/mame.202300158>

© 2023 The Authors. Macromolecular Materials and Engineering published by Wiley-VCH GmbH. This is an open access article under the terms of the Creative Commons Attribution License, which permits use, distribution and reproduction in any medium, provided the original work is properly cited.

DOI: 10.1002/mame.202300158

hole-punch, sintering of polymers,<sup>[8,9]</sup> while IR light, X-rays, and other electromagnetic radiation have been widely used to characterize the chemical structures of polymers.

Shape-memory polymers (SMPs) have been attractive in the last two decades and paid great attention from the aspects of both academy and industry. SMPs can recover their original shapes from temporary ones upon different stimuli, which find great applications in many fields.<sup>[10,11]</sup> Chemical structures and network architectures determine the performance of SMPs.<sup>[12]</sup> The successful preparation of SMPs having required original shapes and structures is critical.<sup>[12,13]</sup> In addition, the precise and on-demand trigger of SMPs is necessary to realize their valuable applications.<sup>[14,15]</sup> Finally, the exploration of SMPs' applications in accurate control of both shapes and functions needs further investigations.<sup>[16,17]</sup> The chain of structure-preparation-stimuli-application contributes to the main research topics of SMPs.

Light as a kind of electromagnetic radiation has been widely involved in every research field of SMPs, including structural characterization, precise preparation of original shapes, use as non-contact stimuli source, and optical properties tuning of SMPs. In this paper, we review the involvement of light in structure-preparation-stimuli-application of SMPs, trying to give a brief relationship between light and SMPs as illustrated in **Figure 1**.

The first section discusses applications of optical/spectroscopic approaches that provide information for understanding structure-property relations in SMPs. In particular, the applications of X-ray spectroscopies techniques including X-ray scattering, reflection, and absorption spectroscopies are discussed to detect changes in crystalline structures and orientation during the shape-memory process for semicrystalline SMPs.<sup>[18,19]</sup> UV-vis spectroscopy is typically used for measuring the optical characteristics of photo-responsive SMPs, and it also can be applied for the configuration of chemical bonds and quantitative determination of solutions with SMPs at the nanoscale.<sup>[20,21]</sup> Further, photophysical phenomena that existed in some SMPs can be detected by fluorescence spectroscopy, which then is related to their conformational changes during the shape-memory process.<sup>[22,23]</sup> Varying degrees of molecular structures and orientations can be determined by IR and Raman spectroscopies by identifying chemical bonds in polymeric systems, which gains useful information on structural changes in SMPs.<sup>[24–27]</sup> In addition, elastic properties as an important factor for enhancing the accurate control of the shape-memory process can be determined by Brillouin spectroscopy, while nanoparticles (NPs) blended into SMPs can be analyzed by optical extinction spectroscopy.<sup>[28,29]</sup>

The second section describes how to build SMPs with light. On one hand, this section describes different photochemical reactions used to construct crosslinking networks at the molecular scale. Various irreversible photo-crosslinking reactions and

reversible photo-crosslinking reactions and their applications in the field of SMPs are described in detail. Irreversible photo-crosslinking reactions are usually used to construct permanent shape networks, while reversible photo-crosslinking reactions can be used to construct both permanent shape networks and temporary networks for shape fixation and restoration.<sup>[12,30]</sup> On the other hand, different 3D photocuring technologies and their characteristics are introduced at the scale of industrial processing technology, and 4D printing is realized using advanced processing technology combined with SMPs, which enhances the level of digital design and manufacturing of smart materials.<sup>[31,32]</sup>

Instead of light beams used to characterize the chemical structures of SMPs or to create them with unique original shapes directly, light having different wavelengths has also been used to trigger the shape change of SMPs due to photochemical or photothermal mechanisms. In this section, photothermal fillers at micro-/nanoscale which can present wide spectrum absorption are introduced and used to create SMP composites (SMPCs).<sup>[33–41]</sup> The approaches to enhance filler dispersion in SMPCs are discussed, which ensure both good thermal conductivity and mechanical property reinforcement. More importantly, many organic functional groups and inorganic fillers present selective absorption toward light with unique wavelengths including UV light, visible light, and so on.<sup>[33,42]</sup> The assembly of SMPs and SMPCs having such absorption units can achieve the control of multiple shape changes upon light irradiations.<sup>[33,43–45]</sup>

Finally, in addition to light usage, the shape change of SMPs can present optical properties tuning. The last section, thus, concentrates on how to take advantage of shape-memory effect (SME) to tune the optical characteristics of polymers. First, different kinds of SMEs are introduced, especially discussing their unique functions for controlling optical properties, such as tunability, feasibility in re-programming, and multi-sensitivity.<sup>[46–48]</sup> Afterward, various structures of SMP color-changing materials and their synthetic strategies are introduced based on different working principles, including photonic structures, wrinkles, 3D structures, and biomimetic structures.<sup>[49–54]</sup> The deformation-induced alteration in optical properties is discussed for each structure. Finally, relevant examples are presented where the precise control of optical properties using SMPs can be applied in various fields such as sensors, rewritable paper, energy harvesters, and anti-counterfeiting.<sup>[55–58]</sup> In addition, limitations in the use of SMPs as optical materials and their other potential applications in the future are foreseen.

## 2. Optical/Spectroscopic Techniques for Characterization of SMPs

When a substance interacts with the incident light beam, either absorption, emission, or scattering of the radiation happens.<sup>[59,60]</sup> The variations in intensity or direction of the radiation due to the energy level transition of particles or wave scattering can be measured as a function of wavelength or angle, generating a certain spectrum. Those spectra provide a wealth of information about atomic and molecular structures as well as critical qualitative and quantitative chemical analysis.<sup>[60]</sup> Meantime, spectroscopic methods own advantages of quick analysis, easy operation, good selectivity, high sensitivity, and low possibility for sample damage. Spectroscopic techniques, thus, are used as potent tools

M. Herath  
Department of Engineering Technology, Faculty of Technological Studies  
Uva Wellasa University  
Badulla 90000, Sri Lanka  
J. Epaarachchi  
School of Engineering, Faculty of Health, Engineering and Sciences  
University of Southern Queensland  
Toowoomba, QLD 4350, Australia

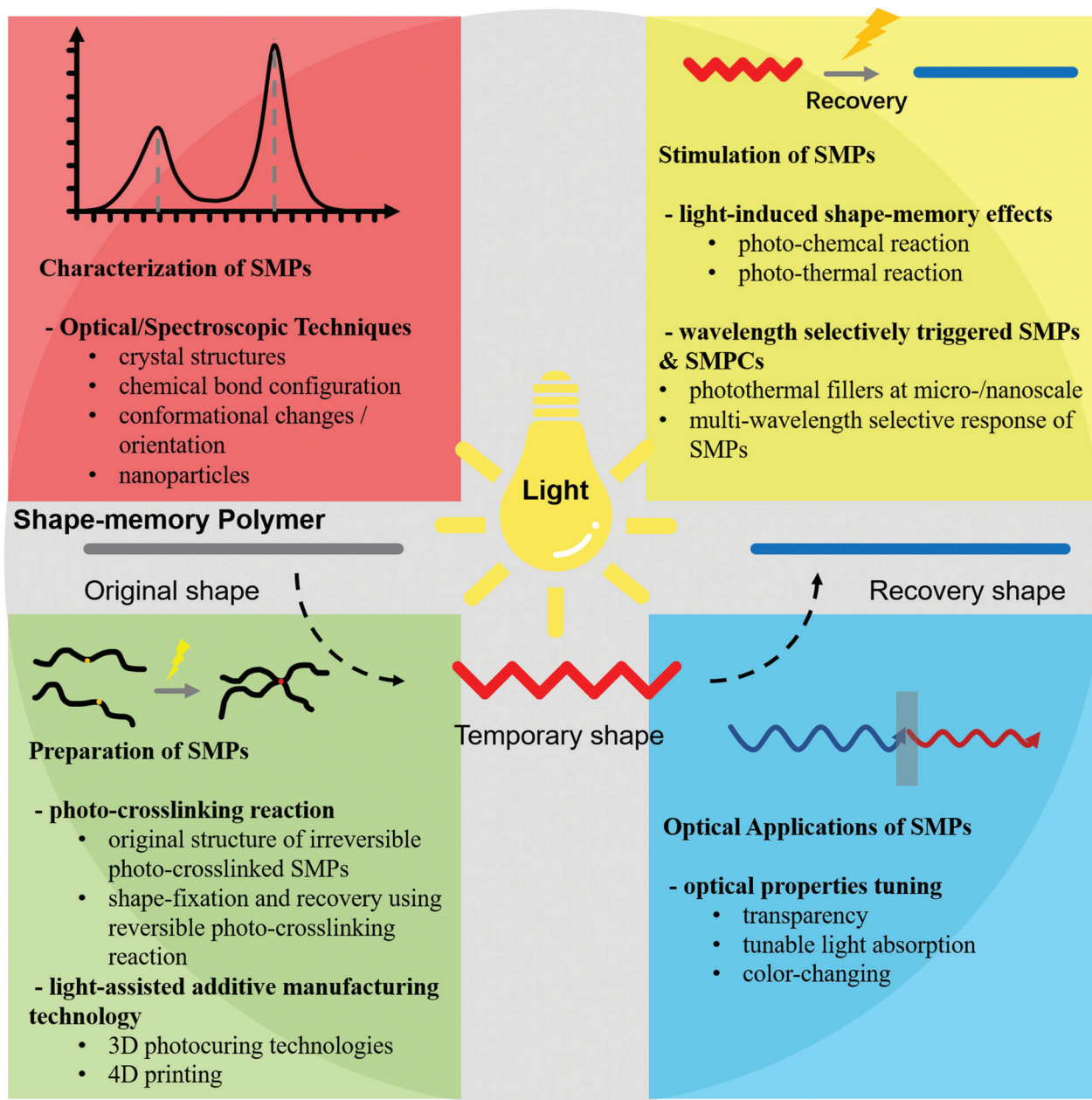


**Figure 1.** Summary of the 4 aspects between light and SMPs.

for analyzing chemical compositions, studying reaction mechanisms, and testing molecular structural models in synthetic chemistry, biochemistry, medicine, and materials science.<sup>[61–64]</sup>

Shape-memory process of polymeric materials relies on the alignment of molecules and molecular order-disorder transformation. Atomic and molecular level characterization allows the understanding of the correlation between their structural variations in micro-/nano-scale lengths and the macro-scale shape changing during shape-memory processes. Therefore, spectroscopic measurements are essential for fast detecting, non-destructive testing, and in situ monitoring of SMPs. This section intended to give an overview of the utilization of optical spectroscopic techniques (as outlined in **Table 1**) for the examina-

tion of structural variations in polymers and composites throughout their shape-memory process, including block polymers, polymer blends, and liquid crystal (LC) elastomers. The obtained outcomes offer a comprehensive understanding of the interplay between the structural attributes and the shape-memory performance of SMPs.

### 2.1. X-Ray Spectroscopic Techniques

X-ray spectroscopic techniques are based on the interaction of radiation at a wavelength range of 0.01–10 nm with electrons of the inner shell of an atom, which can reveal structural,

**Table 1.** List of spectroscopic techniques for SMPs.

Techniques	Light source	Characterization
X-ray scattering	0.01–20 nm	<ul style="list-style-type: none"> <li>• crystalline structure<sup>[65]</sup></li> <li>• orientation<sup>[66,67]</sup></li> <li>• crystallinity<sup>[67,68]</sup></li> </ul>
UV–vis spectroscopy	180–800 nm	<ul style="list-style-type: none"> <li>• optical characteristics<sup>[20]</sup></li> <li>• chemical bond configuration<sup>[69]</sup></li> <li>• quantitative determination of solution and diverse analytes<sup>[70]</sup></li> </ul>
Fluorescence spectroscopy	180–800 nm	<ul style="list-style-type: none"> <li>• conformational changes<sup>[22]</sup></li> <li>• fluorescence phenomena<sup>[21]</sup></li> </ul>
Raman spectroscopy	450–1200 nm, typical 785 nm	<ul style="list-style-type: none"> <li>• determination of chemical compounds and functional groups<sup>[24,25,71,72]</sup></li> <li>• molecular orientation<sup>[73,74]</sup></li> </ul>
IR spectroscopy	780–2500 nm	
Photoluminescence spectroscopy	300–490 nm, usually at 325 nm	<ul style="list-style-type: none"> <li>• particle in material<sup>[75,76]</sup></li> </ul>
Brillouin spectroscopy	532–780 nm, typical 532 nm	<ul style="list-style-type: none"> <li>• elastic modulus<sup>[28]</sup></li> </ul>
Optical extinction spectroscopy	400–2200 nm	<ul style="list-style-type: none"> <li>• particle in material<sup>[29]</sup></li> </ul>

elemental, and atomic information for assessing molecular mechanisms associated with SMEs in polymeric materials.

### 2.1.1. X-Ray Scattering

X-ray scattering technique based on the elastic scattering of radiation is one of the routine techniques for characterizing crystalline structures. The incident X-rays are scattered into specific directions with the same energy/wavelength as incident X-rays after irradiating a sample. The scattered X-rays are collected by a detector, forming scattering patterns.<sup>[77,78]</sup> The diffraction or interference of reflected light can be defined using the Bragg equation:

$$2d \sin \theta = n\lambda \quad (1)$$

where  $d$ ,  $n$ , and  $\lambda$  are lattice spacing, diffraction order, and peak wavelength, respectively.  $\theta$  is the angle between the incident light and the normal line. Peaks in X-ray scattering patterns corresponding to atom positions within lattice planes, thus, can identify and quantify periodically arranged atoms in polymers.

The investigation of X-ray scattering in polymer systems, particularly multi-phase systems, is typically categorized into three types based on the angular range. These include: 1) Wide-angle X-ray scattering (WAXS), commonly referred to as X-ray diffraction (XRD), which typically explores length scale in the order of molecular dimensions and the information about the arrangement of chain segments; 2) Small-angle X-ray scattering (SAXS), which examines long-range ordering and detects nanostructural organizations; and 3) Ultra-small-angle X-ray scattering, which provides access to structures at the micro-scale.<sup>[77]</sup> These related measurements, thus, can obtain information on crystal sizes, orientation degrees, and internal structures.

SMEs, including one-way and reversible abilities, are initiated by a programming process, where directional rearrangement is induced into molecular structures of samples. The recovery process of programmed SMP samples relies on the entropy-elastic recoil of stretched chains. SMP materials, especially thermos-

responsive SMPs, are mainly based on semicrystalline polymers, and the shape-memory processes take place through the crystallization-melting of crystalline phases in multiphase polymer systems. Therefore, these X-ray scattering techniques are frequently used for SMPs to obtain compositional and structural variations.<sup>[67,68,79,80]</sup>

The X-ray scattering patterns of SMPs in original and temporary shapes can be used to study crystal structural orientation after programming. One of the examples was stated by PDLCL copolymers of  $\epsilon$ -caprolactone (PCL) and  $\omega$ -pentadecalactone (PDL). Their SAXS and WAXS patterns as shown in **Figure 2I** presents a clear preferred orientation of molecular chains after stretching, which showed randomly crystalline chains before.<sup>[66]</sup> The results deduced the microstructure evolution for the fixation of the temporary shape of semicrystalline SMPs. The recovery process can also be monitored by measuring the change in oriented crystalline structures. The stretched and recovered semicrystalline poly(*L*-lactide) (PLLA) films at different programming temperatures were measured by WAXS and compared with each other. Under the stretching at 85°C, a diffraction pattern featuring a singular peak at  $2\theta$  of 16.2° was observed in the sample, which signifies the formation of oriented PLLA crystals along the draw direction. The recovered pattern was similar to the pattern of an undrawn sample, indicating the disappearance of crystal orientation after the recovery to its original state. Similar patterns for pieces at these two states was observed when the sample was programmed at 120°C, indicating a lower recovery ratio for higher programming temperature due to chain slippage.<sup>[80]</sup>

Quantitative analysis of the evolution of crystallites could also uncover micro-molecular structural changes related to the shape-memory properties of semicrystalline polymers. The changes in crystallinity, orientation degree (from WAXS) and a long period of lamellar structure (from SAXS) can be calculated from X-ray scattering measurement. In the context of SMPs based on polyvinylidene fluoride (PVDF) blends, deformation causes the PVDF crystallites to transform from their initial lamellar form into fibrillar crystals. This process leads to a reduction in the crystallinity of the crystalline PVDF through fragmentation, an extension of the long period and an increase in the degree of orientation due to



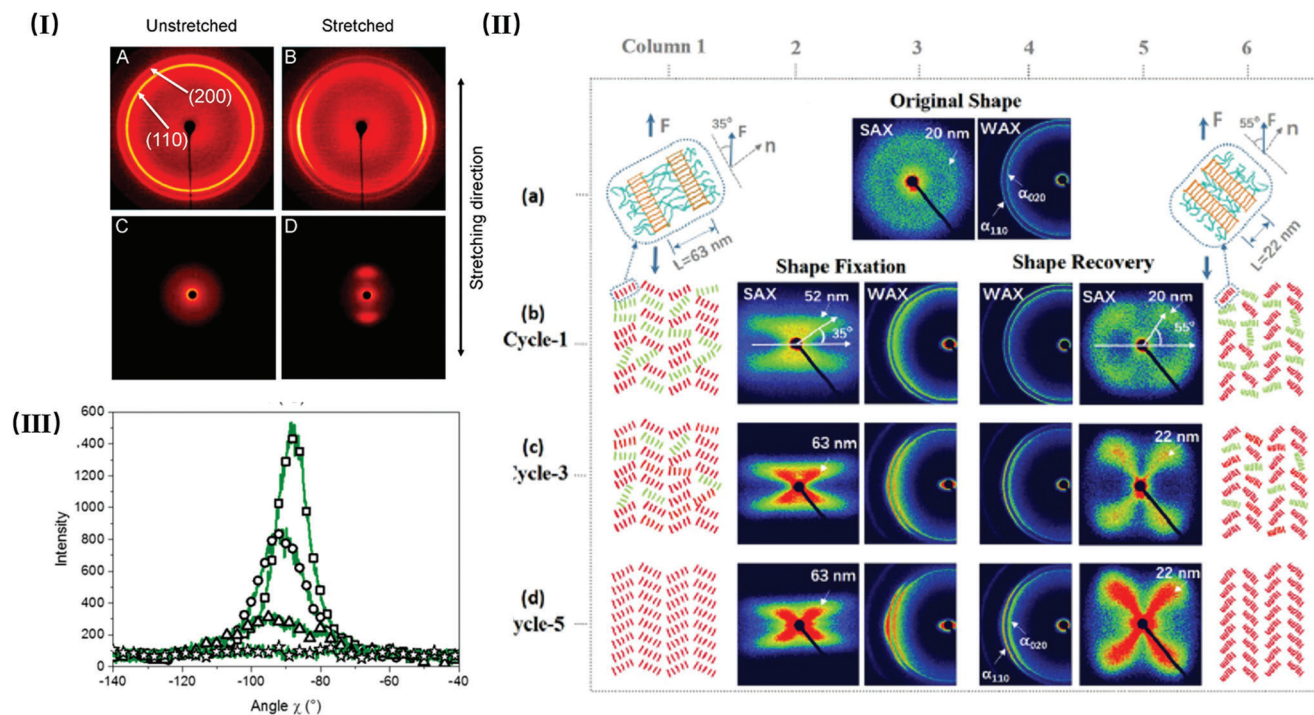


**Figure 2.** I) A,B) WAXD and C,D) SAXS patterns of unstretched and stretched polymer samples. Reproduced with permission.<sup>[66]</sup> Copyright 2017, American Chemical Society. II) SAXS patterns (columns 2 and 5), and WAXS patterns (columns 3 and 4) of PVDF blends during shape-memory cycles and the statistical orientation of the PVDF lamellae (columns 1 and 6, here red-line groups indicate the preferentially oriented lamellae and green-line groups represent the random lamellae). Reproduced with permission.<sup>[65]</sup> Copyright 2020, Elsevier. III) Azimuthal scan from WAXS patterns of PCL crystalline structure in programmed PCL-based SMPs during shape-recovery at 0 (squares), 50 (triangles), and 60 (stars) °C. Reproduced with permission.<sup>[79]</sup> Copyright 2018, American Chemical Society.

the elongation of amorphous segments and the reorganization of lamellar structures. When shape recovered upon stress unloading, the deformed crystalline structures returned to their random organized state (Figure 2II).<sup>[65]</sup> The results of different cycles also demonstrated that the changes in crystallites were observed during the initial three cycles, while all crystalline-related parameters remained unchanged after three cycles.<sup>[65]</sup> The strain-induced supramolecular structures of SMP based on poly(propylene glycol) and 4,4'-methylenebis(phenyl urea) were characterized using SAXS when the sample was stretched from the strain 0%–500%, where periodic structures oriented perpendicular to the drawing direction. The relations between the orientation parameter and strain can be plotted, presenting that the anisotropy increased with increasing the strain and reached 0.4 when the strain was 500%.<sup>[67]</sup> This data supports the hypothesis that polymer chains aligned along the drawn direction and organized dynamic bonds into large supramolecular nanostructures.

These two X-ray scattering techniques enable in situ measurements combined with temperature or uniaxial testing, further giving valuable insight into the behavior of microstructural changes in different stages of shape-memory process. For example, the recovery process of thermo-responsive SMPs can be tested by WAXS measurement with a heating chamber. The programmed PCL based SMP with a strain of 900% was measured during heating. The reduction of a PCL crystal peak in WAXS patterns (Figure 2III) indicated the recovery of the programmed sample started from 30°C when PCL began to melt, and all

PCL crystals melted at 60°C when the diffraction peak of PCL crystals disappeared.<sup>[79]</sup> Besides, X-ray scattering measurements combined with a tensile tester realized the in situ measurement during the shape deformation process to examine the stretch-induced crystalline structures in semicrystalline polymers. The patterns of PCL/PLLA SMP blend with different composition ratios can be measured in the original state during programming and recovery. By analysis of the bands from the amorphous phase and crystalline PLLA as well as the PCL phase, PLLA crystals remained orientated after recovery. An unexpected mechanism has been concluded from the results that both PLLA crystalline structure and PCL amorphous chains orientated to the stretching direction. The orientated PLLA crystals were not affected during the recovery process by heating, and the recoil of aligned PCL chains is responsive to the shape recovery.<sup>[68]</sup>

WAXS measurements can also be performed on the liquid-crystalline structure, where the smectic-C nature of LC elastomer can be detected. The WAXS patterns provide evidence of the orientation occurring in the siloxane backbone, as well as the long-range smectic order that is induced through stretching and fixation of the second shape. The smectic ordering can be lost when heating upon the clearing transition, resulting in shape recovery.<sup>[81]</sup> Grazing-incidence small- and wide-angle X-ray scattering (GISAXS and GIWAXS) are modified versions of SAXS and WAXS, utilizing a grazing-incidence approach, which measure the reflected light from a sample. The grazing mode turns this technique to surface sensitive, where incident X-rays hit a

sample at an angle  $< 0.5^\circ$ , which can provide order and orientation of thin films. This novel technique is usually used for characterizing shape-memory alloy thin films.<sup>[82]</sup> However, it is recently applied for the SME of organic semiconductors, where the martensitic transition was indicated using GIWAXS.<sup>[83]</sup>

Another approach to detecting the nano-scale to meso-scale structure of polymers is resonant soft X-ray scattering (RSoXS), which is sensitive to chemical bond orientation.<sup>[84]</sup> Though currently rare work has been reported for characterizing SMP using RSoXS, it becomes a promising technique for gaining accurate structural information of polymers compared to transitional scattering techniques.

### 2.1.2. X-Ray Reflectivity

X-ray reflectivity (XRR) is the method used to investigate the surface and interface properties of thin films. By measuring the reflected X-rays and determining the electron density profile perpendicular to surface, valuable information including composition, thickness, roughness, and density of the surface can be obtained.<sup>[85]</sup> Langmuir films are particular types with a thickness of several nanometers. The crystalline structures in Langmuir film based on shape-memory PDLCL copolymers can be confirmed by XRR, and the thickness of the film can be determined between 1.5 and 3 nm.<sup>[86]</sup>

### 2.1.3. X-Ray Absorption Spectroscopy

The advanced technique known as near-edge X-ray absorption fine structure (NEXAFS), or X-ray absorption near edge structure (XANES) measures the spectrum of the energy absorbed by the sample in the edge region where a sample absorbs X-ray.<sup>[87]</sup> Qualitative and quantitative analyses of the chemical bonding and orientation of molecules in the sample can be operated in the sampling depth of  $\approx 10$  nm using NEXAFS, which is relevant for characterizing polymeric components at the interface and thin film surface.<sup>[88]</sup> Recently, this technique has been used to determine the bond length change during the programming of thermoset SMPs, which illustrated the stress and energy storage during the shape deformation.<sup>[89]</sup>

## 2.2. UV-Vis Spectroscopy

UV-vis spectroscopy is an analytical method to explore the absorption of UV and visible light by molecular chromophores in a sample. Elemental concentrations in a sample can be determined using absorption spectra based on the Beer-Lambert law.<sup>[90]</sup>

For the characterization of SMPs, UV-vis spectroscopy can be an effective technique to measure optical characteristics of samples, especially for photo-responsive SMPs. A nontraditional all room-temperature SME has been reported to be realized by blending SMPs containing polyester/polyether-based urethane acrylates with tripropylene glycol diacrylate, which exhibits the collapse and swelling of macropores with a diameter of 350 nm. A perceived color change can be observed related to the concentrations of swelling analytes in the mixture. A quantitative colorimetric analysis, thus, was carried out using UV-vis spectroscopy

to differentiate the color changes induced by different ethanol concentrations in octane. Reflection spectra of cold-programmed microporous samples and the recovered samples in the solution with varying ethanol concentrations have been detected and compared as shown in **Figure 3I**.<sup>[20]</sup> The full recovery of the photonic crystal configuration was observed in the spectrum of the sample recovered in the 5500 ppm ethanol, which matched with one of the original SMP membranes.<sup>[20]</sup> Another SMPs based on photo-responsive coumarin-containing polycaprolactone were studied. The spectra obtained after exposure to the wavelengths of 365 and 254 nm exhibit a decrease and recovery in the absorption peak  $\approx 320$  nm, respectively, indicating the reversible photo-crosslinking reaction of the coumarin groups. The shape recovery can be activated by the cleavage of the crosslinked cyclobutene ring that fixed the temporary shapes.<sup>[91]</sup>

UV-vis spectroscopy is also available to characterize solid SMPs at the nanoscale, such as NPs, when dispersed in a solvent. For example, block copolymer (BCP) particles have been reported by Kim et al. to obtain reversible shapes activated by irradiation with UV and visible lights by a spiroopyran-dodecyltrimethylammonium bromide (SP-DTAB) surfactant.<sup>[21]</sup> The photoisomerization behavior of SP-DTAB was monitored using UV-vis spectroscopy. A distinct absorption peak at 501 nm in the spectrum of the aqueous surfactant solution under UV irradiation as shown in **Figure 3II** indicated the extended  $\pi$ -conjugation of the hydrophilic, ring-opened merocyanine form of SP isomer, which then disappeared upon visible light due to the photoisomerization to the hydrophobic ring-closed SP form.<sup>[21]</sup> This result demonstrated that the ability of the SP-DTAB surfactant to undergo wavelength-dependent isomerization facilitated the reversible transformation of NPs, allowing them to shift between spherical onion-like particles and ellipsoidal particles.<sup>[21]</sup>

The most common use of UV-vis spectroscopy is for quantitative measurement of solutions, but it can also provide valuable insights into the analysis of a solid-state sample. Due to the exceptional sensitivity ( $< 10^{-5}$  molar) of UV-vis spectroscopy, it can be applied to identify polymer impurities.<sup>[92]</sup> It is a typical method to blend NPs into SMPs to generate advantages of either uniform heating, high recovery speed or magnetic/electrosensitivities.<sup>[93]</sup> An example of this concept is demonstrated by the light-controlled shape-memory poly(vinyl alcohol) with gold nanorods (AuNRs) that can convert optical energy into heat for shape recovery upon light absorption. The comparison of polarized UV-vis-NIR absorption spectra of un-stretched samples and stretched samples demonstrated that the AuNRs in the films oriented in the direction of the stretching. This result indicated the selective shape recovery under polarized light (**Figure 3III**).<sup>[70]</sup> Li et al. presented another type of wavelength-selective SME of multi-walled carbon nanotube (MWCNT)/epoxy composites. The photo-responsive behaviors of MWCNT are proved by UV-vis spectra, demonstrating its function to manipulate the SME of the multi-composite due to their wavelength-selective photo-responsive behavior.<sup>[94]</sup>

It is also a common use of UV-vis spectroscopy for determining the configuration of chemical bonds and for quantifying various analytes, including metal ions, conjugated organic compounds, and large biological molecules. A SMP with a  $\text{Fe}^{3+}$ -coordinated polyacrylic acid (PAA) network has been reported based on reducing  $\text{Fe}^{3+}$  to  $\text{Fe}^{2+}$  under visible light irradiation.

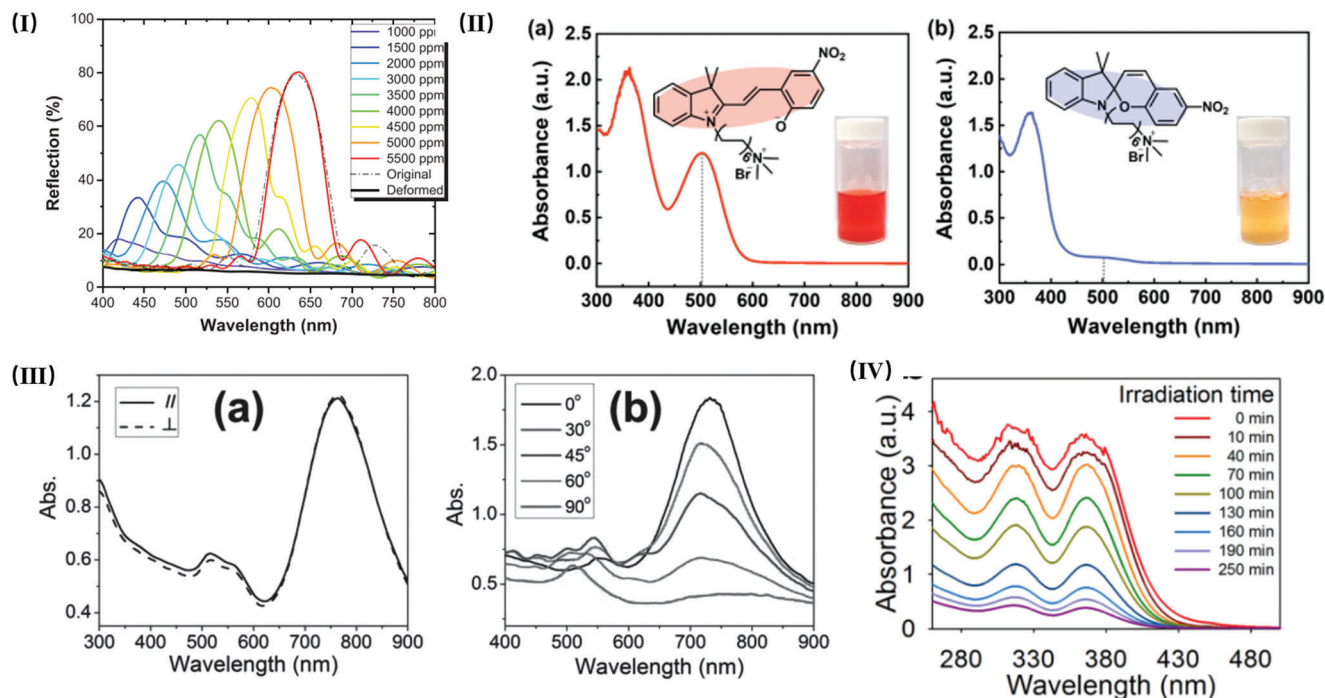


**Figure 3.** I) Normal-incidence optical reflection spectra of a cold-programmed macroporous SMP membrane after cold programming and recovering from ethanol-octane solutions containing different concentrations of ethanol. Reproduced with permission.<sup>[20]</sup> Copyright 2018, Wiley-VCH. II) UV-vis spectra of SP-DTAB sample in water after irradiation with a) UV and b) visible light for 6 h. Reproduced with permission.<sup>[21]</sup> Copyright 2021, American Chemical Society. III) Polarized UV-vis-NIR absorption spectra of (a) un-stretched poly(vinyl alcohol) (PVA)/AuNRs composite films and (b) stretched films to a draw ratio of 5 at different angles between the polarization direction of the incident light and the film stretching direction. Reproduced with permission.<sup>[70]</sup> Copyright 2013, Wiley-VCH. IV) UV-vis spectra of PAA-20 after visible light irradiation for different times. Reproduced with permission.<sup>[69]</sup> Copyright 2018, American Chemical Society.

The UV-vis absorption spectra (Figure 3IV) showed a decrease in the peaks representing  $\text{Fe}^{3+}$  at 318 and 365 nm, indicating the reduction of ferric ions during the recovery under visible light exposure.<sup>[69]</sup> The shape-memory mechanism of the staging-responsive SMPs can also rely on the analysis of the UV-vis spectrum. For example, as the UV radiation time increased, the absorption peak at 332 nm of the shape-memory polyurethanes (PUs), which corresponds to the  $\pi-\pi^*$  transition of the azo groups in the trans isomer of azobenzene, decreased, while the absorption peak at 436 nm representing the  $n-\pi^*$  transition of the azo groups in the cis isomer of azobenzene increased. This photoisomerization of the trans isomer of azobenzene into a cis configuration realized the staging-responsive SME in polymers.<sup>[95]</sup>

### 2.3. Fluorescence Spectroscopy

Fluorescence spectroscopy is a method used to analyze fluorescence emitted from excited molecules by photons. The fluorescence spectroscopy measurement provides detailed information regarding molecular processes, including conformational changes in polymer systems. Shape-memory hydrogels utilizing supramolecular chemistry crosslinks to fix temporary shapes have been developed to show good shape-memory performance at room temperature. The fluorescence spectrum shown in **Figure 4I** of the programmed sample displayed a typical peak

at 618 nm corresponding to the transitions of  $\text{Eu}^{3+}$  complexes compared to the spectra of samples in original and recovered shapes.<sup>[22]</sup> This result indicated that the fluorescent alginate- $\text{Eu}^{3+}$  complexes acted as switching crosslinks in the shape-memory hydrogels.

The fluorescence technique can be used to detect photophysical phenomena that exist in SMPs. An instance of the use of in situ fluorescence spectroscopy, in combination with a programmable hot stage, is the analysis of the relations between temperature and fluorescence color of SMP blends.<sup>[23]</sup> The shape-memory particles can display shape changing due to photo-switchable surfactants. The photoluminescence was used to investigate the emission characteristics of BCP particles. The spherical particles were stabilized by the RO surfactant and suspended in water, which exhibited a significant peak at 615 nm as shown in **Figure 4II**. Therefore, the particle shape to the optical signal was correlated.<sup>[21]</sup>

### 2.4. IR and Raman Spectroscopy

IR absorption and Raman scattering are two main vibrational spectroscopic techniques that can identify and determine chemical compounds and molecular structures in polymeric systems. Characteristic peaks in a spectrum represent molecules and functional groups corresponding to the unique “fingerprint” frequencies of molecule vibrations. IR spectroscopy measures the



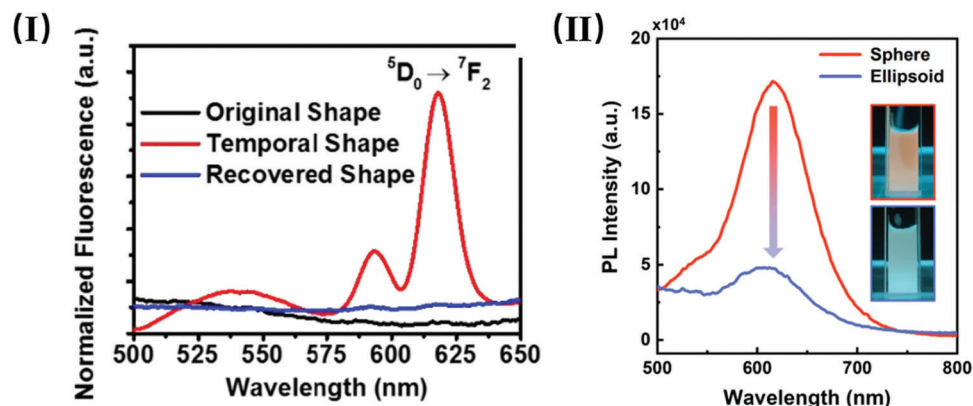


**Figure 4.** I) The fluorescence spectra of the shape-memory hydrogels containing alginate-Eu<sup>3+</sup> complexes in the original, temporal, and recovered shapes. Reproduced with permission.<sup>[22]</sup> Copyright 2018, American Chemical Society. II) Photoluminescence spectra of an aqueous suspension of the spherical (orange) and ellipsoidal (blue) PS10k-b-P4VP10k shape-memory particles, where the insets are their fluorescence optical images. Reproduced with permission.<sup>[21]</sup> Copyright 2021, American Chemical Society.

transition between molecular vibrational energy levels due to the absorption of incident IR radiation by vibrating molecules. Raman effect relies on the inelastic scattering occurring when molecules vibrate and scatter a monochromatic light.<sup>[96]</sup> The two fundamentals of IR and Raman spectroscopies yield complementary information because of the different sensitivity to the vibrations of chemical bonds. For example, IR spectroscopy is sensitive to polar functional groups like hetero-nuclear bonds, while Raman scattering is active to symmetric vibrations, such as homonuclear molecular bonds.<sup>[97]</sup> The selection of inspection methods should depend on the required information of detected samples.

#### 2.4.1. Raman Spectroscopy

Raman scattering is a powerful spectroscopic technique for identifying chemical components and functional groups in polymeric materials. Raman spectroscopy is based on the interaction between the incident radiation and vibrating molecules in a sample, which causes the incident radiation to undergo inelastic scattering and become distorted.<sup>[98]</sup> The Raman spectra present scattered intensity and wavelength shift correlation, where peak locations are assigned for chemical bonds and functional groups in polymeric systems.<sup>[99]</sup>

Raman technique is widely used for studying carbon-centered materials and presenting well-defined bands in spectra. The established polymer band libraries enable fast identification of chemical structures as well as crystalline and amorphous carbon compositions in SMP chains. The recycling of crosslinked SMP material was achieved by functionalizing the star-shaped PCL with photo-cross linkable coumarin-based end groups. The characteristic peaks of coumarin at 1562 and 1617 cm<sup>-1</sup> as shown in **Figure 5I**, corresponding to the stretching modes of the —C=C— bonds in the pyrone ring, were determined by Raman spectroscopy to present the conversion of the coumarin in relation to the dimerization degree under light irradiation. Meantime, the degree of conversion of coumarin was calculated quantitatively by analyzing the ratio of band intensities at 1562 cm<sup>-1</sup>

in Raman spectra before and after exposure to UV irradiation, which effectively established the relationship between the degree of coumarin dimerization and shape-memory properties.<sup>[24]</sup> The spectral characteristics of carbon-based materials can be influenced by external factors such as temperature and strain. This implies that bond shifts can be employed to verify the extension of polymer chains in a SMP after programming. For example, the bands at 1367 and 1587 cm<sup>-1</sup> were reported to represent the stretching vibration of —CH<sub>2</sub> and the aromatic stretching groups, respectively, which disclosed the elongation of hard segments in microstructures of shape-memory PU after deformation.<sup>[25]</sup>

As mentioned before, for thermo-responsive SMP based on semicrystalline polymers, the orientation degree in crystalline and amorphous phases are vital factors in understanding the relations between macroscopic shape-memory properties of polymeric materials and their microstructural variations. Polarized Raman scattering is a potent technique that can be used to gather data on the distributions of molecular orientation. Polarized Raman spectroscopy provides an advantage over X-ray scattering, which measures only the crystalline structures, and dichroism IR, which has low accuracy. This technique can determine high-order coefficients for distribution functions that offer a quantitative measurement of the level of molecular orientation.<sup>[73]</sup> Studies on the thin film of shape-memory PU have demonstrated the efficacy of polarized Raman spectroscopy as the method for characterizing phase separation and average molecular orientation. To probe local molecular alignment and phase separation in samples, the depolarization ratio between the vibrational modes of the two benzene rings at 1616 cm<sup>-1</sup> in hard segments domains (**Figure 5II**) were employed to illustrate partially aligned hard micro-domain in the PU film.<sup>[100]</sup> For elastomeric thermoplastic PUs with a water-responsive rapid, rapidly switchable SME, Zhu et al. have also applied polarized Raman spectroscopy to manipulate the micro-structural changes of samples. The peak at 1095 cm<sup>-1</sup> in the spectrum, which corresponds to the C—O stretching vibration in the ring structure of cellulose was used to calculate the quantitative orientation parameter to represent the orientation in microdomains along the stretching direction in the original shape after programming and recovery processes.<sup>[101]</sup>



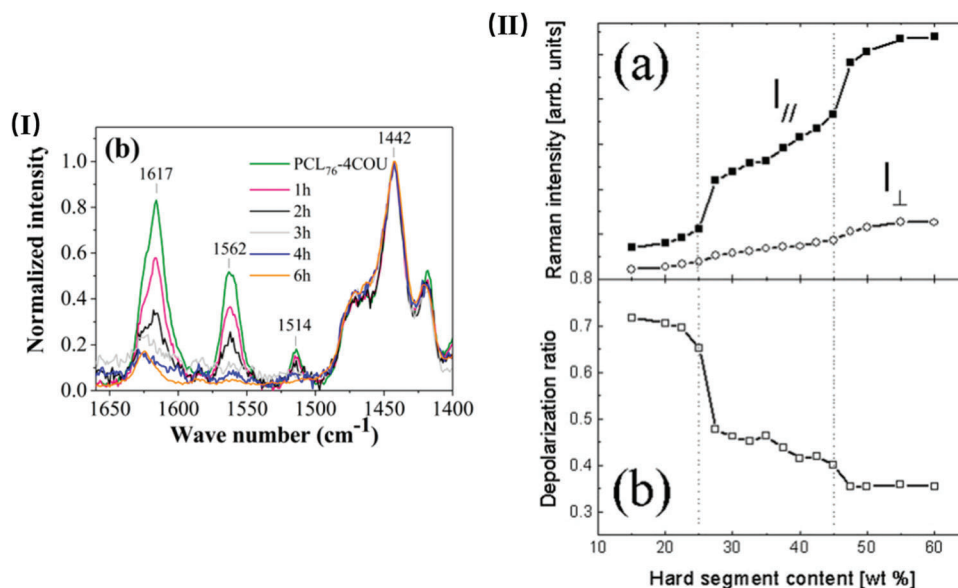


**Figure 5.** I) Raman spectra of PCL76-4COU-Bzph0 before UV irradiation (green curve), after 60 min (pink curve), after 120 min (black curve), after 180 min (gray curve), after 240 min (navy blue curve), and after 360 min of UV irradiation (orange curve). Reproduced with permission.<sup>[24]</sup> Copyright 2019, American Chemical Society. II) a) Polarized Raman intensities of the PU films with various hard segment contents, here,  $I_{//}$  and  $I_{\perp}$  denote the signals with polarization parallel and perpendicular to that of the excitation laser, respectively, b) the plot of peak intensity at  $1616\text{ cm}^{-1}$  vibrational mode with various hard segment contents. Reproduced with permission.<sup>[100]</sup> Copyright 2007, Wiley Periodicals.

In order to address the low sensitivity issue caused by weak Raman scattering of molecules, Surface Enhanced Raman Spectroscopy (SERS) is used to boost the Raman scattering by utilizing certain nanostructured materials, such as metal NPs, which allows the structural analysis of low-concentration compounds.<sup>[102,103]</sup> Owing to the ultra-high sensitivity, this technique was also applied for quantitative analysis of SMPs. Silver NPs were successfully decorated on shape-memory polystyrene sheets to produce thermally induced hot spot effects. Aromatic thiols can be used as probes to obtain high-quality SERS spectra, which were easily acquired with enhancement factors exceeding  $10^8$ .<sup>[104]</sup> Gaobardo et al. also reported the fabrication of wrinkled SMP films with gold NPs, which leveraged the structural tunability to program the wavelength and amplitude of wrinkles. The gold wrinkling provided a practical enhancement in the signals of SERS, and the intensities of the peak at  $1090\text{ cm}^{-1}$  of 4-mercaptopyridine can be compared to those before and after shrinking.<sup>[105]</sup>

Tip-enhanced Raman spectroscopy (TERS) is a spectral mapping technique that integrates Raman spectroscopy and scanning probe microscopy, similar to AFM-IR as previously discussed. This technique involves focusing a sharp metal tip onto the center of a laser beam and accurately positioning it at various regions on a sample surface.<sup>[106,107]</sup> For instance, Weng et al. reported the application of a voltage to the tip to deform the suspended graphene sheet during TERS experiments. Young's modulus of graphene can be estimated as  $1.48\text{ tPa}$  by this method.<sup>[108]</sup> Though rare research has been done on SMPs using TERS techniques, it has excellent potential for investigating in situ structural deformations in materials utilizing the TERS tip.

#### 2.4.2. IR Spectroscopy

IR spectra of polymeric samples are results of the excitation of vibrational modes of molecules. The peaks observed in the IR spectrum of a sample can be regarded as the "fingerprint" associated with different chemical bonds and groups presenting in molecules, which is used to determine the chemical structure of molecules. In addition, quantitative analysis can be carried out from the IR spectra by calculating the absorbance of IR energy by a molecule, which is directly proportional to its density.<sup>[109]</sup> IR spectroscopy can be classified into three types depending on the range of frequency: NIR, mid-IR (MIR) and far-IR (FIR). MR spectroscopy with the wavenumbers from  $500$  to  $4000\text{ cm}^{-1}$  is usually maintained using interferometer-based Fourier Transform IR (FTIR), typically used for studying fundamentals of molecular vibrations in polymeric materials.

FTIR is sensitive to hydrogen bonds, which can measure the formation of hydrogen-bonded groups in a SMP to state the structural transition for shape fixation. For example, the shape recovery of solvent-responsive SMPs can be triggered after being immersed in solutions. The FTIR spectra displayed **Figure 6I** verified that the IR band at  $1724\text{ cm}^{-1}$  of the free C=O stretching vibration was shifted to the bonded C=O stretching band at  $1740\text{ cm}^{-1}$ .<sup>[71]</sup> Further, the intensity of hydrogen-bonded bonds increased with immersion time in a solvent, indicating that the shape recovery process was actuated by forming hydrogen bonds.<sup>[71,110]</sup>

FTIR has been used extensively to investigate the polymorphs of PVDF, which has been widely studied because of its pyro- and piezoelectricity.<sup>[111,112]</sup> PVDF-based polymers can exhibit excellent SMEs. To illustrate, the  $\beta$ -phase content in the original

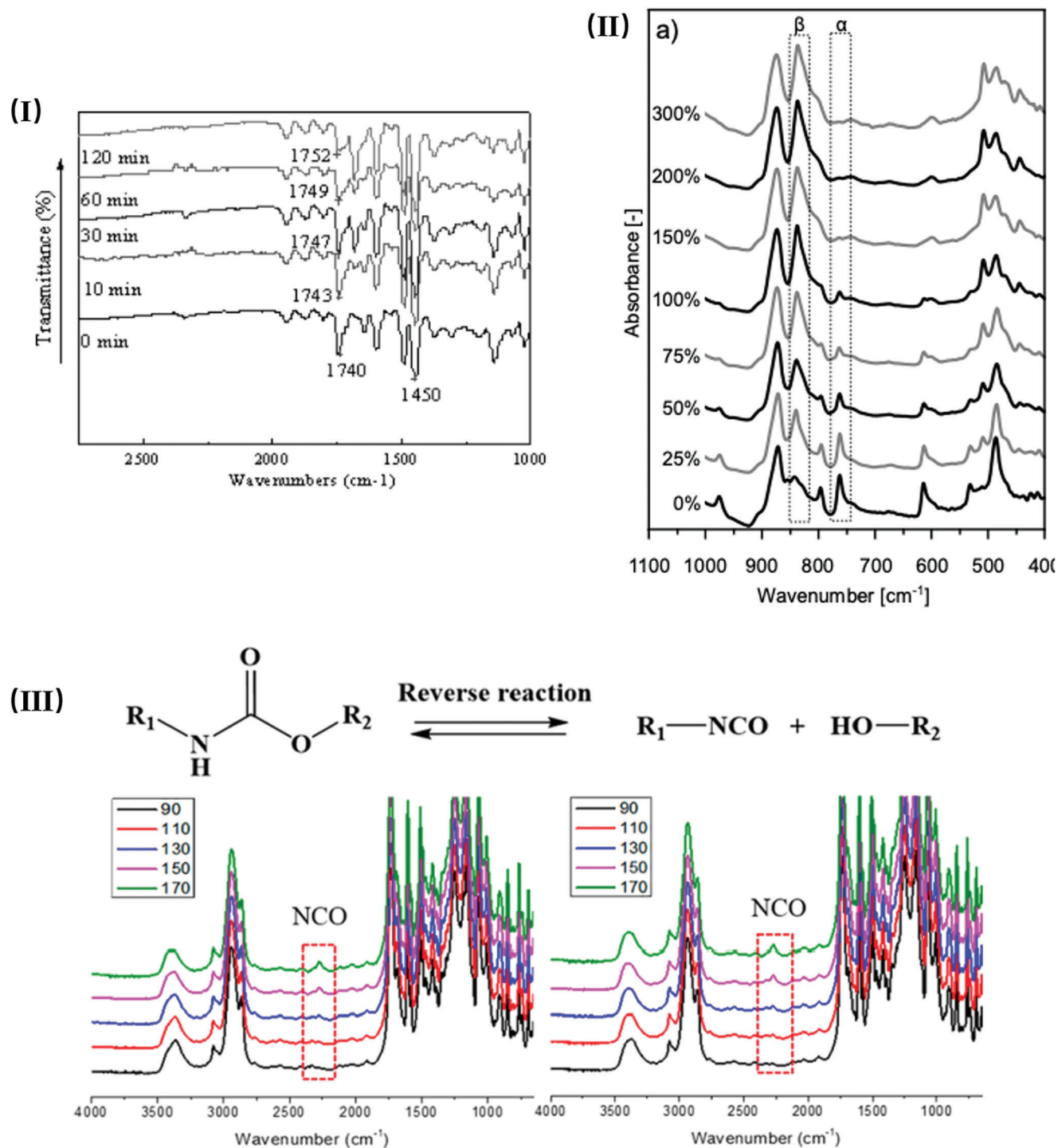


**Figure 6.** I) The C=O stretching region in FTIR spectra of styrene-based SMP after different immersion hours. Reproduced with permission.<sup>[71]</sup> Copyright 2008, Wiley-VCH. II) ATR-FTIR spectra of x-PVDF programmed to different strains. Reproduced with permission.<sup>[72]</sup> Copyright 2015, Wiley-VCH. III) FTIR spectra of the reversion of the carbamate bond. Reproduced with permission.<sup>[114]</sup> Copyright 2018, American Chemical Society.

state of PVDF after the program and after recovery was calculated using the absorbances of  $\alpha$ - and  $\beta$ -phases at 764 and 840 cm<sup>-1</sup>, respectively, from FTIR analysis as shown in Figure 6II.<sup>[72]</sup> The findings suggested that the fixation of PVDF based SMPs relied on the transition from  $\alpha$ -phase to oriented  $\beta$ -phase in PVDF. The

highest content of  $\beta$ -phase in programmed PVDF-based SMP samples exhibited the highest recovery ability.<sup>[72,113]</sup>

LC polymers with a unique anisotropic shape-changing ability have become promising shape-memory materials. IR is a crucial characterization method to study the temperature-induced phase

transition behavior of LC polymers. The phase transition of LC polymers results from a change in the orientation of internal LC moieties. The study of phase transition behavior, thus, usually starts from the basic structural units using IR. A reconfigurable PU-LC elastomer has been reported by Wen, et al., whereby structural rearrangement upon applying external stress relied on the reversible addition reaction of carbamate bonds, which present in the isotropic phase at a high temperature. The FTIR spectra in Figure 6III elucidated the urethane bond reversion dynamics. The fact that isocyanate with an IR peak at  $2225\text{ cm}^{-1}$  appeared upon heating and disappeared after cooling confirmed the reversible nature of this linkage in the samples with exchangeable carbamate functional groups.<sup>[114]</sup>

Compared to X-ray scattering for determining the orientation degree of crystals, IR spectroscopy is also a potential method for characterizing chain orientation and transformation in polymeric samples under deformation and relaxation, which is essential for understanding the shape-memory mechanisms in polymeric materials.<sup>[26,27]</sup> For example, the orientation of amorphous PCL chains in PCL/poly (vinyl chloride) blends during its deformation and recovery process can be calculated from the vibration peaks of carbonyl groups in dichromic FTIR spectra, indicating that the amorphous PCL region acted as the switching domains at low switching temperature in the triple-shape-memory process.<sup>[74]</sup> Even rapid polymer orientation kinetics can be detected by ultrarapid scanning FTIR with a millisecond resolution.<sup>[115]</sup>

Recently, atomic force microscopy-based IR spectroscopy (AFM-IR) has been reported to acquire IR spectra with a resolution at and beyond the nanoscale, which surpasses the constraints of light diffraction.<sup>[116,117]</sup> The AFM-IR technique can be applied to investigate nano-properties and gain microstructural information about SMPs. Shape-memory epoxy resins have been reported to undergo a polymerization-induced micro-phase separation process. The micro-morphology of samples can be indicated by the AFM-IR map, where regions with a low intensity of the stretching vibration of aliphatic bonds at  $2930\text{ cm}^{-1}$  represented phases containing a high content of soft segments.<sup>[118]</sup> Further, the relations between shape-memory behavior and the microstructure of a polymer system can also be explained by AFM-IR. Huang, et al., described the development of a thermal-responsive shape-memory silicone rubber composites (SRCs) with three distinct transition temperatures. The AFM-IR maps of SRC samples revealed a dark region, which represented the two switching phases of poly(methyl methacrylate) (PMMA) and poly(ethylene-co-methacrylic acid) with a peak observed at  $1735\text{ cm}^{-1}$  of C=O vibration. This information can be used to identify the chemical compositions of the sample and build a linear functional relationship between the recovered scale and the content of switching domains.<sup>[119]</sup>

## 2.5. Other Spectroscopic Techniques for SMPs

### 2.5.1. Photoluminescence (PL) Spectroscopy

PL spectra are a fast and efficient method to investigate specific energy levels and acquire details on the properties of materials, particularly the composition of semiconductor samples, the

thickness of quantum well or the monodispersity of quantum dot samples. In SMP composites with carbon or graphene quantum dots, PL measurements were usually carried out to explore the luminescence properties of composite films related to the quantum dots content.<sup>[75,76]</sup>

### 2.5.2. Brillouin Spectroscopy

Brillouin light-scattering (BLS) spectroscopy, which is also known as Brillouin–Mandelstam light-scattering spectroscopy, is the method of using the inelastic scattering of light for investigating the elemental excitations of materials such as phonons or magnons, which are either thermally generated or coherently excited. This technique can be used to determine the elastic properties of materials by measuring the frequency shift of the scattered light. The glass transition temperature ( $T_g$ ) of a sample can be determined by sweeping the temperature and then calculating the slope variation in the Brillouin shift depending on temperature changes. It has been proven to be an effective method of measuring the precise  $T_g$  for a SMP, which requires accurate control of shape-changing. It had another advantage that the testing sample could be in any shape, size and volume without preparation or the need to apply stress.<sup>[28]</sup>

### 2.5.3. Polarized Optical Extinction Spectroscopy

Optical extinction spectroscopy is a technique to measure the amount of radiation transmitted through a sample in relation to the wavelength of the incident light. This technique is commonly used for analyzing metallic particles. When NPs are blended into SMPs, they can also apply to determine the optical properties. In the work of Yadav, plasmonic NPs were embedded in SMPs for photothermal stimulation to control shape recovery. When analyzing stretched SMP films containing NPs, changes in the coupling between the NPs can be observed in their polarized extinction spectra, where the maximum of the optical extinction corresponds to the surface plasmon resonance. Therefore, the extinction spectra of the SMP sample during programming and recovery process revealed the correlations of plasmon coupling in the NPs with the strains and temperatures.<sup>[29]</sup>

In conclusion, X-ray and spectroscopic techniques have played a crucial role in characterizing SMPs to offer insightful information about the chemical composition molecular structure, and conformational variation of SMPs. The future prospects for optical spectroscopic techniques in characterizing SMPs appear promising, where the advanced spectroscopic methods with improved sensitivity and spatial resolution will allow more precise characterization of local structural changes. Further, the integrations of spectroscopic techniques with other analytical tools, such as microscopy and imaging techniques, can provide a more comprehensive understanding of the underlying mechanisms of SMPs.

## 3. Preparation of SMPs with Different Original Structures and Shapes using Light

The light-related construction of SMPs, including photocrosslinking and photo-fabrication, is an important part of the

relationship between SMPs and light. In the scope of molecular structure design, photo-crosslinking is used to build firm network points in permanent shape and molecular switches in secondary shape networks of SMPs. The curing method of polymer networks has been changed from overall heat curing to local photocuring based on photo-crosslinking technology, which can restrict the area of crosslinking as well as control the space and time during the molding process.<sup>[12,30,120,121]</sup> Photo-related preparation methods can produce precise and sophisticated shapes of SMPs through the synergistic effect combined with advanced 3D printing systems, and can push advanced manufacturing to practical products in different applications.<sup>[31]</sup>

The overview of light-related construction in this section is divided into two parts: the interaction between light and molecular structure at the structural level and the advanced 3D/4D printing technology based on light at the macro level.

From the structural level, the regulation of molecular structure is mainly dependent on the design and construction of network points in crosslinked networks of SMPs and molecular switches to realize SMEs. Network points decided the permanent shape of SMPs, which are generally created by chemical crosslinking or physical crosslinking.<sup>[122]</sup> The main way of chemical crosslinking is to form covalent bonds, which is more stable than chain entanglement, crystallization, and glass solidification, that is, physical crosslinking. The shape-memory recovery performance of chemical crosslinking is also better than that of physically crosslinking in SMPs. The network points made by photo-crosslinking are mainly composed of irreversible covalent bonds, and traditional molecular switches are based on thermal phase transitions of polymer chain segments, such as crystallization-melting and glass transitions.<sup>[123,124]</sup> Currently, reversible dynamic functions such as reversible heat-curing and photo-curing, as well as pH reversible response are becoming increasingly popular.<sup>[125–127]</sup> This also gives more flexibility in changing the permanent shape after fabrication compared with the irreversible covalent bonds, which is benefit for a sustainable consideration.

From a macro perspective, advanced manufacturing technology is an important part of realizing the fabrication of smart materials. Additive manufacturing technology is widely used due to characteristics of digital design and precise molding, and it can also be called 3D printing technology in a narrow sense. 3D printing technology provides flexibility and cost efficiency for the manufacture of complicated and on-demand products. However, it can only be used to usually generate static structural products rather than dynamic structural materials.<sup>[128]</sup> Recently, advancements have been made via 3D printing, creating innovative smart materials.<sup>[129–131]</sup> The products have the characteristics of physical properties variation over time under specific environments and stimuli, including electricity, light, solvent, magnetism, heat, etc. This capability is commonly referred to as 4D printing, which adds the dimension of time under static geometric structure determined by 3D printing to realize the dynamic change of materials over time.<sup>[132]</sup> The technologies employed in 4D printing are fundamentally rooted in 3D printing technologies, with differences arising in the selection of materials and parameters in printing processes. The 4D printing products are typically fabricated using stimuli-responsive materials, or engineering materials containing designed networks capable of achieving desired motions in response to external stimuli. The latter portion of this

section introduces the basic principles and technical characteristics of various photo-crosslinking printing technologies and the detailed insights of the mechanisms and processes involved in these printing methods are discussed.

### 3.1. Molecular Structure Design of Photo-Crosslinked SMPs

Photo-crosslinking reaction is mainly divided into two categories: irreversible and reversible photo-crosslinking. As mentioned above, irreversible photo-crosslinking is used to construct the network points of SMPs, while reversible one can be used in the construction of molecular switches. Currently, common irreversible photo-crosslinking methods mainly include photo initiator-acrylate free-radical polymerization, thiol-ene/yne addition, photo initiator-epoxy ion polymerization, azide-alkyne cycloaddition and photooxidative coupling.<sup>[133–136]</sup> Reversible photo-crosslinking methods mainly depend on the cycloaddition reaction of functional groups, including coumarin group, thymine group, cinnamic acid group, stilbene group, and anthracene group. **Table 2** presents a classification of commonly employed photo-crosslinking methods, while the subsequent discussion follows the categorization based on the reversibility of photo-crosslinking reactions.

#### 3.1.1. Irreversible Photo-Crosslinking Reaction

The majority of photo-crosslinking reactions exhibit irreversible characteristics, where the most prevalent applications involving the crosslinking of acrylate systems via the initiation of photoinitiated free radicals. Units incorporating acrylate groups as either monomers or acrylate-terminated prepolymers offer versatility in their application of 3D printing processes. The ratios between these two categories can determine the appropriateness for different 3D printing cases and influence the product performance.<sup>[138]</sup> Another type of irreversible photo-crosslinking reaction is photoclick chemical reaction, including thiol-ene/alkyne and azide-alkyne cycloaddition reaction. The photooxidation reaction commonly used in biological protein systems is also one of the methods for irreversible photo-crosslinking, which is suitable for crosslinking in an aqueous environment.<sup>[139]</sup>

*Photo Initiator-Acrylate:* The photo initiator-acrylate crosslinking is the most common photo-crosslinking method at present. The reaction conditions of this method are simple and effective, and the curing speed is very fast. A photo initiator must be added to the system to link acrylate groups together through free radical polymerization to form a crosslinked network as shown in **Figure 71**. The addition of multifunctional acrylate crosslinking agents to the system can increase the crosslinking density of the network and effectively adjust physical properties of the product. Safranski et al. prepared a series of photo-crosslinked SMPs mixed with mono-functional (meth)acrylates and 16 multi-functional (meth)acrylates, and explored the impacts of monomer ratio and crosslinker content on the network structures and product performances. All samples were prepared with 2,2-dimethoxy-2-phenylacetophenone as the photo initiator and photocured under 365 nm UV light.<sup>[144]</sup>



**Table 2.** List of photo-crosslinking technologies for SMPs.<sup>[137]</sup>

Categories	Photo reversible	Photo initiator	Reaction conditions	Photo reversible conditions
Photo initiator-acrylate	N	Y	UV, visible, NIR (photo initiator-dependent)	N/A
Thiol-ene/yne	N	Y	UV, visible, NIR (photo initiator-dependent)	N/A
Azide-Alkyne Cycloaddition	N	Y	UV, visible (photo initiator-dependent)	N/A
Photooxidative coupling	N	Y	UV, visible (photo initiator-dependent)	N/A
Coumarin	Y	N	UV, visible > 320 nm	UV < 280 nm
Cinnamic acid	Y	N	UV > 300 nm	UV < 260 nm
Stilbene	Y	N	UV, visible > 300 nm	UV < 280 nm
Anthracene	Y	N	UV, visible > 350 nm	UV < 300 nm

Zarek et al. used different degrees of methacrylate-terminated PCL prepolymers for 3D printing photo-crosslinking molding, and prepared a variety of complex structures such as the Eiffel tower and eagles.<sup>[145]</sup> The samples were prepared with 2,4,6-trimethylbenzoyl-diphenyl-phosphineoxide (TPO) as photo initiator under 385 nm UV light. These products all realized the thermal stimulus response, and the shape recovery process is shown in **Figure 8I**.<sup>[145]</sup>

Sheiko et al. produced a crosslinked network using acrylate-modified polyoctyl adipate (POA) macromolecules under 365 nm UV light with 2,2-diethoxyacetophenone (DEAP) as photo initiator.<sup>[146]</sup> The melting of partial crystalline segments can induce a non-uniform change in volume of crosslinked POA, which realized bidirectional SME under stress-free condition.<sup>[146]</sup> Tak-

ing advantage of this point, it can be designed as a reversible opening and closing change of petals, as shown in **Figure 8II**.

Current mainstream application of the photo initiator-acrylate system is 3D light-curing printing, and the molecular structure design of the acrylate monomer needs to meet the requirements of product performance and light-assisted printing technology. Precise 3D printing has strict requirements for different monomer ratios, molecular weights of monomers, the content of crosslinking agent and the concentration of photo initiators. Spiegel et al. presented a versatile light-controlled 4D printing system using shape-memory ink both at the macroscale and microscale.<sup>[138]</sup> In the system, the network chain was built with isobornyl acrylate, poly(ethylene glycol) diacrylate and tricyclo[5.2.1.0]decanedimethanol diacrylate were used as

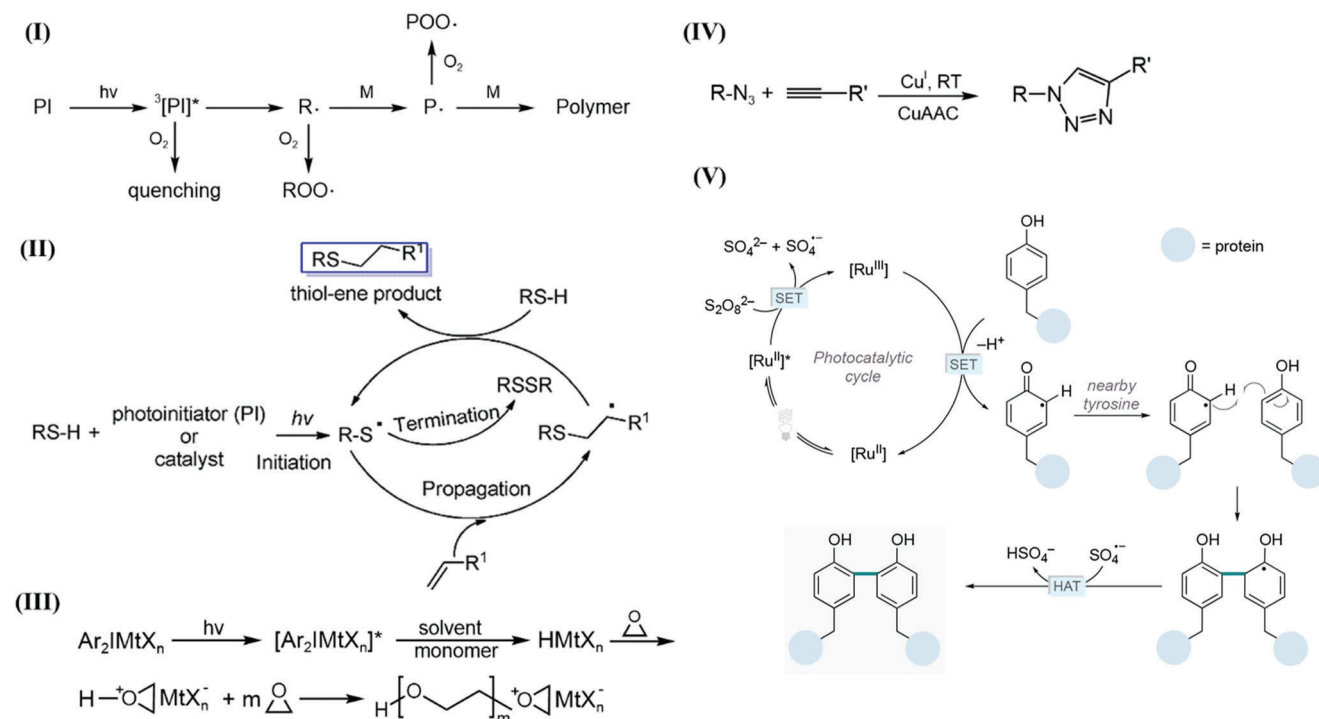


**Figure 7.** The schematic diagrams of irreversible photo-crosslinking reactions. I) The mechanism of photo initiator-acrylate reaction. II) The mechanism of thiol-ene/yne addition reaction. Reproduced with permission.<sup>[140]</sup> Copyright 2018, Wiley-VCH. III) The mechanism of photo initiator-epoxy reaction. Reproduced with permission.<sup>[141]</sup> Copyright 1999 Wiley Periodicals. IV) The mechanism of azide-alkyne cycloaddition reaction. Reproduced with permission.<sup>[142]</sup> Copyright 2011 Wiley-VCH. V) The mechanism of photooxidative coupling reaction. Reproduced with permission.<sup>[143]</sup> Copyright 2022, American Chemical Society.

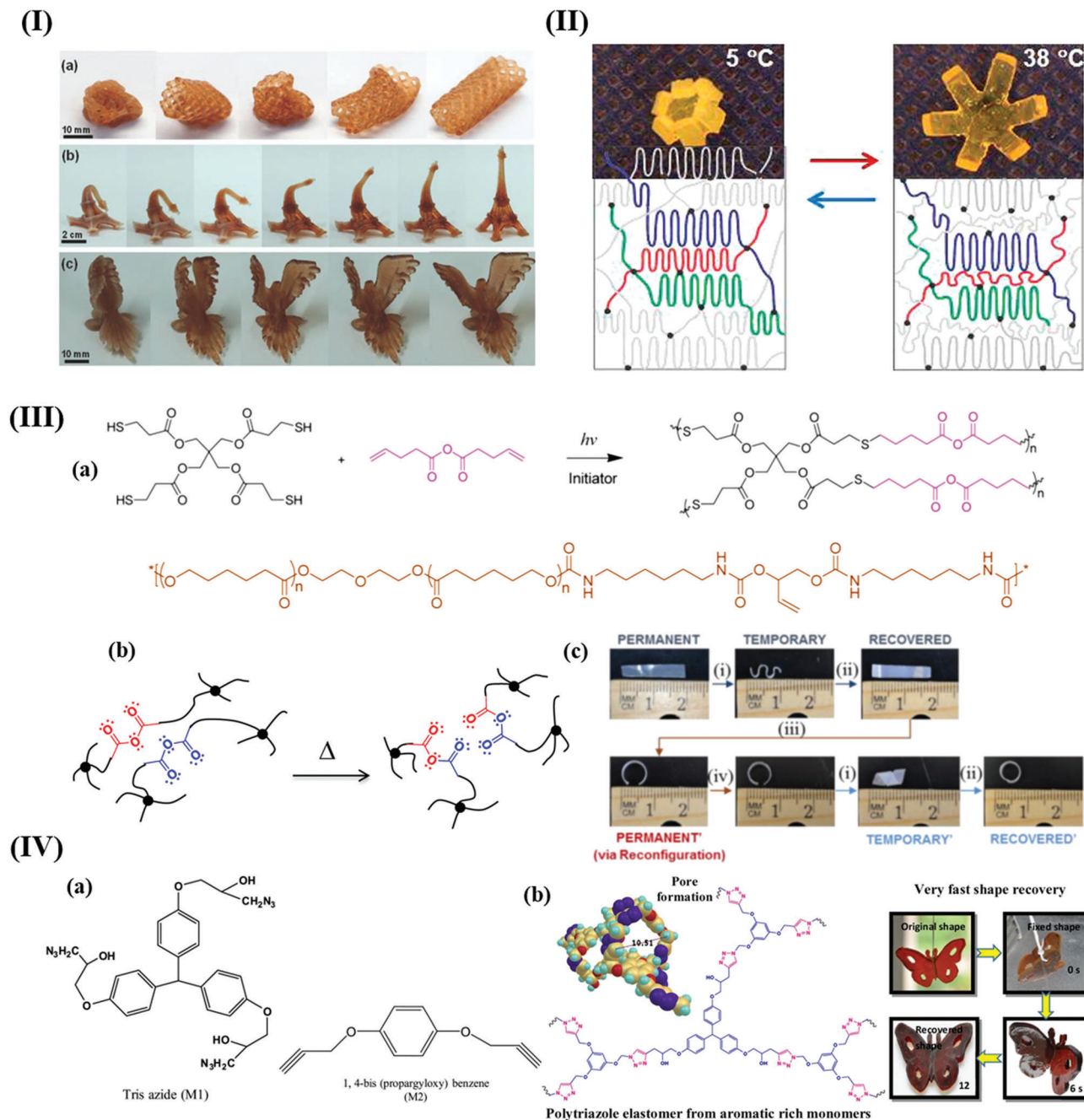


**Figure 8.** I) SLA printing of molten macromolecules with methacrylate groups, respectively printed cardiovascular stents, Eiffel Tower and eagle shapes, and the shape recovery function under thermal stimulation. Reproduced with permission.<sup>[145]</sup> Copyright 2016, Wiley-VCH. II) The molecular structure of crosslinked acrylate-modified POA prepolymer using 365 nm ultraviolet light and reversible opening and closing actions of artificial petals using bidirectional SME. Reproduced with permission.<sup>[146]</sup> Copyright 2014, American Chemical Society. III) a) Preparation of reconfigurable shape-memory materials with three functional units, b) thermodynamic covalent rearrangement of poly(anhydride) segments, and c) demonstration of shape recovery and reconstruction of anhydride-based shape-memory materials. Reproduced with permission.<sup>[160]</sup> Copyright 2016, American Chemical Society. IV) CuAAC was triggered by multifunctional azides and multifunctional propargyl monomers under heat to prepare elastomeric SMPs with fast response. Reproduced with permission.<sup>[167]</sup> Copyright 2018, Elsevier.

crosslinkers. The poly(ethylene glycol) diacrylate can also be taken as the soft segments of the network. Compared with microscale products printed with two-photon lithography, the macroscale products printed with DLP added HexA and Sudan I as additives to improve photocuring efficiency. All the products

were prepared with TPO as photo initiator under 385 nm UV light.<sup>[138]</sup>

The drawback of free radical polymerization reactions is that the presence of oxygen can lead to the formation of peroxyradicals, which could inhibit the activity of free radicals. This

interference can significantly slowed down or even halt the entire photocuring reaction.<sup>[147]</sup> Therefore, SMPs prepared through photo initiator-acrylate crosslinking usually had heterogeneous network structures with a wide range of chain lengths between network points. Compared to the SMPs prepared by thiol-ene polymerization, the SMPs prepared by photo initiator-acrylate crosslinking had a wide  $T_g$  range. The crosslinking uniformity of free radical acrylate system was relatively poor, and the toughness and shape-memory response of the material were not as good as thiol-ene systems.<sup>[148]</sup>

**Thiol-Ene/yne:** As a classic reaction in click chemistry, thiol-ene/yne reactions have been widely used in the formation of network by photopolymerization, especially in the chemical modification of biological materials. Thiol-ene/alkyne crosslinking refers to the addition reaction of thiols with various unsaturated groups to form covalent bonds as illustrated in Figure 7II. Such reactions can be initiated by heat, redox, and free radicals, among which photo initiator-based thiol-ene/yne reactions are commonly used for photo-crosslinking.<sup>[149–151]</sup> Compared to the photo initiator-acrylate system, the photo-crosslinking of thiol-ene/yne demonstrates notable advantages, including rapid reaction kinetics and insensitivity to oxygen inhibition. The resulting crosslinked network is uniform and has minimal volume shrinkage.<sup>[152,153]</sup> The preparation of conventional SMPs products usually use thiol-ene reaction to photo-crosslink prepolymers. Curing rate increases in the case of selecting a suitable photo initiator and functional monomer with polythiol groups. Compared with the acrylate system, the modulus of products decreases while toughness significantly improves. An exemplary study conducted by Ding et al. showed that the utilization of an efficient step-growth thiol-norbornene system can fabricate SMPs with high homogeneity.<sup>[154]</sup> The resulting SMPs exhibit a uniform network structure, enabling a high shape recovery ratio and rapid response. Besides, it also had multiple SMEs within a narrow  $T_g$  range. This study serves as a compelling demonstration of the efficacy of the thiol-ene system in synthesizing well-defined SMPs. Similarly, Anthamatten et al. also prepared a kind of well-defined shape-memory networks by employing a base-catalyzed reaction of acrylate-terminated PCL with multifunctional thiols.<sup>[155]</sup> The resulting networks exhibited uniform molecular weight distribution between network points, resulting in exceptional thermal and mechanical properties, as well as outstanding shape-memory characteristics. In contrast, the mechanical and thermal behavior of SMPs crosslinked by free radical polymerization was undesirable. In another study from Anthamatten et al., the triggering temperature of shape-memory PCL networks adjusted by non-crystallizable molecular linkers and molecular weight of PCL prepolymer through base-catalyzed thiol-ene reaction. They found that longer linkers and PCL prepolymer with lower molecular weight would affect the crystallization process and decrease the  $T_g$ . This feature can be applied to design SMPs triggered by body temperature for medical applications.<sup>[156]</sup> Prepolymers containing PEG segments have low photo-reactivity. It is difficult to achieve good crosslinking effect by conventional photoinitiated free radical polymerization, and the crosslinking effect of such prepolymers can be optimized by thiol-ene reaction.<sup>[157]</sup> The covalent bonds formed by thiol-ene reaction are used in SMPs as permanent network points. SMPs can be prepared with reconfigurable shapes using ther-

modynamic covalent bonds, such as Diels–Alder bonds and exchange of ester bonds. Some exchange reactions can be realized with organic base, like 1,5,7-triazabicyclo[4.4.0]dec-5-ene (TBD), and some exchange reactions can take place by heating, such as anhydride bond.<sup>[158,159]</sup> The intermolecular rearrangement with exchange reactions can effectively realize the dynamic changes of crosslinked network.

The reconfigurable shape-memory material prepared by Mather et al. was a typical triple functional network. The PCL prepolymer was responsible for SME and the polyanhydride prepolymer was responsible for the dynamic reconfiguration function. These two functional segments were integrated into one polymer network by thiol-ene photo-crosslinking reaction in order to achieve complex shape changes, as shown in Figure 8III.<sup>[160]</sup>

Thiol-ene photo-crosslinking reaction has the advantages of simplicity and efficiency. It can be used to prepare bidirectional SME materials, which can be photocured to form a permanent network when the material is not stretched. The secondary shape was photocured to maintain the chain segments' orientation after uniaxial stretching. The deformed network structure and the oriented mesocrystalline can relieve part of the stress caused by stretching to realize bidirectional SME. Anthamatten et al. used excess acrylate-terminated PCL and trimercapto-based compound for two-stage crosslinking. The first stage was thermal crosslinking of some groups in the initial shape, and the second stage was photo-crosslinking after uniaxial stretch orientation to capture the oriented state.<sup>[161]</sup> Upon cooling, the oriented PCL segments crystallized, and the film elongated along the orientation direction. The crystallized parts melted upon heating, then the orientated force disappeared and the film shrank again. As a result, the bidirectional SME with a uniform actuation of >15% can be realized under the cyclic heating and cooling processes.

**Photo Initiator-Epoxy:** The photo initiator-epoxy system also serves as a common photopolymerization system, wherein photo initiators produce cationic active centers that initiate the ring-opening polymerization of epoxy monomers and prepolymers upon UV irradiation, as shown in Figure 7III. Onium salts, such as iodonium salts and sulfonium salts, are extensively utilized as cationic photo initiators. It can coexist with polymer monomers in the absence of light irradiation and have good latency. The photoinduced cationic polymerization is suitable for a variety of active monomers and prepolymers, such as acetals, cycloethers, epoxides,  $\beta$ -lactones, sulfides, silicone, and unsaturated monomers and prepolymers.

Compared with photoinduced free radical polymerization, photoinduced cationic polymerization can offer advantages such as resistance to oxygen inhibition, fast and complete curing even  $n$  ambient air.<sup>[162]</sup> In the ring-opening polymerization of epoxides, the volume shrinkage of cationic polymerization is significantly lower than that observed in acrylate-based systems.<sup>[163]</sup> In addition, the active center of photoinitiated cationic polymerization exhibits a prolonged lifespan, enabling the effect of delayed curing, shortening the lighting time and improving production efficiency in practical production. The rate of photoinduced polymerization depends not only on the properties and concentration of photo initiators, illumination intensity and duration, polymerization temperature, but also on the structural of monomers in the system. Alicyclic epoxides typically have low



viscosity before curing and strong adhesion after curing, high polymerization activity and favorable mechanical properties.<sup>[164]</sup>

Schenning et al. designed an interpenetrating network (IPN) of hybrid LC with triple-SME. The actuator was fabricated by photopolymerization of a hybrid acrylate-oxetane mixture containing both the free-radical photo initiator, 2,4,6-trimethylbenzoyldiphenyl phosphine oxide (Irgacure 819), and the cationic photo initiator, triarylsulfonium hexafluorophosphate salts. The LC-IPN with dual independent networks exhibited two distinct  $T_g$  ranges, contributing to the one-way triple-SME.<sup>[165]</sup> Huang et al. introduced the epoxy-acrylate hybrid photopolymerization to the light-assisted 3D printing. The resulting photo-cured hybrid polymers composed of both epoxide and acrylate monomers had the advantages of low volume shrinkage and high curing rate. The printed products with hybrid polymers had high tensile strength and good toughness. The exceptional mechanical properties were attributed to the combination of epoxide and acrylate materials and the formation of IPN structure with two types of networks. The shape fixation and recovery ratios are  $\approx 99\%$  and  $100\%$  in 10 cycles of folding tests, which proved the good shape-memory performance and good cycling stability. The hybrid shape-memory polymer had great potential for applications in different areas.<sup>[166]</sup>

**Azide-Alkyne Cycloaddition:** The azide-alkyne cycloaddition reaction is catalyzed with monovalent copper ions as shown in Figure 7IV, which is often referred as copper-catalyzed azide-alkyne cycloaddition (CuAAC). This reaction has characteristics of simple and rapid reaction, high yield, and orthogonal biology. At present, the principle of CuAAC based on stimulus response is to reduce the bivalent copper ions to the univalent copper ions or to directly add the univalent copper ions, which has been widely used to prepare high-performance and multifunctional polymers based on thermal triggering. For example, Ramdas et al. blended aromatic trifunctional azide compounds with multifunctional propargyl monomers and then added cuprous iodide to the reaction, which was carried out under heating conditions, to obtain an elastomeric SMP with rapid shape-memory recovery ability, as shown in Figure 8IV.<sup>[167]</sup>

To make CuAAC response to photo-stimulation, it is necessary to find some photochemical reactions that can reduce divalent copper ions to monovalent copper ions. Bowman et al. added benzoin dimethyl ether (DMPA) photo initiator to the CuAAC system to generate electron-rich active sites for the reduction of divalent copper ions under  $5 \text{ mW cm}^{-2}$  intensity at 380 nm (Black-Ray Model B 100 AP), thereby realizing photoinitiated CuAAC. The generated SMP network was uniform and had a narrow  $T_g$  range, as well as excellent shape-memory and recovery ability.<sup>[168]</sup>

In addition to building networks for SMPs, CuAAC reaction can also be used for surface functionalization of SMPs without compromising its desired thermal-mechanical properties. Song and Xu introduced the fluorescently labeled peptide to the surface of POSS-PLA SMP by Azide-Alkyne cycloaddition reaction to mediate biomaterial-cell interactions. Shape-memory polyacrylates with azido end groups were synthesized with the urethane chemistry of 3-azido-1-propanol. The end group of fluorescently labeled peptide was functionalized with alkyne. The versatile SMPs with biodegradability and biofunctionability has tremendous promise for tissue engineering applications, such as tissue scaffolds and implants.<sup>[169]</sup>

**Photooxidative Coupling:** The photooxidative coupling method is a biologically safe photo-crosslinking method suitable for aqueous environments, and it plays an important role in protein coupling and biohydrogel synthesis. The mechanism as shown in Figure 7V is to generate oxygen free radicals in the side chain of the polymer, and then couple two free radicals to crosslink the polymer. Jeon et al. purified recombinant hybrid mussel adhesion protein (MAP) that is rich in tyrosine side groups. The protein is blended with ruthenium bipyridine complex  $\text{Ru(II)bpy}_3^{2+}$  and sodium persulfate solution. The oxidation reaction occurred under the blue light of 460 nm, and the active hydrogen of tyrosine side group was deprived to generate free radicals. Two activated tyrosine groups were coupled to form covalent bonds among chains to realize photo-crosslinking of proteins. They used this photo-crosslinking material system for biological tissue adhesives, which has the advantages of easy operation, good biocompatibility and stability in wet environment.<sup>[170]</sup>

### 3.1.2. Reversible Photo-Crosslinking Reaction

Reversible photo-crosslinking is a kind of reaction that does not rely on photo initiators and uses ultraviolet rays of different wavelengths to couple or cleavage photo-responsive groups. Currently known reversible photo-crosslinking reactions can all be attributed to reversible photocycloaddition. The reversible photo-crosslinking groups used in SMPs are all introduced into the two ends or side groups of the linear prepolymer, and photoactive multifunctional molecules can be introduced for photo-crosslinking reactions with modified groups. Reversible photo-crosslinking can be used for building SMPs network points and introducing molecular switches. The reversible photo-crosslinking as network points is mainly used in thermos-induced SMEs. The reversible opening and closing of network points enables SMPs to switch between thermosetting and thermoplastic networks. The shape reconfiguration of the initial permanent shape of SMPs can be achieved on demand, offering advantageous prospects for the sustainable utilization of SMPs. The development of SMPs using sustainable substances gives the concern regarding the recycling and global environmental issue. Reversible photo-crosslinking as molecular switches is mainly used in photochemical SME, but the photo-crosslinking reaction as a molecular switch is affected by wavelength, light intensity, penetration depth and position of photoactive groups. The energy efficiency is extremely low, and the photo-crosslinking density is also less, resulting in poor secondary shape fixation and slower shape recovery. The core of the reversible photo-crosslinking reaction is to develop photo-responsive structures that are friendly to light wavelengths and have molecular structures with high reaction efficiency. At present, four kinds of reversible photo-crosslinking groups are mainly used, including coumarin, cinnamic acid, stilbene, and anthracene, as shown in Figure 9I.<sup>[137]</sup> The photo-crosslinking reactions of coumarin, cinnamic acid, and stilbene belong to [2+2] cycloaddition, and the photo-crosslinking reaction of anthracene belongs to [4+4] cycloaddition.

**Coumarin:** Coumarin is widely used in photoactive polymers due to its [2+2] photocycloaddition properties close to the visible



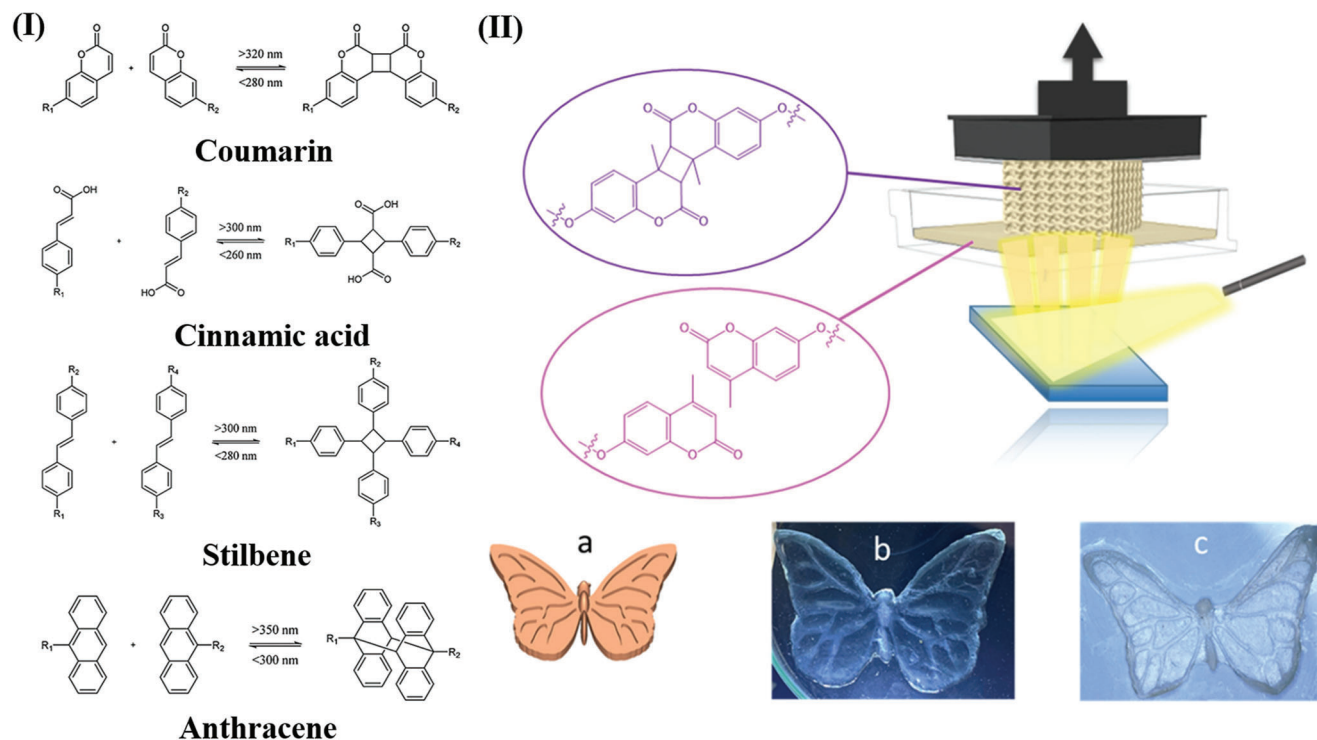


**Figure 9.** I) Structures of four reversible photo-crosslinking groups and their reversible cycloaddition process. Reproduced with permission.<sup>[137]</sup> Copyright 2019, Royal Society of Chemistry. II) 4D printing based on photo-crosslinking with coumarin groups realized thermal motion of butterfly wings. Reproduced with permission.<sup>[172]</sup> Copyright 2022, Elsevier.

light absorption band, which can perform dimerization reactions in sunlight, and the photocycloaddition at the 320–365 nm absorption band works best. When irradiated with UV light with the wavelength of  $< 280$  nm, the cyclobutene structure of the coumarin dimer in the network is cleaved and decomposed into two olefin monomers. Due to its high reversibility, biocompatibility and band safety, coumarin has great potential in the fields of biomedicine, artificial organs and decoration coatings.

Zhao et al. coupled hydroxyl groups of PVA with 7-carboxymethoxycoumarin esters to synthesize modified functional PVA materials with coumarin side groups. The material can be irradiated with 360 nm ultraviolet light for different times to obtain different degrees of crosslinking. After shape fixation ensured by sufficient crosslinking, it can be used as the initial shape of the SMPs, showing a good thermally induced SME.<sup>[171]</sup> However, Benkhaled et al. copolymerized coumarin methacrylate and 2-ethylhexyl methacrylate to synthesize thermally induced shape-memory copolymers P(EHMA-co-CouMMA) with coumarin side groups. The photo-crosslinking effect and shape-memory recovery ability of polymers were controlled by adjusting the content of photoactive monomers. After photo-crosslinking, the  $T_g$  and Young's modulus of the polymer film were increased, and the mechanical property was enhanced, but the shape recovery ratio was reduced. They realized the preparation of butterfly wings through photo-crosslinking printing technology, which can change in motion during the heating process, and successfully applied the coumarin group to the field of 4D printing, as shown in Figure 9II.<sup>[172]</sup>

**Cinnamic Acid:** The earliest light-induced SMPs in history were realized by reversible photo-crosslinking of cinnamyl groups. Lendlein et al. introduced cinnamyl groups into chemically crosslinked amorphous elastomeric materials with a  $T_g$  of  $< -20^\circ\text{C}$ . The good elasticity of the matrix at room temperature can ensure shape fixation due to photo-crosslinking without the influence of glassy solidification. The temporary shape was fixed by photo-crosslinking by ultraviolet irradiation of  $\lambda > 260$  nm, and the dimer was dissociated by ultraviolet light of  $\lambda < 260$  nm, as to realize the light-induced SME without thermal effect. The reversibility of the cinnamate dimerization was  $\approx 40\%$ , which can activate the shape recovery from the fixed state, but it cannot completely restore its original shape.<sup>[42]</sup> Affected by the thickness and photo reversible efficiency, only part of the photo-crosslinking can dissociate the dimer. Films with high light transmittance and small temporary shape change rate has better light-induced SME effect and good repeatability. In the normal environment, the cinnamyl dimer was very stable and can be used as the network point of the system. Therefore, the photo-crosslinking of the cinnamyl group was also a convenient method for preparing triple-SMPs.<sup>[173,174]</sup>

Compared with other dimers, photo-dimer of cinnamic acid had a large volume, which can reduce the free volume of space before and after illumination, so as to adjust the gap of the network to control the permeability and anti-erosion ability of the film. For example, it can be applied to crosslink non-permeable PMMA membranes.<sup>[175]</sup> In addition, the aromatic group adjacent to the double bond in cinnamyl group utilized  $\pi$ - $\pi$  conjugation

to facilitate the alignment of reactive groups, thereby enhancing the efficiency of dimer formation.<sup>[176]</sup>

Furthermore, coumarin-terminated SMPs exhibit excellent mechanical properties, enabling a good shape recovery capabilities. The reversible crosslinking and decrosslinking processes also allow for repeated shape-memory cycles. For instance, Jérôme et al. designed a star-shaped PCL with a functionalized chain end of 7-hydroxypropoxy-4-methylcoumarin. The permanent shape can be reconfigured by photocleavage and photodimerization process of coumarin groups. The crosslinking density of network can be remotely controlled to realize the fine-tuning of SMEs. The shape recovery process was triggered by heating > 60°C. The shape fixation and recovery ratios were both desirable. They also verified that the photodimerization process of functionalized 4-arm PCL can be accelerated by addition of benzophenone, which helped reconfigure the permanent shape in a short time.<sup>[24]</sup> Yi et al. fabricated a coumarin-terminated shape-memory polyurethane based on PCL as thermoplastic segments. The polyurethane had good mechanical properties with 746% elongation and 55.5 MJ·m<sup>-3</sup> toughness. The photo reversible reaction of coumarin groups gave the network good self-healing performance and permanent shape reconfiguration. The PU can also be recycled and processed for multiple times due to its remold ability and plasticity.<sup>[177]</sup> The configuration of permanent shape made SMPs transformed into sustainable materials. The reversible curing methods help reduce the dosage of fossil resources and promote the recycling use of environmentally friendly materials.

**Stilbene:** Stilbene is a [2+2] photocycloaddition group that has many similar properties to the cinnamyl group. Usually, the absorption wavelength of the photodimerization reaction is > 300 nm, while the absorption wavelength of the photodissociation is < 280 nm. The ultraviolet absorption wavelengths of group dimerization and dissociation can be adjusted by different modifications of the benzene rings at both ends of stilbene. In addition, the vinyl groups modified by different conjugated rings can also undergo corresponding photodimerization reactions. Kashida et al. introduced stilbene derivatives on DNA base pairing scaffolds, and adjusted the absorption wavelength of stilbene dimerization by changing the group species on the distal benzene ring. At the same time, the design of the base pairing position also helped to enhance photo-crosslinking efficiency of stilbene derivatives side groups, as shown in **Figure 10Ia**.<sup>[178]</sup> Truong et al. replaced the benzene ring at one end of stilbene with pyrene. First, they synthesized (E)-4-(2-(pyren-1-yl)vinyl)benzoic acid, and connected it to the amine end of the polymer chain through carbodiimide catalyzed coupling, and achieved long polymer chains double ended with styrylpyrenes. Since the pyrene structure extended the  $\pi$ -conjugated structure, the energy required for the  $\pi$ - $\pi^*$  transition was reduced, thereby extending the photodimerization absorption band to the visible light band. The photo-crosslinking reaction can occur under the irradiation of 400–500 nm. As shown in **Figure 10Ib**.<sup>[179]</sup> In addition, non-aromatic conjugated vinyl compounds also have similar photodimerization reactions. Gabilondo et al. used furan rings instead of benzene rings to form a new photoreactive system. 5-methylfurfural reacted under alkaline conditions to form 5-[2-(5-Methyl furylene vinylene)] furancarboxyaldehyde (MFVF). MFVFs were grafted to the side groups of gelatins by Schiff base

reaction, and then the Schiff bases were reduced to stable C–N covalent bonds, thus forming a photoreactive crosslinked modified gelatin product at last, as shown in **Figure 10Ic**.<sup>[180]</sup> This new photoreaction system absorbs ultraviolet light  $\approx$  365 nm to carry out photodimerization reactions.

**Anthracene:** The photocycloaddition of anthracene is a [4+4] cycloaddition process. The photodimer of anthracene does not produce cyclobutane, so the volume change before and after the reaction is small, and the dimer is more stable. At the same time, due to the strong  $\pi$ - $\pi$  interaction of anthracene structure, the arrangement of the anthracene groups will be promoted, which is also conducive to improving the photodimerization efficiency, thereby precisely controlling the crosslinking density of the system. In addition to photodissociation, anthracene dimers can also undergo thermal dissociation, usually at temperatures > 150°C. Compared with other structures, the anthracene structure has more efficient photo reversibility. Combined with its natural stacking properties, it has excellent and fast light-controlled reversible crosslinking abilities, and has been widely used in smart materials. At first, Yang et al. introduced anthracene side groups into PLA-poly(tetramethylene oxide) glycol (PTMEG) copolymers in order to realize a triple-SME strategy with dual non-overlapping stimulus responses. The anthracene groups undergo photodimerization at 365 nm and the dimers were photo-dissociated at 254 nm. At the existence of grafted anthracene side groups, PTMEG and PLA still had stable thermal phase transition properties. Therefore, the system can realize SME through photo reversible crosslinking, when the phase crystals were used as permanent network points, and the system can also realize SME through reversible thermal phase transition when the photo reversible crosslinking was used as permanent network points. If these two crosslinking methods were combined during one crosslinking process, the system can achieve a triple SME, as shown in **Figure 10II**.<sup>[181]</sup>

Wang et al. introduced anthracene groups into epoxy elastomers that exhibit multi-responsive shape-memory effects with light and heat. The photodimerization of anthracene groups leads to an increase in the modulus and  $T_g$  of the material, and the dimerized anthracene groups will gradually form an aggregate structure in the network, with obvious layer arrangement and distribution. The dimer can be covalently fractured by heating to restore its original shape.<sup>[182]</sup> Compared with other photodimerization systems, the large conjugated ring of anthracene molecules has good mechanical properties, and the unreacted anthracene molecules have the tendency to arrange naturally. Liu et al. took advantage of this property to introduce anthracene side groups into polyether ether ketone. Through the photodimerization reaction, the crosslinked PEEK material had better mechanical properties and a more stable shape-memory ability, and its shape recovery ability was also stronger than that of the unmodified material.<sup>[183]</sup> Another example is a UV reconfigurable shape-memory polyurethane with anthracene groups reported by Tian et al. They incorporated a kind of diol chain extender containing anthracene group as side groups into the hard segment. The permanent shape can be fixed via the photodimerization of anthracene groups under UV irradiation. When the temperature was > 150°C, the network of permanent shape can be de-crosslinked. The SME of PU was realized by melting transition of PCL soft segments at 50°C. The shape fixation ratio and

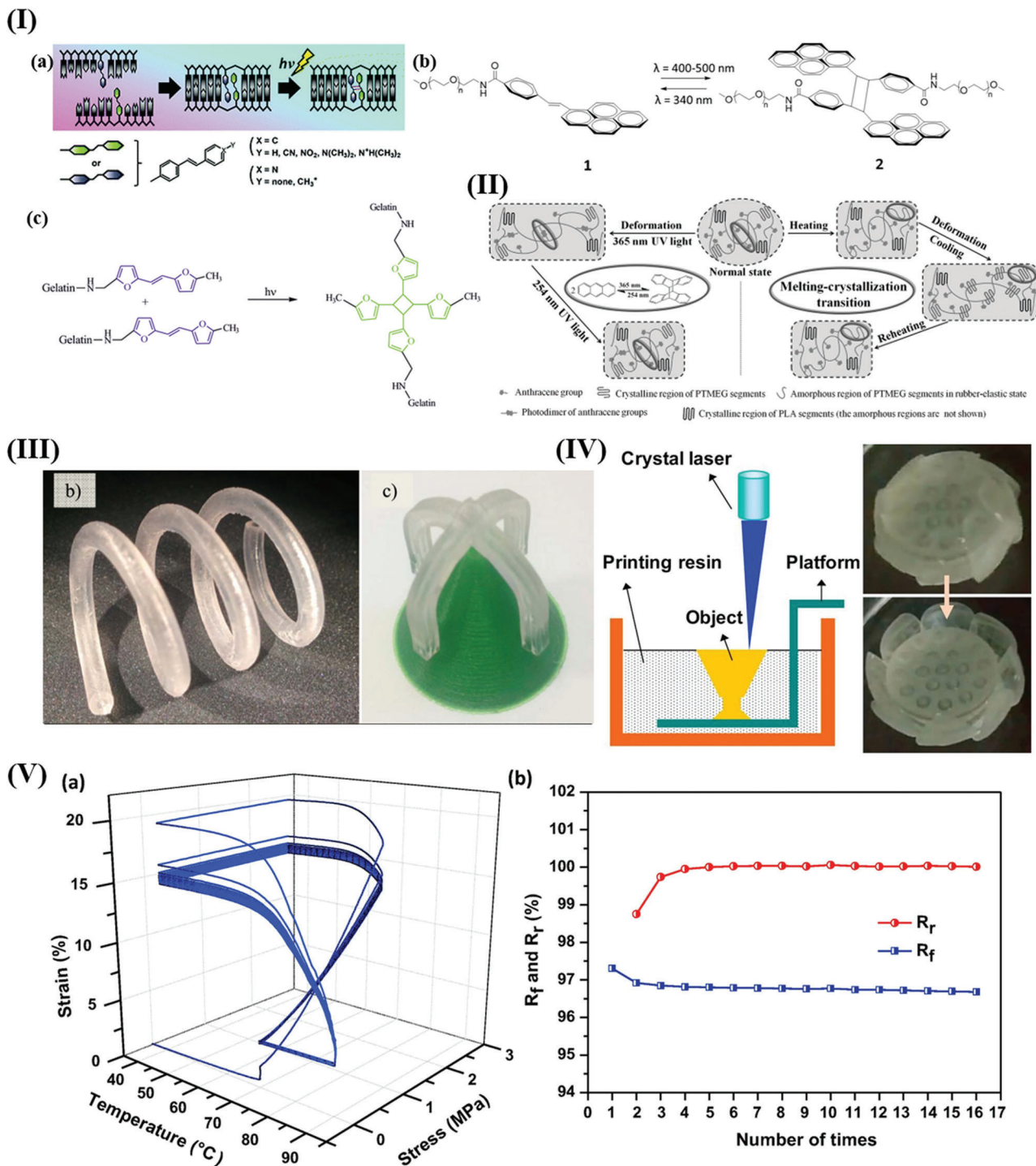


**Figure 10.** I) a) The DNA base-pairing scaffold modified by stilbene derivatives undergo photodimerization reaction under ultraviolet light, and the absorption wavelength of photodimerization reaction can be changed by adjusting different types of modification groups of stilbene derivatives. Reproduced with permission.<sup>[178]</sup> Copyright 2015, Royal Society Of Chemistry. b) The end groups of chains modified with styrylpyrenes extended the photodimerization absorption band to the visible light region. Reproduced with permission.<sup>[179]</sup> Copyright 2018, American Chemical Society. c) Non-aromatic conjugated groups can also carry out photodimerization reaction, such as furan. Reproduced with permission.<sup>[180]</sup> Copyright 2015, Elsevier. II) Introducing anthracene side groups into PLA-PTMEG copolymers to realize dual-stimuli-responsive triplet SME under the mechanism of reversible photodimerization and thermal phase transition. Reproduced with permission.<sup>[181]</sup> Copyright 2017, Wiley-VCH. III) The shape-memory actuators with internal microvascular were printed by SLA and can be activated by heat flow. Reproduced under the terms of CC BY 3.0 license.<sup>[187]</sup> Copyright 2016, the Author(s). Published by IOP Publishing Ltd. IV) Lotus-shaped SMP printed with PU macromonomers. Reproduced with permission.<sup>[188]</sup> Copyright 2018, Elsevier. V) The shape-memory and recovery process of photocured polymer printed with PU macromonomers. Reproduced with permission.<sup>[188]</sup> Copyright 2018, Elsevier.



recovery ratio were both high even under the strain reaching 270%.<sup>[184]</sup> Therefore, the selection of an appropriate photodimerization system, including consideration of the compatibility between the photoactive groups and matrix materials, as well as the interactions between these groups, is crucial in achieving desirable SME and ensuring favorable mechanical properties in the resulting products.

### 3.2. Advanced Light-Assisted Additive Manufacturing Technology

Additive manufacturing (AM) is a technology that uses materials to gradually accumulate to manufacture solid parts or products. Different from traditional removal-cutting material processing technology, additive manufacturing is a method based on the principle of bottom-up construction technology. In a narrow sense, additive manufacturing is the most widely used forming process at present. It refers to the technology of layering and accumulating materials based on the principle of discrete-accumulation, combining the 3D data of the product with CAD/CAM technology and using different energy sources (manufacturing methods).

In the past two decades, AM technology has achieved rapid development. Based on different classification principles, it can also be called rapid prototyping, rapid prototyping, rapid manufacturing, and 3D printing. This section mainly introduces the 4D printing principles and applications of SMPs additive manufacturing based on various 3D printing technologies. At the same time, this section explains the characteristics of products manufactured by different printing technologies. The referred 3D printing technologies in this section are all related to photopolymerization. This section introduces five printing technologies based on the principles of 3D photopolymerization, including stereolithography (SLA), digital light processing (DLP), polymer jet printing (Polyjet), direct ink writing (DIW), and two-photon lithography (TPL). Continuous liquid interface production (CLIP) technology and projection micro-stereolithography (PμSL) belong to the upgraded version of DLP technology, and are also classified as DLP in this section. The following are the above five optical-forming technologies and their applications in the 4D printing of SMPs.

#### 3.2.1. Stereolithography

Chuck Hull was the first to realize 3D printing products using SLA in 1984.<sup>[185]</sup> SLA uses an ultraviolet laser beam as a light source. By deflecting the outlet laser beam, a high-intensity single-point laser beam is generated. The laser beam finally acts on the surface of photosensitive resins to trigger photocrosslinking reaction of the resin, which contributes to selective photocuring. When a layer of pattern is cured, the platform is lowered to allow resin solution to respread on upper layer. Photocuring occurs again, and the operation is repeated until the 3D model is completely printed. SLA technology has high resolution and precise control, but the printing time is long. Due to the use of a continuous laser, the products printed by SLA technology have great smoothness.

Sharifi et al. used poly(D,L-lactide-co-trimethylene carbonate) dimethacrylate macromers to fabricate porous materials with

good biocompatibility by SLA technology.<sup>[186]</sup> The material has a very excellent SME and can keep the secondary shape stable at low temperature. When the temperature is close to 40 °C, the deformed SMP can return to the original shape. The computer-aided design of the porous structure can make the material both light and structurally strong. SLA is used in many biomedical fields. On one hand, it can realize the designed structure according to the program instructions through a non-contact photocuring process. On the other hand, it has the printing characteristics of a smooth transition, which is difficult for other photocuring printing methods.

The applications of biological materials, especially cardiovascular materials, have high requirements for the surface smoothness of the final products, otherwise it is easy to cause blood coagulation or hemolysis. Lantada et al. used SLA technology to easily print complex geometric shapes and used it for the development of shape-memory materials containing microvascular system inside. Through computer-aided design of geometrically complex vascular system, the final developed SMP can be activated by thermal fluid, as shown in Figure 10III.<sup>[187]</sup> In order to facilitate the preparation of shape-memory materials to be used in 4D printing, people have shifted their focus to the preparation of shape-memory PU macromonomers. PUs with shape-memory functions can be rapidly molded by photocuring. Yu et al. used the reaction of TDI, polytetramethylene ether glycol (PTMG), and ethylene oxide modified bisphenol A to obtain the prepolymer that was blocked with hydroxyethyl acrylate to obtain PU macromonomers. The photocurable resin was blended with macromonomers, small molecule monomers IBOA, DGEDA, and photo initiator PI184. The blended photocurable resin was copolymerized under SLA laser irradiation, and can be printed into lotus-shaped SMPs, as shown in Figure 10IV.<sup>[188]</sup> The photocured polymer has high UV curing activity and excellent shape-memory properties, including remarkable shape recovery ratio, high shape recovery ratio, good shape fixation ratio and excellent durability, as shown in Figure 10V.<sup>[188]</sup>

#### 3.2.2. DLP

DLP uses a UV surface light source to locally photo-cure the surface of resin, so its printing speed can be hundred times faster than that of SLA. People can directly choose the projection with ultraviolet rays for copolymerization, and the equipment itself produces regionalized ultraviolet patterns for printing. This printing method has low requirements for equipment and is easy to operate, but it has obvious light pixels. Therefore, the surface of the products is rough. The printing mode of DLP is usually to irradiate ultraviolet light from the bottom of resin solution. The platform moves up for a short distance after printing of each layer, and then adjusts to a suitable height to print the next layer. In addition to UV projection curing, the current mainstream uses dynamic mask technology to control the curing pattern. The first dynamic mask method is LC display (LCD), which adds a layer of LCD board between the light source and resin, and generates different patterns through computer control. However, the pixel size of LCD is large, and the switching speed of the refraction element is low. The transmitted light density is low as well. These problems hinder the contrast of the



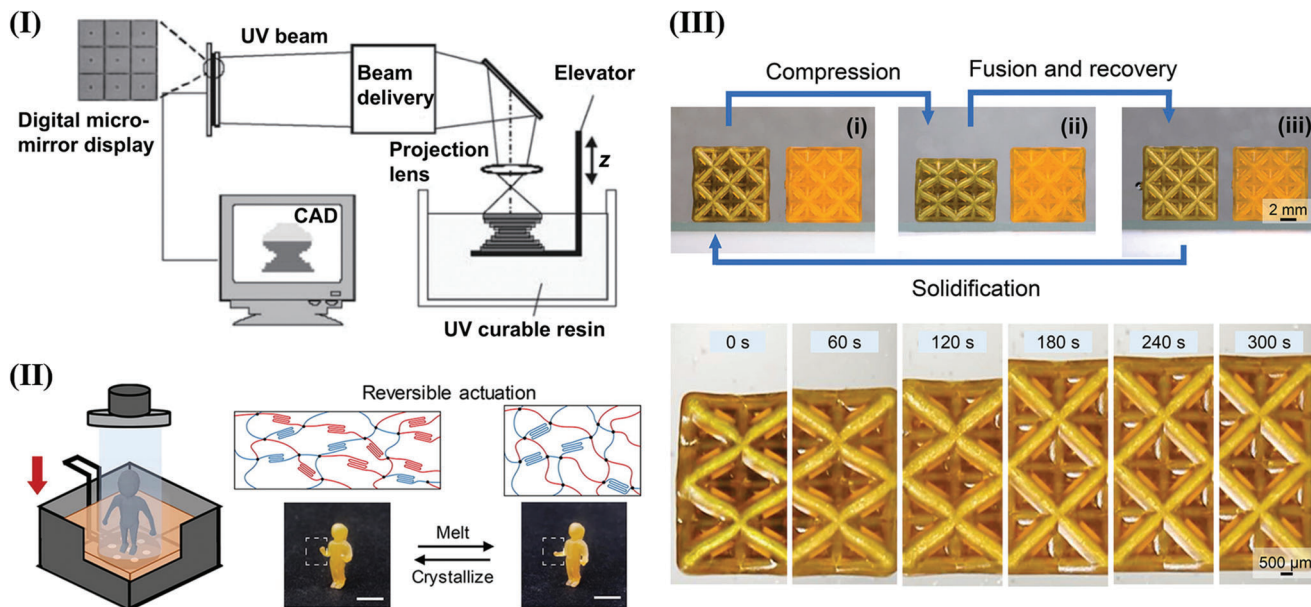


**Figure 11.** I) The working principle of DMD. Reproduced under the terms of CC BY 3.0 license.<sup>[190]</sup> Copyright 2020, the Author(s). Published by IOP Publishing Ltd. II) The realization of bending actions through local crosslinking gradient and crystallization of PCL. Reproduced with permission.<sup>[191]</sup> Copyright 2021, Elsevier. III) The SME of superstructure material made with elastomer and liquid metal Ga. Reproduced with permission.<sup>[192]</sup> Copyright 2020, Wiley-VCH.

transmitted pattern and affect printing accuracy. Another method is the digital micromirror device (DMD), which was first designed and developed by Sun et al.<sup>[189]</sup> DMD was assembled using a group of controlled micron-sized mirrors that can control the path of UV light by rotating at different angles, and correct the path of ultraviolet light toward the photosensitive resin. The working principle is shown in **Figure 11I**.<sup>[190]</sup> Ordinary micromirror devices have a large number of mirrors, up to more than two million. The mirror projection can be adjusted according to the mask pattern, and then the light can be adjusted to transmit through narrowing lens. The printing resolution can be controlled to a few microns. This ultra-high precision DLP technology is also known as projection microstereolithography (PμSL). Another upgraded version of DLP printing technology is called continuous liquid interface manufacturing (CLIP) that was developed from an improved 3D printing technology produced in 2014. In the CLIP process, an oxygen-permeable and light-permeable polytetrafluoroethylene film is used as the bottom of the resin tank to form an oxygen interface layer at the window. Oxygen entering the interface inhibits free radical photopolymerization and prevents resin curing. A dead zone with a thickness of tens microns is formed on the interface, and the cured resin does not adhere to the release film. The interspace of the bottom area can allow the uncured resin smoothly to replenish the printing area for fast printing, and the printing speed reaches 100 times higher than that of DLP. It also contributes to the continuous printing process where the light source can use continuous UV projection to make the printing transition smooth and the product surface slippery.

Xie et al. used DLP to photo-cure polyester prepolymers containing double crystal components of polycaprolactone and

polypentadecanolactone, and obtained different degrees of crosslinking by controlling the exposure time of different regions for obtaining 4D printing products that can undergo reversible deformation at low temperature. Among them, the polypentadecanolactone component has the characteristics of low temperature stability and high temperature melting, which can be used to fix the semi-permanent shape, while polycaprolactone can undergo the reversible phase transition at low temperature and can be used to make reversible changes in shape. The design of crosslinking degree can control crystallization degree of different regions to realize complex actions such as bending,<sup>[191]</sup> as shown in **Figure 11II**. Khalid et al. used PμSL technology to print hollow polyacrylate superstructures, and then infused them with liquid metal Ga. Solidified gallium can improve the fracture toughness and structural strength of superstructure materials. When the material was immersed in hot water at 90°C, metal Ga melted and the elastic stress of the shell material was released. The superstructure material returned to its original shape, as shown in **Figure 11III**.<sup>[192]</sup>

In the field of shape-memory hydrogels, Zhang et al. used CLIP technology to print sodium alginate shape-memory gels with blended acrylamide, methylenebisacrylamide and sodium alginate. An interpenetrating hydrogel network was formed by photo-crosslinking. Calcium chloride solution was added during the secondary deformation. The temporary shape can be fixed by the ionic crosslinking of sodium alginate and calcium ions. The addition of EDTA solution can remove calcium ions, and then the hydrogel lost the ionic crosslinking and returned to the original shape, which achieved the SME as shown in **Figure 12I**. In order to make the hydrogel printing with a high resolution, crystal violet and methylene blue were added to the solution to limit the scattering of ultraviolet rays.<sup>[193]</sup>

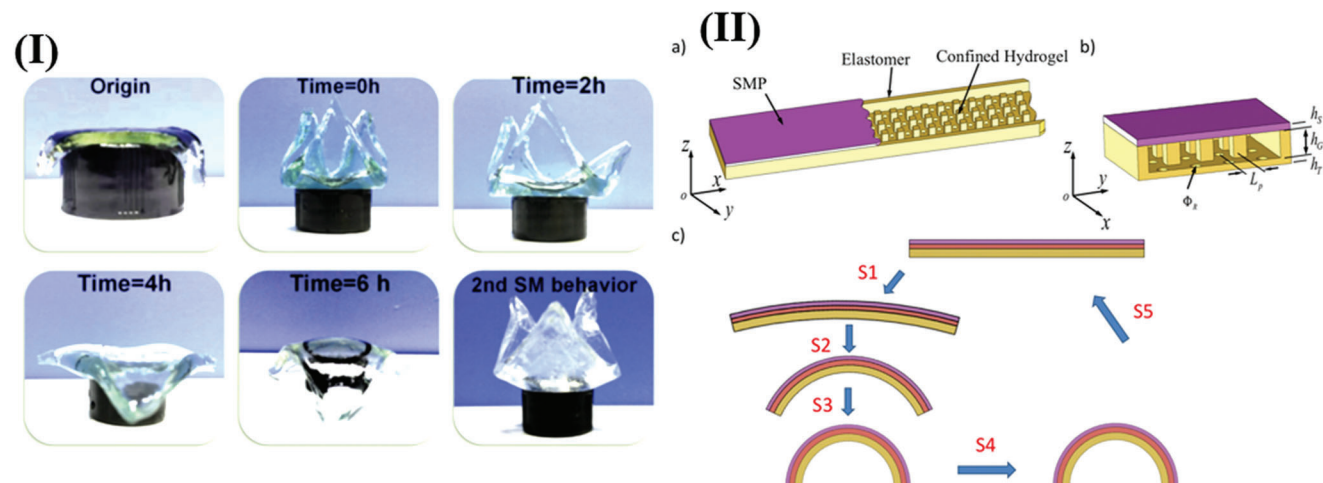


**Figure 12.** I) The SME of crosslinked hydrogel with  $\text{Ca}^{2+}$  in EDTA solution. Reproduced with permission.<sup>[193]</sup> Copyright 2020, Elsevier. II) a) The reversible actuator made by 3D printing where the hydrogel layer is in the middle of the SMP and the elastomer layers. b) Structural parameters for efficient actuation. c) Schematic plots of the reversible actuation. Reproduced under the terms of CC BY license.<sup>[194]</sup> Copyright 2016, the Author(s). Published by Springer Nature.

### 3.2.3. Polyjet

Polyjet is a unique inkjet 3D printing technology of StrataSys company. The working principle of this technology is to spray ultra-thin liquid photosensitive resin materials onto the tray layer by layer. Curing takes place and produces a fully solidified model. The advantage of Polyjet lies in its high printing accuracy and good smoothness. It can be used for multi-nozzle and multi-material photocuring printing. The disadvantage is that the printing speed is very slow and it needs a support structure. Mao et al. prepared shape-memory splines built from a variety of materials with different moduli. Figure 12IIa shows that the splines have triple-layer structure.<sup>[194]</sup> The layer of SMP is on the top, the layer of elastomer is at the bottom and the layer of hydrogel and elastomer columns is in the middle of the structure. Multi-response SMP splines were fabricated by utilizing the water-absorbing swelling force of the hydrogel and the shape-memory property of the SMP layer. The swelling tension of the hydrogel was used to shape the quadratic shape, and the SMP layer can fix the shape after swelling at low temperatures. When the moisture was dried and the temperature reached the  $T_g$ , the original permanent shape can be restored and the mechanism is shown in Figure 12IIc.<sup>[194]</sup>

### 3.2.4. DIW

Direct ink writing is a simple and fast method of 3D printing. The printing ink is extruded directly from a needle and the shape is set immediately, before the material is cured to determine its permanent shape. The most widely used materials have the properties of shear thinning or rapid self-curing. In addition, DIW products can also be cured under ultraviolet light, which can be cured after one layer is printed, or it can be cured during printing. Because its printing effect is relatively mild, DIW is suitable for the printing of cell-bound biomaterials.<sup>[195]</sup>

Wilt et al. prepared epoxy materials with shape-memory effects using a dual functional epoxy resin system under UV-assisted DIW printing. This epoxy resin system can be cured both with UV light and heat. The epoxy ink can be first cured through radical polymerization of photocurable acrylates under UV light, then it can be thermally cured in the next step. The dual-cured network exhibited SMEs under the stimulation of heat. When the epoxy material was heated above its  $T_g$  at  $76^\circ\text{C}$ , it can be transformed into a temporary shape. The shape was fixed when the temperature went down below  $T_g$ , and it can return to its printed shape or permanent shape when the epoxy material was reheated above its  $T_g$  for 18 s.<sup>[196]</sup> Diba et al. used DIW in the form of extrusion and curing for printing. They used gelatin NPs whose surface was modified with methacrylate to blend in light-curable inks, which were printed by extruding assisted with UV light. The permanent shape of printed products was determined through deep curing in the deformed state. The temporary shapes were fixed by gel drying and the permanent shape can be restored by wetting to achieve the shape-memory behavior between the flat shape and the curled shape as shown in Figure 13I.<sup>[197]</sup>

### 3.2.5. Two-Photon Lithography

2D structures are usually fabricated by standard photolithography technology which is based on the principle of one-photon absorption. Two-photon lithography (TPL) is a bottom-up and non-linear processing technology applied in the fabrication of sophisticated, well-defined 3D micro and nanostructures.<sup>[198]</sup> Photo initiators at the focus region of a femtosecond laser in liquid resin are triggered by a two-photon absorption process. As a result, the polymerization and cross-linking processes are able to take place at very precise region. The wavelength of laser is usually in NIR spectral region.<sup>[52]</sup> Compared with single-photon absorption used in conventional rapid prototyping, the two-photon process has two obvious advantages. On one hand, due to negligible linear absorption in NIR region of most commercially available

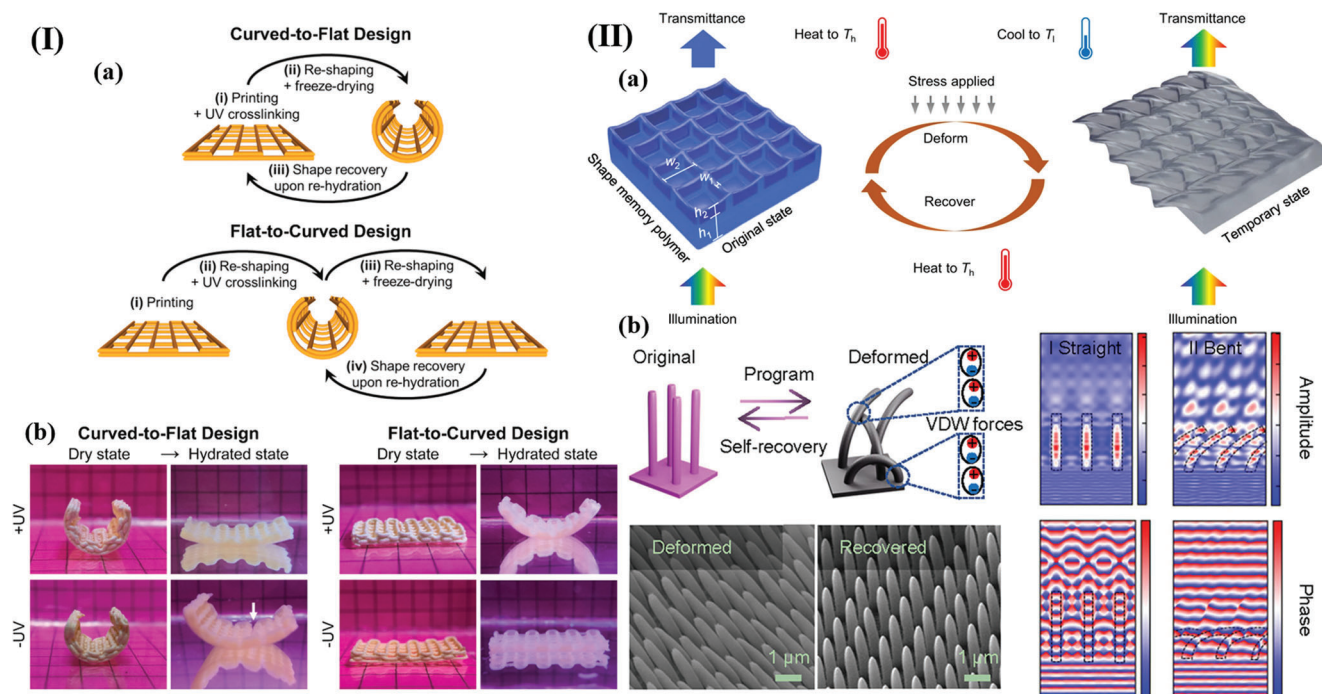


**Figure 13.** I) Shape-memory effects of printed hydrogel models: a) Schematic illustration of technological processes of models with shape-memory ability; b) Digital photographs of different model designs at dry state and their shape recovery performance in the hydrated state upon immersion in aqueous media. Reproduced with permission.<sup>[197]</sup> Copyright 2021, Elsevier. II) a) Schematic illustration of color and shape change of a 3D-printed constituent nanostructured element in SMP. Reproduced under the terms of CC BY license.<sup>[52]</sup> Copyright 2021, the Author(s). Published by Springer Nature. b) the mechanism of structural color change through SME with high-resolution reconfigurable structural color. Reproduced with permission.<sup>[199]</sup> Copyright 2022, American Chemical Society.

polymers, the polymerization can be directly induced inside the material by laser beam without triggering any unexpected photochemical process outside of the focus region. On the other hand, the polymerization rate is proportional to the quadratic of the laser intensity, contributing to high 3D spatial resolution.<sup>[52]</sup>

Two-photon lithography is widely used in the field of optical devices. Zhang et al. used TPL to prepare submicron shape-memory grids. They performed resolution tests achieving  $\approx 300$  nm half pitch gratings. The submicron-level geometry of the SMP structures can be controlled to achieve a series of structural colors. When the nanostructures recover from a flattened state to an upright state upon heated above its composition-adjustable  $T_g$ , a large-scale visual response can be observed, as shown in Figure 13IIa. This 4D printing approach can be potential applied in many precision manufacturing fields, such as optics and sensors.<sup>[52]</sup> In another work, Zhang et al. also used the high-resolution characteristics of TPL to prepare stiff SMPs for high-resolution reconfigurable nanophotonics, as shown in Figure 13IIb. They explored how to use the SMP nanopillars array to modulate the amplitude and phase of light at the single-pillar level. At the same time, the ability of nanopillars with high storage modulus to overcome the friction in the pillars and the van der Waals force with the bottom surface was also explored when the secondary deformation restored the original shape with high aspect ratio structure, thereby realizing the ability of reconfigurable optical control.<sup>[199]</sup>

In summary, the aforementioned five photocuring 3D printing technologies represent prevalent photo-forming methods

employed in producing shape-memory materials, which offering suitability for different photo-forming 3D printing scenarios. TO provide a comprehensive overview, we summarized the light source requirements, printing resolution, printing area, and printing speed of these five photocure printing technologies in Table 3.

The SLA and DLP 3D printing technologies employed resin interfacial polymerization to build models layer by layer. SLA, with the line printing mode, allows for model printing with large size but slower printing speed. The printing resolution is determined by the size of the laser beam spot. Its resolution is lower than that of DLP, but suitable for printing complex models with small dimensions. The printing material for SLA is made of photosensitive resin, which should exhibit stability in visible light, low viscosity, and small swelling degree. Cationic photopolymerization serves as the basis for the photocuring process in SLA, ensuring minimal volume shrinkage and high printing accuracy.<sup>[203]</sup> While there are limited options for resins in cationic photopolymerization, the utilization of free radical resins in hybrid photosensitive resins can enhance its printing speed and reduce the production costs.<sup>[204]</sup>

DLP uses surface projection mode to accelerate printing process but with a limited projection area.  $\mu\text{SL}$  equipped with DMD can ensure the advantage of high printing resolution. CLIP, on the other hands, utilizes oxygen interface layer to change the printing direction and feeding mode to realize continuous plane printing, which greatly enhances the printing speed and increases the surface smoothness of model, and solves the problem



**Table 3.** Conditions and characteristics of different printing technologies.<sup>[200–202]</sup>

Printing methods	Light source	Printing resolution	Printing area	Printing speed
SLA	355nm Laser beam	75–200 $\mu\text{m}$	380 mm $\times$ 380 mm to 1500 mm $\times$ 750 mm	Slow
DLP	385–405nm LED lamp	0.6–90 $\mu\text{m}$	2 mm $\times$ 1 mm to 230 mm $\times$ 143.75 mm	Very fast
Polyjet	No limit	34 and 68 $\mu\text{m}$	342 mm $\times$ 342 mm, 490 mm $\times$ 390 mm,	Slow
DIW	No limit	200 $\mu\text{m}$ to 50 mm	30 mm $\times$ 30 mm to 10 m $\times$ 10 m	Fast
TPL	680–1040 nm Laser beam	$\approx$ 100 nm	10 $\mu\text{m}$ $\times$ 10 $\mu\text{m}$ to 2.2 mm $\times$ 2.2 mm	Very slow

of step roughness of traditional DLP. DLP employs similar printing materials to SLA but rely on free radical photopolymerization as their photocuring mechanism. However, cationic photosensitive resin cannot be utilized in DLP due to the challenges in exciting cationic photoinitiators.<sup>[200]</sup> CLIP requires printing materials with a lower viscosity compared to DLP resin, which makes it easier to supplement the resin quickly. In addition, the resin needs to maintain a certain oxygen concentration at the bottom to stop the polymerization by oxygen inhibition, which realizes the bottom-to-up printing mode.<sup>[205]</sup>

The multi-nozzle array of Polyjet printing technology allows spraying and curing of multiple materials at the same time, facilitating the formation of complex models with diverse mechanical properties and regional functional distribution. It requires a continuously and controllably supplied photosensitive ink with rapid photocuring speed and low viscosity flow, which limited its material selection. The printing material used in Polyjet is mainly supplied by Stratasys. It offers more than 20 types of base materials and the incorporation of an independent light with the nozzle array enables the use of various types of photopolymerization.

DIW printing technology is primarily used for 3D printing of functional hydrogel models. The printing resolution depends on factors including the size of extrusion head, the rate of ink extrusion, the moving speed of platform and the rheological characteristics of inks. DIW accommodates a wide range of materials and equipments, and is commonly used for the printing low-precision products as well as the printing models containing other functional materials. DIW requires rheologically suitable inks with shear thinning behavior, which could easily transform to a fluid state during printing and quickly restore mechanical properties after extrusion. They must also possess good photosensitivity for in situ photocuring, forming a stable self-supporting structure. Furthermore, the ink mixed with solid materials also need to have a suitable solid content to prevent the block of nozzle and avoid the changes of rheological properties.<sup>[206]</sup>

TPL is currently the most accurate photocuring 3D printing technology, but with the limitation of its low printing speed and small model size. It achieves photocuring directly within the material using laser beams and without inducing unintended photochemical reactions in other areas. The printing resolution of TPL is very high, but the cost is expensive. At present, TPL is

mainly used for manufacturing polymeric micro-nano structures with specific photoelectric properties for scientific research purposes. The resin employed in TPL should process transparency in the visible and near-infrared wavelength ranges to enable deep laser penetration without side reactions. The resin should achieve rapid curing effect and the polymerization should be limited to the focus point by adding a certain concentration of inhibitors, which helps to terminate the polymerization process. Currently, the printing materials used in TPL are available commercial resins, such as photoresist SU8, acrylic resin, and epoxy resin.<sup>[207–209]</sup>

Overall, each of these photocuring 3D printing technologies has its unique advantages and specific material requirements, making them suitable for various applications and printing scenarios.

#### 4. Light-Induced SMPs and SMPCs

Light offers a remote, localized, and non-contact means of triggering SMPs “on-demand” without affecting surrounding conditions. There are two main mechanisms for creating photo-responsive SMPs: photomechanical and photothermal effects. In photomechanical mechanism, certain reversible bonds that are sensitive to UV light are introduced in polymers. In photothermal mechanisms, thermally-induced shape deformation is converted into a remotely triggered one using polymer composites containing SMPs and photothermal fillers. Instead of fillers that are reported to have a wide absorption peak, other fillers that can be selectively heated by light with certain wavelengths are investigated as well. More importantly, the assembly of photo-responsive polymers with high wavelength selectivity as the units into a single material system is required to achieve complicated or multiple shape deformations of photo-responsive polymers.

##### 4.1. Fillers with Wide Absorption Spectrum

Traditional SMPs mainly focus on thermal response, and most of the shape changes of SMPs are triggered by direct contact or heat exposure, which makes the application range and

scenarios of traditional SMPs limited. In addition, traditional SMPs often have drawbacks such as low mechanical strength, short service life, and environmental unfriendliness. In order to solve the above problems, researchers have tried to introduce functional fillers into shape-memory polymers through physical doping, grafting, and crosslinking, so as to improve their shape-memory and mechanical properties. At the same time, the SMP drive mode is more diversified, such as optical drive, magnetic drive, electric drive, and so on. In this section, the preparation methods of various new SMPs are described in detail as well as their advantages and disadvantages are compared.

#### 4.1.1. Graphene

**Graft:** Bai et al. prepared a photothermal shape-memory material with good self-healing properties by preparing a thermosetting PU with 0.1 wt% graphene oxide (GO) content. The shape recovery ratio of the composite was higher than 95% under 1.4 W·cm<sup>-2</sup> irradiation. PCL was grafted onto GO nanosheets by ring opening polymerization. The graft polymer (GO-PCL) was synthesized by ring-opening polymerization of  $\epsilon$ -caprolactone using hydroxyl group on GO as initiating agent. Then GO-PCL was crosslinked with methylene diphenyl diisocyanate (MDI) to structure the polymer network.<sup>[210]</sup> Du et al. found that doping 2 wt% of multifunctional GO (mfGO) into disilene-containing PU (dPTD) can improve the shape-memory, self-healing, flame retardant properties of the matrix. Due to the crystallization induction effect, photothermal effect and dynamic exchange characteristics of diene bond of mfGO, the shape-memory performance and recovery ratio of mfGO after three visible–near–IR light cycles reach > 90% and 76%, respectively. Under alkaline conditions, the amino group of polyethylenimine (PEI) reacted with the epoxy group of GO, and the phosphor-hydrogen bond of 9,10-dihydro-9-oxa-10-phosphaphenanthrene 10-oxide (DOPO) reacted with the amino group of PEI-GO graft under the action of catalyst. The terminal isocyanate group of isocyanatopropyltriethoxysilane (IPTS) reacted with the remaining hydroxyl and carboxyl groups of DOPO-PEI-GO, and the Si(OEt)<sub>3</sub> group of the IPTS unit was further converted into Si–O–Si chains through hydrolysis and condensation processes.<sup>[211]</sup>

**Copolymerization:** Du et al. found that functionalized GO (FGO) can be used as a multifunctional enhancer to improve mechanical and photothermal properties of PU composites after the isocyanate terminated molecules are covalently attached to the FGO surface. The preparation process of FGO attached to the isocyanate terminated molecules was prepared, and then the FGO was compounded with the polymer matrix. The mixture was poured into molds for curing and drying.<sup>[212]</sup>

**Crosslinking:** The addition of epoxide (EP) groups on the GO surface can enhance the mechanical properties of the composite and form a denser crosslinking network. The shape recovery time of the composite containing 1 wt% crosslinked EP bisphenol A diglycidil ether functionalized rGO (DGEBA-f-rGO) was 6.5 s under 808 nm NIR laser irradiation. The rapid actuation of the material stems from the  $\pi$  conjugate enhancement in the rGO in the crosslinked DGEBA-f-rGO and the covalent interactions, leading to an uniform dispersion of the graphene network in the polymer matrix. Hyperbranched PU (HBPU) was synthesized by a two-

step method, and then GO was pretreated to increase the amount of –COOH on the GO surface to obtain DGEBA-f-rGO.<sup>[213]</sup>

**Physical Doping:** Using graphene oxide as filler, infrared induced SMPCs were prepared by the crosslinking reaction between polyvinyl butyral (PVB) and 4,4'-methylene diene, named PMGD.<sup>[214,215]</sup> The main preparation processes of PMGD were as follows: GO, PVB, and MDI were dispersed in dimethylformamide (DMF) in turn, and then dibutyltin disalicylate (DBTDL) was added to obtain film samples after post-processing.<sup>[214]</sup> By doping gold NPs/reduced GO (AuNP-RGO) with cross-linked PCL, the photothermal conversion efficiency and speed of SMPCs were improved simultaneously. The synthesis process of AuNP-RGO nanocomplexes was similar to the transfer method. GO was prepared by the Hummers method and gold colloids were then added to the reduced GO colloids.<sup>[215]</sup>

Shape-memory PVA/PAA-GO film prepared by Li et al. can repair physical damage with the aid of water. The fracture stress of PVA/PAA-GO film with PAA-GO content of 3 wt% is 70.4 MPa, and the Young's modulus is 2.8 GPa. Due to the stable network formed by the hydrogen bond interaction between PVA and PAA-GO, the film shows excellent shape-memory performance. Acrylic acid and ceric ammonium nitrate aqueous solution were added to the aqueous solution of GO for polymerization reaction. After the reaction, acrylic monomers and salts were removed by dialysis, and then PAA-GO nanosheets were obtained by centrifugation and drying. Finally, PVA/PAA-GO films were prepared.<sup>[216]</sup>

NIR photo-responsive shape-memory scaffolds with graded porous structure can be obtained by incorporating g-GO NPs into poly(D,L-lactic acid-co-trimethylene carbonate) (PLMC) matrix. Poly(L-lactic acid) with carboxyl end groups (PLLA-COOH) was used as a hydrophobic surface modifier to prepare g-GO NPs by hydrophobic modification on the surface of GO NPs (**Figure 14I**). Then GO/PLMC based shape-memory scaffolds can be directly obtained by freeze-drying emulsified scaffolds.<sup>[34]</sup>

Wang et al. prepared a kind of RGO/water-based epoxy resin (WEP)/RGO sandwich composite film with a good photothermal and electrical response. rGO short fibers were prepared, and the dried fibers were dispersed in deionized water and filtered through vacuum to obtain uniform flocculation GO dispersions to form rGO paper. The RGO/WEP/RGO composite film was prepared by spreading the mixed powder of WEP and curing agent evenly on the GO paper, followed by covering the top of the powder layer with another layer of GO paper (**Figure 14II**).<sup>[217]</sup> These materials were compressed into a sandwich structure film.<sup>[217]</sup>

Allyl isocyanate modified GO (iGO) can act as a multifunctional crosslinker at low content, as a nucleator at high content, and as a reinforcing filler, while the optical absorption of iGO can lead to the melting of PU soft segments with 90% shape recovery. Vinyl PU crystalline soft segment was prepared by high molecular weight PCL. After the vinyl PU and iGO were dissolved in DMF, the photo initiator was added, and the dispersive solution was cast before drying and curing.<sup>[218]</sup> When RGO is incorporated into PU, physically and chemically crosslinked structures can be formed in the composite material, and the mechanical properties, thermal stability and photothermal effects of PU are improved. Du et al. fabricated Diels–Alder crosslinked polyurethane/functionalized reduced graphene oxide composites (DAPU-FRGs) through in situ polymerization. Under

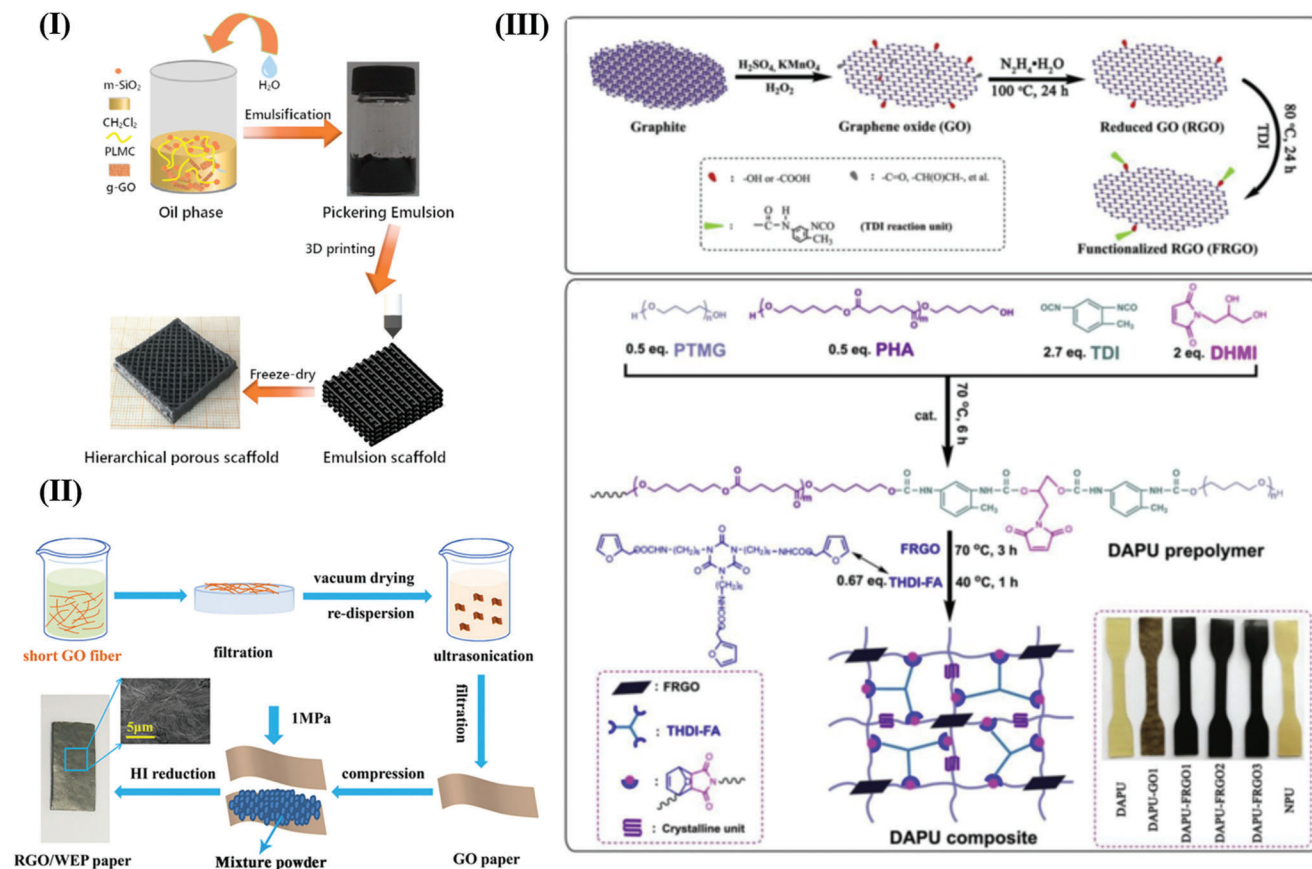


**Figure 14.** I) Schematic illustration of the fabrication of GO/PLMC based shape-memory (GSPM) scaffolds by freeze drying of 3D printed Pickering emulsion templates. Reproduced with permission.<sup>[34]</sup> Copyright 2021, Wiley Periodicals. II) Preparation procedures of RGO/WEP/rGO sandwich structure composite film. Reproduced with permission.<sup>[217]</sup> Copyright 2019, Elsevier. III) Synthetic routes of FRGO and DAPU composites. Reproduced with permission.<sup>[193]</sup> Copyright 2020, Elsevier.

NIR light, DAPU-FRGOs composites doped with 2 wt% FRGO showed rapid shape-memory and self-healing. The hydroxyl-terminated PU prepolymer containing maleimide group and FRGO were prepared, before the Diels–Alder PU composite (DAPU) was prepared as shown in Figure 14III.<sup>[193]</sup> Zhang et al. prepared PU composite films (azobenzene compound 4-cyano-4'-pentyloxyazobenzene/4-cyano-4'-pentyl biphenyl/GO/SMPU (5CAZ/5CB/GO/SMPU) that showed different optomechanical bending deformation and stretching under different light-induced mechanisms. GO was ultrasonically dispersed in DMF, and then SMPU solution and LC mixture containing 5CAZ were stirred evenly. The obtained solution was cast and dried into composite film.<sup>[219]</sup>

#### 4.1.2. Carbon Black (CB)

**Copolymerization:** The surface of the shape-memory substrate was modified by different means to make it respond to different stimuli. Wang et al. prepared a bilayer SMPU consisting of a SMPU-azobenzoic acid (Azoa) layer and a SMPU-CB layer (Figure 2a). Azoa and CB as functional fillers can respond to UV light and IR light respectively, so different stimulus light sources

can be selected to trigger the material deformation or shape recovery. When the content of Azoa and CB are 5 wt% and 0.5 wt% respectively, and the thickness ratio of SMPU-Azoa layer to SMPU-CB layer is 1/1.3, the reversible bending Angle and velocity of SMPU bilayer can reach ideal values (Figure 15I). PCL, Glycerol (GL), Isophorone diisocyanate (IPDI) and CB were pre-treated to obtain the prepolymer after chain extension reaction in a three-necked flask. Finally, the prepolymer solution was post-processed to obtain the film sample (Figure 15II).<sup>[35]</sup>

**Physical Doping:** CB has excellent photothermal conversion efficiency. PU and CB were dissolved in DMF, and the solvent was volatilized after the mixture was stirred evenly to form a photo-responsive shape-memory material. The composites were added to an extruder and the photo-responsive shape-memory filament was prepared at 150 °C as the 3D printing raw material. A 3D printer was used to print the photo-responsive shape-memory device at 240 °C.<sup>[220]</sup> Liu et al. used CB as filler and epoxy resin as a matrix to prepare a smart material that can respond to 1.064 μm NIR light, and the shape recovery ratio of this material is > 97%. Flexible polypropylene glycol diglycidyl ether was introduced into the epoxy crosslinking network to improve the flexibility of the polymer chain segment. The curing agent was added, and the nano-scale CB particles were evenly dispersed in the resin



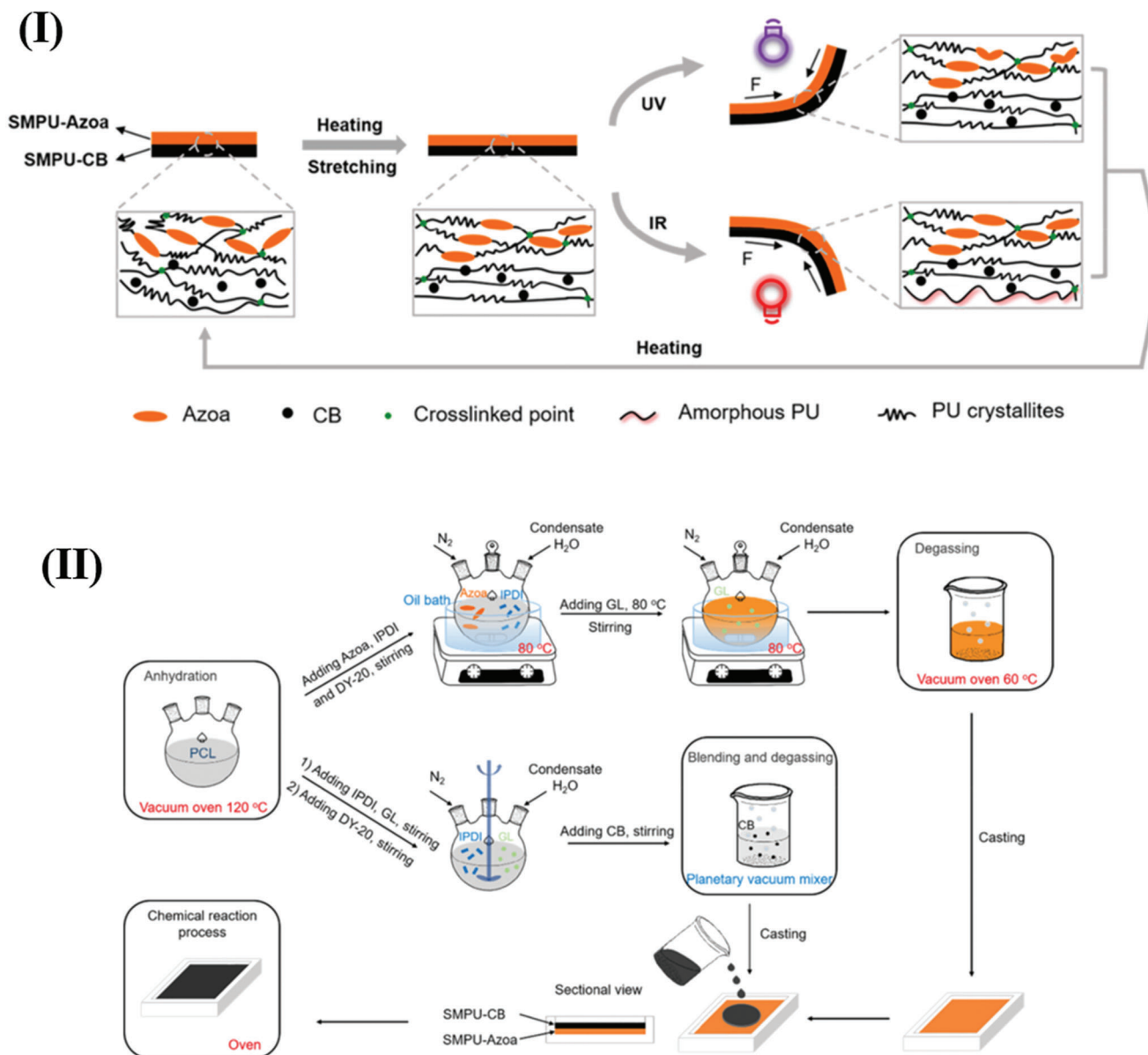


**Figure 15.** I) Photo-responsive mechanism for the reversible deformation of SMPU-AC bilayer to UV and IR lights; II) Schematic representation of the synthetic route for SMPU-AC. Reproduced with permission.<sup>[35]</sup> Copyright 2021, Elsevier.

matrix under the action of mechanical agitation and ultrasonic dispersion. The final sample was obtained after the prepolymer was injected into the mold for degassing and curing.<sup>[221]</sup>

#### 4.1.3. Carbon Nanotubes (CNTs)

**Graft:** Wang et al. reported a CNTs-graft-poly(tetrahydrofurfuryl methacrylate-co-lauryl acrylate-co-1-vinylimidazole) copolymer (CNTs-g-P(TMA-co-LA-co-VI)). The mechanical properties of CNTs-g-P(TMA-co-LA-co-VI)/Zn<sup>2+</sup> with CNTs content of 1.1 wt% were significantly improved after the metal ligand was cross-linked with Zn<sup>2+</sup> ions. CNTs-g-P(TMA-co-LA-co-VI) copolymer was prepared by reversible addition-

fragmentation chain transfer polymerization (RAFT) and metal-ligand crosslinking as shown in Figure 16I.<sup>[222]</sup> The properties of the copolymer can be controlled by changing the composition and crosslinking degree of the copolymer side chains (Figure 16II).<sup>[222]</sup> Another paper reported a CNT-coated conductive elastomer with dual-stimulated shape-memory and self-healing performance. CNTs/CNT-g-P(TMA-co-LA-co-VI)/Zn (CNTs/CHSMPs) was facilely fabricated by coating CNTs on the surface of a crosslinked CNT-based graft copolymer, CNT-g-P(TMA-co-LA-co-VI)/Zn.<sup>[223]</sup>

**Crosslinking:** Wanyan et al. reported the crosslinked poly(L-malic acid)/CNTs nanotubes (PLMA/CNTs) shape-memory nanocomposites with excellent optical absorption efficiency and photothermal conversion stability.<sup>[224,225]</sup> CNTs were grafted onto

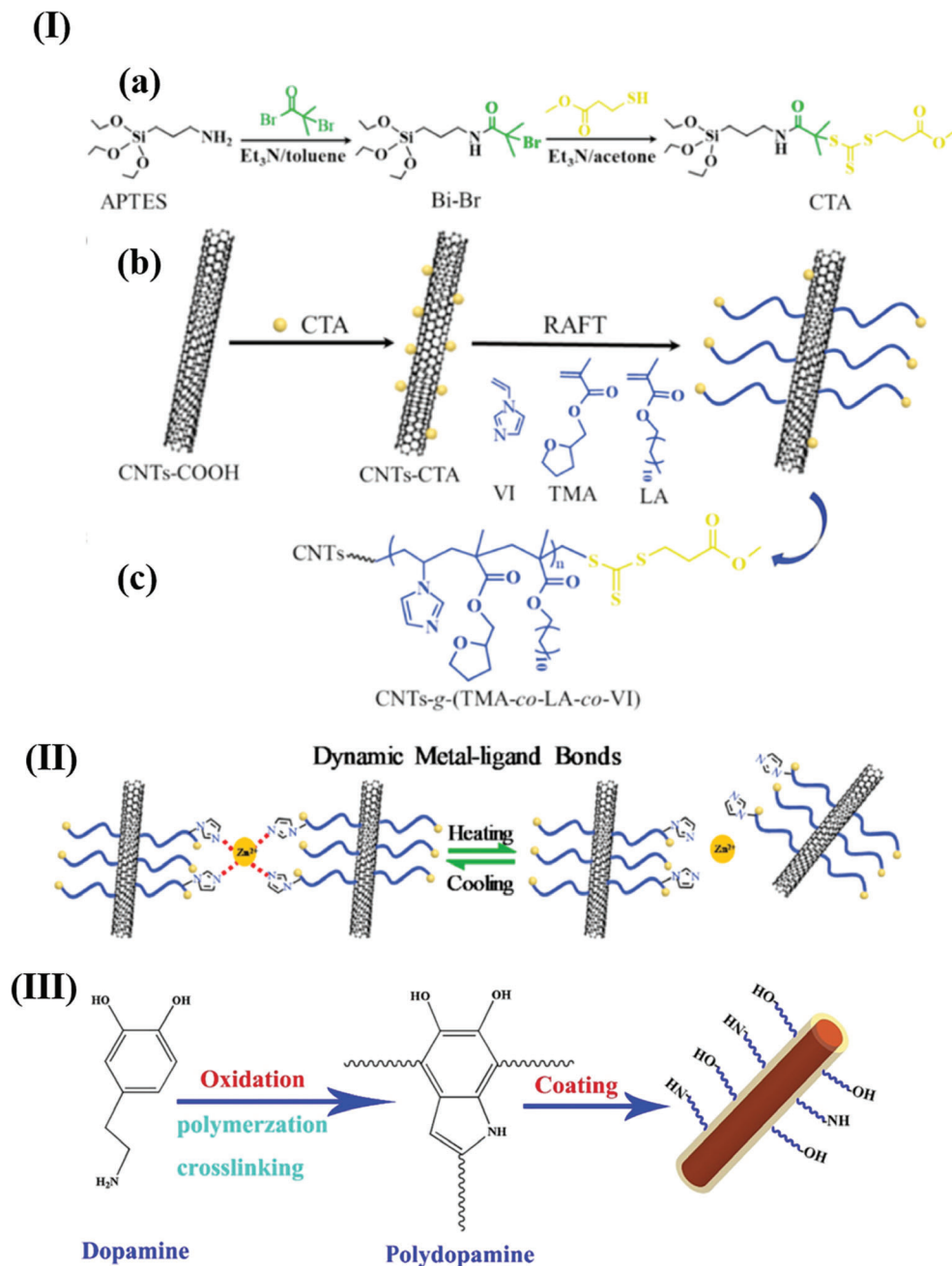


**Figure 16.** I) Schematic diagram for the synthesis of a) RAFT agent (CTA), b) CNTs-CTA, and CNTs-g-P (TMA-co-LA-co-VI). c) The chemical structure of CNTs-g-P(TMA-co-LA-co-VI). Reproduced with permission.<sup>[222]</sup> Copyright 2020, Elsevier. II) Illustration of the association and disassociation process of  $\text{Zn}^{2+}$ /VI metal-ligand bonds in response to stimulus. Reproduced with permission.<sup>[222]</sup> Copyright 2020, Elsevier. III) Schematic of modification of MWCNTs by DA. Reproduced with permission.<sup>[227]</sup> Copyright 2020, Elsevier.

PLMA oligomers, and then the cross-linker was added to the system. The mixture was poured into the mold for curing and forming, and a sheet sample was finally obtained.<sup>[224]</sup> Bai et al. reported a recyclable SMPs SBS-20FU-CNTs. The mechanical properties, resilience and solvent resistance of the materials were greatly improved by the presence of only 1 wt% CNTs. Diels-Alder (DA) reactive polymer SBS (SBS-20FU) was synthesized by

furfuryl mercaptan, and then CNTs were added to SBS-20FU solution. During the cooling process, DA reaction occurred to form a crosslinked structure.<sup>[225]</sup>

**Physical Doping:** This section aims to explore some doping methods to improve photothermal and electrical properties of SMPs, while producing as little negative effect as possible on shape-memory properties.

Xu et al. introduced CNTs in poly (ethylene-cooctene)(POE) to construct the segregation structure and fabricate the photoelectric driven reversible SMPs. The POE/S-CNT composite containing 2 vol % CNT is characterized by high electrical conductivity and light absorption (760 nm), and this property can ensure that the composite is activated at low voltage ( $\leq 36$  V) and suitable light intensity ( $250 \text{ mW cm}^{-2}$ ). POE and CNTs were pulverized to get powders with the size of 76–600  $\mu\text{m}$  using a pulverizing machine at low temperature, and then the POE/CNT composites were compression molded into sheets with different particle sizes and mixing ratios.<sup>[226]</sup> Bi et al. reports a composite material that can be used as a raw material for 3D printing. After three shape-memory cycles, the shape fixation rate of the composite with CNTs content of 3 wt% is > 90%, and the shape recovery ratio is higher than 75%. When the content of CNTs is 5 wt%, the thermal conductivity of the composite can reach 3.6 times that of the composite without fillers. Dopamine (DA) was self-polymerized into polydopamine (PDA) on the surface of MWCNTs, and the modified MWCNTs covered by PDA were formed. Subsequently, modified CNTs were mixed with thermoplastic polyurethane(TPU)/PCL/CNC/DMF solution, before the mixed solution was poured into the mold and dried to obtain a composite film. The composite filament was applied to a fused deposition modeling 3D printer, and the NIR induced shape-memory model was obtained by using the composite filament. DA is oxidized on the surface of MWCNTs and self-polymerizes to form irreversible covalent PDAs, such as high-strength phenolic hydroxyl ( $-\text{OH}$ ) and amino ( $-\text{NH}-$ ) groups as illustrated in Figure 16III.<sup>[227]</sup> Ha et al. prepared PU nanocomposites with excellent thermal properties by doping boron modified single-wall CNTs (SWCNTs). The boron-doped SWCNTs (B-SWCNTs)/PU mixed solution was poured into the mold and dried to form a film to prepare the composite film.<sup>[36]</sup> Lu et al. added boron nitrides to SMPs, thereby improving the thermal conductivity of shape-memory nanocomposites. DSC results showed that increasing the CNT content helped to increase the thermoweight of the material. The embedding of boron nitride promotes the heat transfer of CNTs to the polymer matrix and improves the thermal conductivity of SMP composites. SMPCs containing 4 wt% boron nitride and 4 wt% CNTs have the highest recovery speed and the highest  $T_g$  (107.8°C).<sup>[37]</sup>

#### 4.1.4. $\text{Fe}_3\text{O}_4$ Nanoparticles

**Crosslinking:** SMPCs can also be fabricated using  $\text{Fe}_3\text{O}_4$  inter-networking structure materials. The catechol group terminated PCL-PTMEG (PCL-PTMEG-DA) was synthesized, and then a certain amount of treated  $\text{Fe}_3\text{O}_4$  NPs was mixed with PCL-PTMEG-DA.  $\text{Fe}_3\text{O}_4$  NPs and PCL-PTMEG-DA could be crosslinked to prepare dynamic network.<sup>[228]</sup>

**Physical Doping:** SMPs with excellent thermal/electric/magnetic effects can be prepared by physical blending with  $\text{Fe}_3\text{O}_4$ . To repair the damage generated during deformation, Huang et al. designed a shape-memory assisted self-healing polylactide(PLA)/epoxidized natural rubber (ENR)/ $\text{Fe}_3\text{O}_4$  thermoplastic vulcanizates via dynamic curing. ENR/ $\text{Fe}_3\text{O}_4$  blend and PLA/Irganox 1010 (0.2phr (PLA+ENR) blend were prepared, and then mixed evenly in a two-roll

mill before dicumyl peroxide (DCP) was added to initiate the crosslinking of ENR.<sup>[229]</sup>

Du et al. fabricated SMPCs with two-way SMEs and self-healing capacity. Catechol group terminated PCL (PCL-DA) was synthesized, and then  $\text{Fe}_3\text{O}_4$  NPs with coating agent sodium oleate was synthesized by controlled chemical coprecipitation method.  $\text{Fe}_3\text{O}_4$  NPs and PCL-DA were mixed in chloroform, to create PCL-DA- $\text{Fe}_3\text{O}_4$  network polymer (Figure 17I).<sup>[230]</sup>

#### 4.1.5. $\text{Fe}^{3+}$ Ions

**Coordination:** The two transition temperatures of poly (ethene-co-vinyl alcohol) (EVOH) give the composite a triple shape-memory behavior, and the NIR photoinduced responsiveness of the composite is due to the addition of iron tannic acid (FeTA) NPs as a photothermal conversion factor. The composite exhibits high driving recovery stresses. EVOH with shape-memory characteristics was prepared by using hexamethylene diisocyanate (HDI) as a chemical crosslinking agent. Then, a certain amount of EVOH and  $\text{FeCl}_3$  were mixed and crosslinked under appropriate conditions. Then the mixture was soaked in tannic acid to form FeTA NPs.<sup>[231]</sup> Due to the specific photothermal effect of each ion, the light-induced shape-memory characteristics of ionomers can be freely adjusted via the type and content of metal ions. PVA and PAA were dissolved in water and poured and dried, following by immersion in  $\text{FeCl}_3$  solution. The strength of ion crosslinking was controlled by the immersion time of PVA-PAA in  $\text{FeCl}_3$  solution. The final results show that the increase in cross-linking time contributes to the enhancement of ion cross-linking (swelling degree (Q) rapidly decreases from 177% to 70%).<sup>[232]</sup> The introduction of  $\text{Fe}^{3+}$  into the poly(ethylene oxide)/poly(acrylic acid) (PEO/PAA) blend can induce the formation of coordinated cross-link networks. The coordination of  $\text{Fe}^{3+}$  carboxylate reduces  $\text{Fe}^{3+}$  ions to  $\text{Fe}^{2+}$  under UV light, and  $\text{Fe}^{2+}$  can be oxidized to  $\text{Fe}^{3+}$  in the air. The formation and disappearance of crosslink networks realized the endowment and recovery of shapes. The surface of the matrix was treated with an alcohol solution of ferric chloride to introduce a selective crosslinking structure.  $\text{Fe}^{3+}$  preferentially binds to carboxyl groups near the surface to form a PAA network in the PEO/PAA blend, and the crosslinking density changes along the thickness direction (Figure 17II).<sup>[69]</sup> The ideal crystallization ability of gallic acid-based nonionic waterborne PU (GWPU) offers the nanocomposite with shape-memory performance, and iron gallate (GA-Fe) NPs as photothermal fillers gave the material excellent NIR induced shape-memory performance. The nanocomposites containing 0.3 wt% GA-Fe NPs recovered from the temporary shape to the original shape within 1 min under NIR light irradiation. The composites were prepared as follows: GA-Fe NPs were prepared by adding  $\text{FeCl}_3$  solution to GA aqueous solution and stirring to obtain iron-polyphenol colloidal NPs. Isophorone diisocyanate/poly-1, 4-butylene adipate glycol/dibutyltin dilaurate (IPDI/PBA/DBTDL) mixture was reacted at 85°C for 2 h to obtain linear and NCO-terminated oligomer. Subsequently, polyethylene glycol branched diol (PEGB) was added to the above oligomers to prepare PU prepolymer anchoring hydrophilic polyethylene glycol chains, and 1, 4-butanediol (BDO) and GA were added to the system for condensation and cooling. The



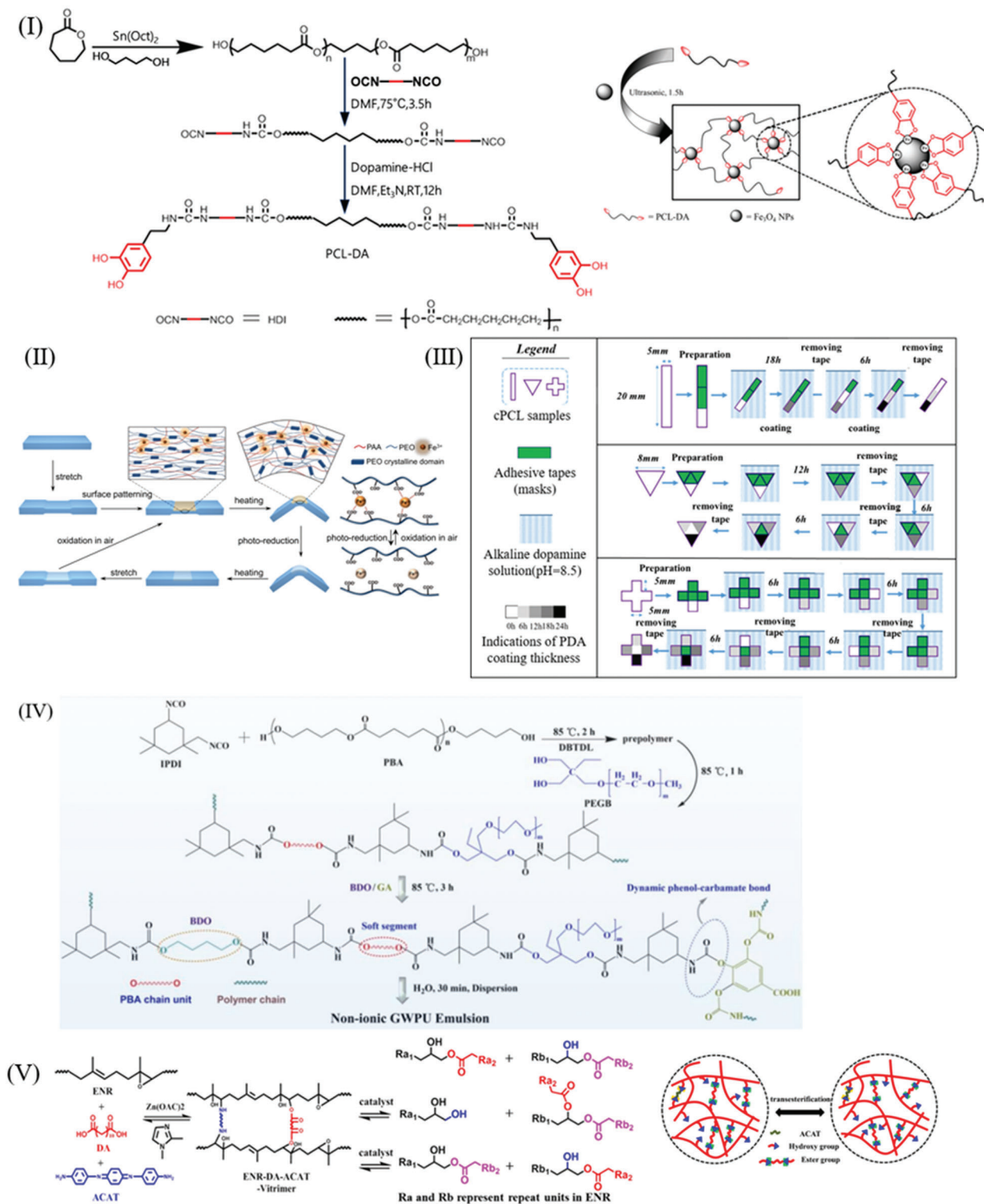


**Figure 17.** Preparation Route of I) the PCL-DA and the PCL-DA-Fe<sub>3</sub>O<sub>4</sub> Networks. Reproduced with permission.<sup>[230]</sup> Copyright 2018, American Chemical Society. II) Schematic illustration of the reversible 2D-to-3D shape transformation process of PEO/PAA blends and the underlying mechanism based on selective suppression of strain relaxation upon uniform heating of the SMP. Reproduced with permission.<sup>[69]</sup> Copyright 2018, American Chemical Society. III) Illustrations of the Preparation of Gradient PDA Coatings. Reproduced with permission.<sup>[38]</sup> Copyright 2022, Elsevier. IV) Schematic of the synthetic route of the nonionic GWPU dispersions. Reproduced with permission.<sup>[235]</sup> Copyright 2018, American Chemical Society. V) Synthetic Protocol of the Crosslinked ENR-DA-ACAT Network, and an Illustration of Reversible Transesterification). Reproduced with permission.<sup>[243]</sup> Copyright 2019, American Chemical Society.

GWPU/GF nanocomposites were prepared by gradually dropping the GA-Fe nanoparticle suspension into the non-ionic GWPU dispersion and stirring (Figure 17III).<sup>[38]</sup>

#### 4.1.6. Polydopamine

Polydopamine(PDA) nanospheres have strong light absorption properties and good photothermal effects. The content of PDA nanospheres is generally 0.025 ~ 0.15%. The increase in the content of PDA nanospheres improves the heating speed and moving speed of the microrobot.<sup>[233]</sup> PDA nanosphere stock solution dispersion was added to the methacrylate-terminated prepolymers/crosslink agent solution and mixed evenly. The mixture was poured into the Teflon mold for UV lamp irradiation, and then ventilated.

Chen et al. synthesized PDA nanospheres by a simple self-polymerization method, and prepared PCL/TPU blend films with different proportions.<sup>[234]</sup> Wei et al. fabricated photoinduced SMPs by introducing gradient PDA coatings on dual SMPs by controlling the impregnation time as shown in Figure 17IV.<sup>[235]</sup> PCL was crosslinked with different content of DCP to prepare SMP substrate named cPCL that was immersed in DA solution to prepare PDA coating. Gradient PDA coating was obtained by soaking different positions of cPCL in the same concentration of DA solution for varying time. The photothermal conversion ability of PDA can endow polynorbornene/PDA (PNB/PDA) composites with ultra-fast NIR response shape-memory properties. The surface temperature of the PNB/PDA composite containing 1 wt% PDA can change from 20 to 74 °C in 50 s under NIR light.<sup>[236]</sup> Tian et al. prepared composites with sun-induced plasticity. PCLDA was obtained by terminal functionalized with PCL diol and acryloyl chloride, and the polymer network was obtained by clicking the click-ene chemical reaction. The resulting samples were dried under vacuum after crosslinking under UV light.<sup>[237]</sup> PDA can be mixed with PU to prepare injection molded shape-memory parts with good photothermal response. PDA has a good photothermal effect, and the composite exhibits a fast photo-responsive shape-memory process when doped with only 0.01 wt% PDA. The dried SMPU and PDA were pre-mixed with a high-speed mixer, extruded and cut into particles by a twin-screw extruder. The dried particles were injected molded to obtain the SMPU/polydopamine particles(PDAPs) composite sample.<sup>[40]</sup> The PDA/WEP composite has the ability to undergo thermosetting and thermoplastic transformation at different temperatures, and the photothermally induced plasticity process can program the material into a new permanent shape. When the content of PDA is 1 wt%, the shape-memory fixation ratio and shape-memory recovery ratio are 97.4% and 67.8%, respectively. PDA and WEP were evenly mixed in deionized water and then dried to form a mixture of molten liquid. Curing agent of 4-aminophenyl disulfide was added to the molten mixture and mechanical agitation was carried out. Then the mixture was transferred to a vacuum drying oven for degassing.<sup>[41]</sup>

#### 4.1.7. Polyaniline (PANI)

**Crosslinking:** Dong et al. found that PANi nanofibers can improve the protective performance of epoxy coating, and when the

scratch area is exposed to NIR radiation, the coating containing PANi has good self-healing performance. The 5 wt% PANi composite exhibits the optimal SME and various self-healing properties. The interface polymerization method was used to prepare PANi nanofibers, and then the epoxy resin and PANi resin were mixed. The epoxy resin was heated to 80°C to improve its fluidity before PANi nanofibers were added to the epoxy resin. After uniform dispersion, the sample was solidified under certain conditions.<sup>[238]</sup>

**Physical Doping:** When PANi is incorporated into the polymer in a blending manner, physical crosslinking points can be formed. The photoinduced shape recovery ratio and speed of the polymer can be improved by increasing the content of PANi. Bai et al. used solution casting method to prepare composite films. The PVA/PANi hydrogel was obtained by melting under certain conditions, before the hydrogel was dried to obtain PVA/PANi composite film.<sup>[39]</sup> Heo et al. used a melt blending method to prepare the composite membrane. The shape recovery ratio of the blend under NIR stimulation increased with the increase of PANi content, and the shape recovery ratio reached 96% when the PANi content was 15 wt%.<sup>[239]</sup> Maleated polyolefin elastomer (mPOE)/PANI blend was fused and blended in Haake mixer at 180°C for 10 min, and the mixture was synthesized after subsequent treatment.<sup>[239]</sup>

#### 4.1.8. Other Fillers

**Black Phosphorus (BP):** The incorporation of BP sheet into the shape-memory substrate can cause the temperature of the shape-memory substrate material to rise rapidly and trigger the shape change of composites. Xie et al. prepared PU SMPs with BP sheet doping concentration of 0.08 wt%, and its shape recovery ratio was close to 100% under 808 nm light irradiation. BP crystals are ground to BP powder and dispersed in 1-Methyl-2-pyrrolidinone (NMP), and the dispersions are sonicated in an ice bath and centrifuged. The PU/black phosphorus (PU/BP) film was then prepared using the solution casting method. The PU/BP composite was prepared by thermoplastic methods.<sup>[240]</sup>

**Titanium Nitride (TiN):** TiN NPs is an absorber of sunlight and near-infrared light. Compared with gold and silver nanoparticles, TiN has higher light absorption efficiency, chemical stability and lower price.<sup>[241]</sup> PCL was synthesized with TiN to form a fast photo-responsive SMP. TiN NPs were modified with hexanoic acid to adjust their surface polarity to make TiN NPs evenly dispersed in xylene as nonpolar solvent. Two-branched 20PCL macromolecular monomers (2b20PCL-m) were synthesized by ring opening bulk polymerization. The xylene solution of 2b20PCL-m was then mixed with the pretreated TiN NP and heated at 80°C to form the crosslinked PCL composite film.<sup>[241]</sup>

**CaCuSi<sub>4</sub>O<sub>10</sub>:** The layered structure of CaCuSi<sub>4</sub>O<sub>10</sub> nanosheets (CUP NSs) is similar to that of other 2D materials, and can be easily obtained through the stripping process. The shed structure has excellent photothermal conversion efficiency, indicating that CUP NSs can be used as an IR-II photothermal agent for shape-memory composites. Yang et al. developed a novel biodegradable SMPs by adding CUP NSs to poly (D, L-lacta-co-trimethylcarbonate) SMP (PDLLA-co-TMC, PT). CUP powder was synthesized by typical sol-gel method,

then the synthesized CUP NSs was placed in NMP solution, and collected by centrifugation after ultrasonic treatment. CUP/PT composite was prepared by solution casting method.<sup>[242]</sup>

**Amino-Capped Aniline Trimer (ACAT):** By incorporating ACAT into a polymer matrix, Feng et al. prepared a covalently crosslinked ENR-DA-ACAT vitreous with recyclable, self-healing, multiple response properties. Zinc(Ac)<sub>2</sub>, 1, 2-dimezimidazole (DMI), DA, and ACAT were mixed with ENR in different proportions. The mixed uncured sample was compressed at 180°C. DMI was used to accelerate the crosslinking reaction, and Zn(Ac)<sub>2</sub> was the transesterification catalyst. ACAT was regarded as the tetra-functional crosslinking agent of epoxy group and a catalyst for transesterification reaction as shown in Figure 17V).<sup>[243]</sup>

**Aniline Black (AB):** Composite films that also have excellent SMEs in aqueous media can be prepared by filling the crosslinked poly(ethylene-co-vinyl acetate) (EVA) substrate with AB. With the increase of AB content (from 0.5 to 2 phr), the shape recovery temperature of EVA composite decreases from 85 to 74°C. AB was added to THF/xylene and dispersed evenly by ultrasonication, and then EVA, triallyl isocyanurate (TAI) and benzophenone (BP) were added to the above mixed solution. The mixture was volatilized by solvent to obtain the film.<sup>[244]</sup>

**Polypyrrole (PPy):** PPy NPs can be selectively distributed in PCL fractions as photothermal fillers, allowing EVA/PCL blends with continuous structures to exhibit excellent photoinduced shape-memory properties. PPy NPs were distilled under reduced pressure to remove impurities, and then EVA and PCL particles were fused and blended using screw rotation speed. The molten product was hot pressed to obtain thin sheet samples.<sup>[245]</sup> Dong et al. synthesized PDA@PPy NPs using PDA particles as fillers and dispersed them in an epoxy matrix to prepare a coating with good self-healing properties that were enhanced by increasing the amount of PDA@PPy NPs. The coating with 5 wt% PDA@PPy NPs showed the optimal self-healing properties. The fluidity of epoxy resin can be improved by adding a certain amount of PDA@PPy NPs at 80°C.<sup>[246]</sup>

In this section, various functional fillers, including graphene, CB, CNTs, Fe<sub>3</sub>O<sub>4</sub> NPs, Fe<sup>3+</sup>, PDA, and PANi used in SMPs systems. Graphene, despite its challenges in terms of high cost, aggregation tendencies and stacking behavior, can provide exceptional properties including high specific surface area, mechanical strength, and thermal effects. It can also be modified, such as reduced graphene oxide (rGO), isocyanate modified graphene oxide (iGO), functionalized graphene oxide (FGO), etc., to improve dispersion and interface bonding. CB is a suitable functional filler to enhance photothermal conversion efficiency and expand wavelength response range. Compared to other fillers, CB requires higher filler content, which may affect the mechanical and optical properties of the materials. CNTs offer properties of high thermal conductivity, strong infrared absorption, good charge transport performance and high electrical conductivity, which facilitate remote control and the development of shape-memory and self-healing capabilities through rapid photothermal and electrothermal conversion. However, CNTs face challenges related to its poor compatibility with the polymer matrix, which remains an area of concern. Fe<sub>3</sub>O<sub>4</sub> NPs and Fe<sup>3+</sup>, as a class of fillers with excellent performance, can be added to the shape-memory substrate as powerful network points, playing a role of crosslinking. This network structure imparts multiple

SMEs to the material. Compared to other fillers, Fe<sup>3+</sup> exhibits high self-healing and shape-memory performance even at low filler concentrations. Moreover, Fe<sub>3</sub>O<sub>4</sub> NPs can introduce magnetic response to hybrid materials, and the dynamic properties of metal coordination interactions can enhance the self-healing ability, although the self-healing speed has not reached a high level at present. DA as a natural compound existing in animals and plants has favorable biocompatibility and biodegradability. Therefore, SMPs containing PDA as a filler owns the advantages of environmentally friendly and recyclable properties, aligning with the urgent demand for polymer materials. In addition, the SMPs with PDA can respond not only to the NIR-induced deformation, but also to Vis-light in the range of 400–500 nm with a low yield. However, due to its good recyclability, the durability of PDA filler SMPs is poor. Now researchers are looking for a balance between the two properties. PANi has a high optical extinction coefficient and strong NIR absorption capacity, which makes it useful for photothermal treatment. In addition, PANi can serve as a photothermal conversion agent to improve water-induced shape-memory properties. However, the dual functionality of PANi nanofibers in coatings, may affect the SME and anticorrosion property of the coating.

In short conclusion, the incorporation of the above discussed functional fillers into SMPs offers the advantage of light-responsive effects, thereby improving the shape-memory, thermal conductivity, self-healing and mechanical properties of SMPs. The light-responsiveness encompasses various ranges, including IR, Vis and UV response, among which NIR response is especially extensive. Among the available stimuli, NIR stimulation has been widely used as remote triggering for shape-memory and self-healing materials. This type of triggering mechanism eliminates the need for direct contact, providing enhanced control precision and broader range of applications. Further, it imposes lower requirements on surrounding environmental conditions.

## 4.2. Selectively Triggered SMPs and SMPCs

Varying the light wavelength, intensity, irradiated position, and polarization permits advanced light-activated SMEs. Furthermore, light-activated reversible SME and multi-SME enhance the applicability of light-induced SMPs and composites for sophisticated SMP applications.<sup>[247–249]</sup> Notably, the wavelength selective SME has been introduced for remote and sequential actuation of light induced SMPs and composites. The light-activated SMP and light-activated SMPCs responsive to selective wavelengths of UV–vis and IR are described herein.

### 4.2.1. UV Light

UV light with high energy presents a lower penetration depth than visible light and NIR light. Two main approaches are reported, regarding UV light triggered shape recovery of SMPs, that is, on one hand, photo responsive molecular switches that usually act as reversible crosslinking points are introduced into SMP networks, and on the other hand, UV light responsive photothermal agents are mixed with SMP to create SMPC.



**Photochemical Reaction:** In 2005, Lendlein et al. reported SMPs containing cinnamic groups that can be deformed and fixed into various shapes by UV illumination with wavelength  $> 260$  nm.<sup>[42]</sup> UV light with a wavelength  $< 260$  nm can trigger the shape recovery. Two different UV wavelengths induce reversible [2+2] cycloaddition of two cinnamate functional groups. Other reports followed via various synthesis approaches. Pendant cinnamamide moieties were introduced in multiblock polyesterurethanes with biodegradable segments.<sup>[250]</sup> N,N-bis(2-hydroxyethyl) cinnamamide (BHECA), biodegradable PLLA, and PCL diols, as well as HDI, were used as raw materials and coupling agent. BHECA and MDI were used as hard segments to create UV triggered SMP with PCL-diols as well. Besides, a series of prepolymers were created containing diethyl 2,2'-(cinnamoylazanediyloxy)diacetate (DCA) or diethyl 3-(cinnamoyloxy)pentanedioate (DCE) as well as 1,8-octanediol or 1,4-cyclohexanedimethanol, which were used for synthesizing poly(ester urethane)s with pendant photo-responsive moieties.<sup>[251]</sup>

Cinnamate-modified PCL was synthesized and used as raw materials in the preparations of homopolymers, random copolymers, and BCPs with cinnamate groups using ring-opening polymerization between caprolactone and diols.<sup>[173]</sup> Then p-chloro-substituted cinnamic acid was grafted onto PVA via esterification reaction.<sup>[171,252]</sup> Photodimerization between pendant cinnamate groups was achieved to create photo induced shape fixation. Radical polymerization was used as well to create methacrylate-based monomers bearing cinnamic acid as photo-responsive moieties and cholic acid as biological compounds, in addition to oligo(ethylene glycol).<sup>[253]</sup>

Anthracene is another photo-responsive group that can undergo [4+4] photodimerization upon the irradiation to UV light  $> 300$  nm. The created new crosslinking points fix chain orientation and a temporary shape. External heat results in the scission of dimerized anthracene, triggering disorientation and shape recovery. N,N-Bis(2-hydroxyethyl)-9-anthracenemethanamine was synthesized and used in the preparation of PU elastomers with dangling anthracene groups.<sup>[184,254-257]</sup> Yang and Wang et al. explored poly(D,L-lactide)-PTMEG (PDLLA-PTMEG) network via UV light irradiation, showing triple-SME and tunable two-way SME.<sup>[254,255]</sup> A series of shape-memory PU elastomers with PCL diols as soft segments were prepared.<sup>[184]</sup> The crosslinking degree and shape-memory performance can be controlled by irradiation time. Epoxy monomer with anthracene groups was prepared and reacted with other epoxy monomers and curing agents to create epoxy elastomers with reversible crosslinking points. An aggregated structure of dimerized anthracene molecules is formed, determined from molecular dynamics simulation results. Upon heating, the agglomeration breaks and partially reverses to the initial state.

Grafting reaction is used for introducing anthracene groups to polymer chains based on esterification or amidation reaction.<sup>[183,258]</sup> Hydroxyl groups were first introduced onto poly(styrene-block-butadiene-block-styrene) (SBS) chains as side groups using thiol-ene click reaction, before anthracene groups were grafted via esterification among such hydroxyl groups and succinic acid mono-anthracen-9-ylmethyl ester.<sup>[258]</sup> The dedimerization of anthracene dimers can erase the de-

formation completely and lead to new shape reconfiguration. Poly(aryl ether ketones) (PAEK) bearing anthracene groups were created based on nucleophilic copolycondensation and subsequent amidation reaction between dangling carboxyl groups and 2-aminoanthracene.<sup>[183]</sup> Photodimerization among anthracene groups brought chemical crosslinking point in PAEK network, leading to enhanced SME over pristine PAEK chains having weak intramolecular forces.

Fang et al. developed an UV light responsive polymer by synthesizing a linear PU elastomer (azo-PU) containing azobenzene groups in the main chains, which presented both SME and UV light-induced shape deformation behavior.<sup>[43]</sup> A functional monomer dihydroxyazobenzene (DHAB) which can undergo photoisomerization upon UV illumination was used as the chain extender to incorporate azobenzene moieties in the main chains of the azo-PU, which consisted of polycarbonate diol (PCDL,  $M_n = 2000$ ) and IPDI. The light absorption peaks in DHAB and azo-PU were attributed to the trans-cis photoisomerization of azobenzene moieties.<sup>[43]</sup>

**Photothermal Effect:** UV light with high energy usually leads to the breakage of weak chemical bonds. Unlike photochemical mechanisms observed in SMPs with cleavable backbones, some compounds are used as functional fillers for UV light as well.  $Zn(Mebip)_2(NTf_2)_2$  (where, Mebip stands for 2,6-bis(N-methyl-benzimidazolyl)-pyridine, and  $NTf_2$  stands for bis(trifluoromethylsulfonyl)-imide) has been used in introducing photo-thermal effect in self-healing hydrogels and SMPs.<sup>[259,260]</sup> Upon irradiation of UV light in the wavelength range 320–390 nm at an intensity of  $950 \text{ mW cm}^{-2}$ , such compound can reach over  $220^\circ\text{C}$  in 30 s due to the absorption of metal-ligand complex.<sup>[260]</sup> A 10% mass ratio of  $Zn(Mebip)_2(NTf_2)_2$  was sufficient to bring epoxy resin as SMP matrix with photothermal effect upon UV light irradiation. The well dispersion did not damage the mechanical property of epoxy resin.

Photothermal effect of azopyridine compounds and their azobenzene analogs were reported and one compound (p-aminodiphenylimide, p-AP) was used in creating UV light triggered SMPs with EVA and epoxy resin as matrix.<sup>[248,249]</sup> Different structures resulted in varied photothermal effects possibly due to the different absorption peak related to  $\pi-\pi^*$  transitions.<sup>[94]</sup> The mechanical properties of EVA were slightly reduced by increasing p-AP loading content from 0.5 wt% to 1 wt%. Even though, reversible shape deformation can be achieved upon light on/off.<sup>[249]</sup> UV light at the wavelength of 365 nm increased the temperature of epoxy resin with 0.75 wt% p-AP up to  $80^\circ\text{C}$ .<sup>[248]</sup> High photothermal effect of p-AP, thus, was presented over  $Zn(Mebip)_2(NTf_2)_2$ .

**Other Effects:** Spiropyran was used to create UV light triggered EVA SMP as well due to light induced plasticization.<sup>[261]</sup> UV irradiation greatly decreased the modulus of EVA composites with spiropyran due to the transition from a closed spiro form to an open zwitterionic merocyanine form. The molecular mobility of amorphous phase in EVA was increased. More specifically, zwitterionic MC form of spiropyran resulted in the plasticization of EVA through the strengthen in the interaction with ester groups of EVA and the enhancement in molecular mobility of noncrystalline phase. In another report, n-hydroxyethyl-3,3-dimethyl-6-nitroindoline spiropyran was grafted into a PU

matrix.<sup>[262]</sup> The increase in spiropyran groups amount in PU chains was beneficial for shape recovery ratio up to 93.7%.

#### 4.2.2. Visible Light

Surface plasmon resonance (SPR) of Au or Ag NPs can create photothermal effect upon light at different wavelengths, determined by shape morphologies. Au nanorods with an average length, width, and aspect ratio of 31.08 nm, 9.24 nm, and 3.64 were synthesized and used in biodegradable polymers for cytotoxicity.<sup>[263]</sup> Au nanorods with low concentration (<1 wt%) were sufficient to bring evident photothermal effect after exposure to 0.3 W IR light. Similarly, Ag NPs could introduce a remarkable SPR and photothermal effect that efficiently generated heat when activated by light at the wavelength of 408 nm.<sup>[264]</sup> Ag NPs also played a role as additional crosslink, increasing tensile property and the performance of SME with the fixation ratio and recovery ratio as high as 99.81% and 99.10%, respectively.

PCL disulfide (PCL-SS-PCL) and poly(ethylene glycol) disulfide (PEG-SS-PEG) were synthesized and facilitated Au and Ag NPs dispersion through ligand exchange.<sup>[264–267]</sup> The existence of Au NPs deteriorated the crystallization of the biodegradable SMP, decreasing both crystallization and melting temperatures.<sup>[265]</sup> A laser power of 0.57 W cm<sup>-2</sup> can increase the temperature of the composites with 0.4 wt% Au NPs as high as 25 °C. In another work, the shape recovery occurs only at a laser power of 4 W cm<sup>-2</sup> at which the composites (with 0.003 wt% Au NPs) reached the temperature of 60 °C.<sup>[266]</sup> Au NPs were coated with poly(ethylene oxide) (PEO) chains or dodecyl chains before the dispersion in epoxy matrix was improved.<sup>[267]</sup>

Due to Beer–Lambert's law, the uniform distribution of Au NPs in SMPs still created non-uniform bending due to the generation of photoinduced temperature gradient effect.<sup>[268]</sup> A single laser beam, thus, enabled the creation of multiple deformations and the control of sophisticated motion. Another approach is to use Au NPs with different wavelengths, which present different characteristic absorption wavelengths. Au nanospheres and nanorods presented absorption peaks at 530 and 860 nm, corresponding to green light and NIR light, respectively. The assembly of two SMPs with different Au NPs realized the sequential shape change upon the irradiations of two different laser beams.

Au NPs were mixed with SMPs with different microstructures to tune the shape change at the microscale for applications in smart surface, microfluidic chip, and biomedical applications.<sup>[269–271]</sup> SMP micropillars (10 μm in diameter, 40 μm in height, and 20 μm in pillar-to-pillar distance) in a hexagonal array were mixed with 0.1–0.2 mol% Au nanorods. The bent pillars were nearly recovered to straight ones, and the recovery time was as short as 5 s upon exposure to green laser at 0.3 W.<sup>[269]</sup> PVA was mixed with Au NPs and created a light-induced microfluidic microvalve. The composites with 0.3 wt% Au NPs can recover to their original shapes within 5 s upon visible light irradiation, generating negative pressure for inhaling liquid samples via recovering the cavity volume from the flat surface.<sup>[270]</sup> More interestingly, Au NPs were mixed with poly(D, L-lactic acid) (PDLLA) to create microparticles that can maintain their anisotropic shape at body temperature but recover toward original spherical shape

upon light irradiation.<sup>[271]</sup> This technology provides another important platform for the applications of light-induced SMPs.

Ji et al. developed diselenide bond-containing PUs with visible light-induced plasticity.<sup>[272]</sup> A 6 W white LED was used as the light source and the light-induced plasticity was characterized by stress relaxation under LED irradiation. As shown in **Figure 18I** two strips were curved into the shape of Se and illustrated their shape-memory behavior combined with light-induced plasticity.<sup>[272]</sup> Jeong et al. demonstrated multicolor 4D printing of SMPs and thereby color-dependent selective light absorption.<sup>[273]</sup> As shown in **Figure 18II** red light was first applied and the blue SMP fibers placed at the bottom of the printed structure recovered, whereas the yellow SMP fibers at the top remained rigid.<sup>[273]</sup> Thus, the entire structure deformed into an n-shape. Applying blue light later caused the entire structure to retain its initial flat state. In contrast, when blue light was first applied, the yellow SMP fibers at the bottom recovered first, whereas the blue SMPs remained rigid. Therefore, the entire structure was bent upward and formed into a u-shape. Applying red light later caused the entire structure to retain its initial flat state.<sup>[273]</sup> A facile strategy to fabricate light active and flexible nanocomposite films based on GO and SMPs was reported. These photo-responsive nanocomposite films showed fast, stable, and reversible photomechanical behavior under visible light due to the photothermal effect of GO and the SME of the polymer matrix.<sup>[274]</sup>

#### 4.2.3. IR Light

IR light has longer wavelengths than those of visible light and it is therefore invisible to the human eye. As mentioned before, IR is usually divided into three spectral regions: NIR, MIR, and FIR. Incorporation of photothermal fillers into a thermally induced SMP matrix is widely reported as a convenient and proven method to prepare light-activated SMPCs triggered by IR light. Unlike the photo responsive SMPs, photothermal-activated SMPCs can be used in a wider range of applications, ranging from the microscale to the large scale.

NIR light of 785, 805, and 860 nm have been occupied to trigger the gold photothermal filler based Light activated SMPCs.<sup>[70,275–277]</sup> Shou et al. developed NIR photo-responsive shape-memory films through the photo-initiated polymerization of PCL macromonomers with acryloyl terminal groups in the presence of AuNRs. To incorporate the AuNRs homogeneously within the films, the surfaces of AuNRs were also modified with PCL via surface-initiated ring-opening polymerization.<sup>[276]</sup>

Zhou et al. reported multi photo responsive SMP hybrids and novel chiral actuators based on W<sub>18</sub>O<sub>49</sub> nanowires.<sup>[278]</sup> Light-activated SMPC has been produced by incorporating oligo(ethylene glycol) (OEG)-modified W<sub>18</sub>O<sub>49</sub> nanowires into crosslinked polyethylene glycol diacrylate (cPEGDA) polymer matrices. The chemical crosslinking points formed by the acrylate group provided the shape fixation capacity, while crystalline PEG segments served as the reversible phase of shape-memory. The OEG ligands on the surface of W<sub>18</sub>O<sub>49</sub> could enhance the compatibility between W<sub>18</sub>O<sub>49</sub> and cPEGDA through hydrogen bonds.<sup>[278]</sup> Because of this enhanced compatibility, OEG-W18O49 nanowires were well dispersed and increased

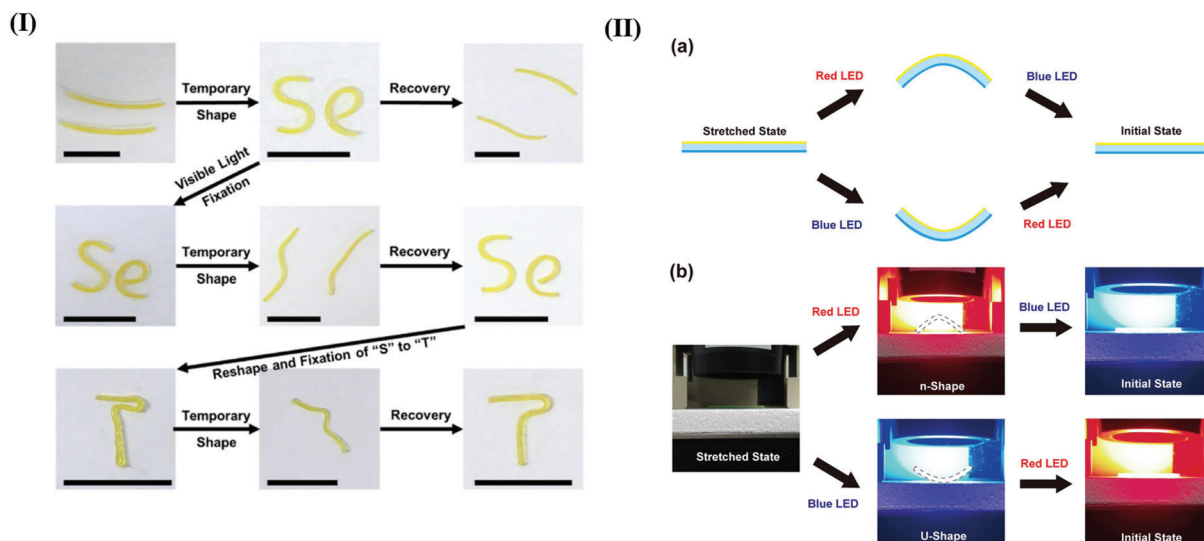


**Figure 18.** Visible light triggered SMPs. I) Shape-memory behavior of diselenide bond-containing PUs under visible light. Reproduced with permission.<sup>[272]</sup> Copyright 2017, American Chemical Society. II) Shape-memory behavior of multicolor 4D printed samples under red and blue light exposure. Reproduced under the terms of CC BY license.<sup>[273]</sup> Copyright 2020, the Author(s). Published by Springer Nature.

the crystallinity of cPEGDA matrices, even at high loading concentrations of 4.0 wt%. Interestingly, the cPEGDA/W<sub>18</sub>O<sub>49</sub> nanocomposites showed efficient photothermal transition and rapid shape-memory behaviors. Also it is proven that the photothermal effect was more efficient under the NIR irradiation than that under UV irradiation. The temperature reached to 167°C in 20 s and 214°C in 1 min due to the irradiation of 1.6 W cm<sup>-2</sup>, 808 nm NIR laser. Under irradiation of 1.6 W cm<sup>-2</sup>, 980 nm NIR laser, the temperature reached 161°C in 20 s.<sup>[278]</sup>

Chen et al. have synthesized a series of novel NIR induced shape-memory ionomers by crosslinking PVA and PAA with various metal ions. The PVA-PAA system was used as the framework and various metal ions (Fe<sup>3+</sup>, Cu<sup>2+</sup>, Ni<sup>2+</sup>, Co<sup>2+</sup>, Cd<sup>2+</sup>, Cr<sup>2+</sup>, Al<sup>3+</sup>) were used as the crosslinked junctions.<sup>[232]</sup> The light induced SME of the ionomer was freely tailored by merely adjusting the species and content of the metal ions, which illustrates the photothermal effect of PVA-PAA and ionomers crosslinked by different metal ions exposed to 808 nm NIR irradiation.

Rare earth organic complexes containing Yb<sup>3+</sup>, Nd<sup>3+</sup>, and Sm<sup>3+</sup> ions, which are being used to produce Light activated SMPs, respond to selective wavelengths of 980, 808, and 1064 nm, respectively.<sup>[33,43]</sup> Accordingly, Nd(TTA)<sub>3</sub>Phen, Yb(TTA)<sub>3</sub>Phen, and Sm(TTA)<sub>3</sub>Phen were incorporated into PU, poly[ethylene-ran-(vinyl acetate)], and poly(methyl methacrylate-co-itaconic acid) SMPs.<sup>[33,43,279]</sup> The commercial availability of the raw materials and the easy preparation approach enable such organic complexes to be cost efficient photothermal fillers for Light activated SMPs.<sup>[33]</sup> Furthermore, it has been reported that such organic complexes show a notable thermal stability up to 270 °C.

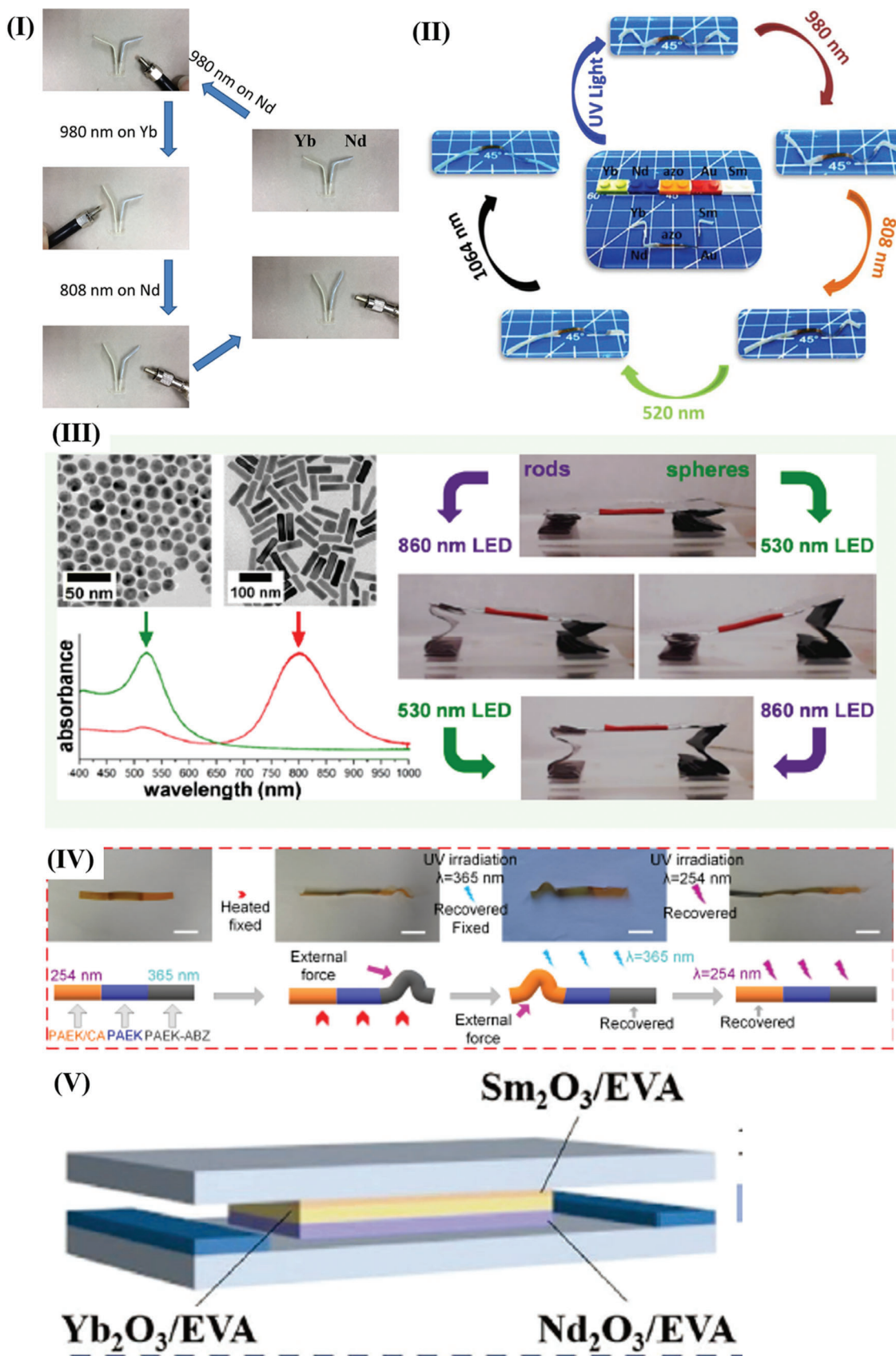
### 4.3. Wavelength Selective Photo-Responsive SME in Polymer

The wavelength-selective photo-responsive SMPs can be constructed using light-active functional groups or light-absorbed

fillers to facilitate the selective shape recovery triggered by light with an appropriate wavelength. The chemical reactions of light-active functional groups in SMPs can occur upon irradiation with a certain wavelength of light. For instance, exposure to UV light can induce the conformational transformation via photoisomerization of azobenzene and arylazopyrazoles molecules in polymer systems, leading to a macroscopic deformation/recovery in shape-memory process.<sup>[280,281]</sup> Incorporation cinnamic groups has been incorporated in SMP networks to adjust the crosslinking density through its photo-reversible cycloaddition reactions upon UV exposure of certain wavelengths. The fixation of a temporary shape and recovery to the original shape can be achieved by the formation and destruction of netpoints.<sup>[250,253]</sup> Alternatively, the photo-thermal effects can be used by adding suitable light-absorbed fillers including Au NPs, CNTs, rare earth organic complexes, and p-aminodiphenylimide, etc., into the SMP matrix.<sup>[14]</sup> The fillers absorb the energy from light with a certain wavelength and convert its energy into heat, triggering the shape-recovery of SMP matrixes. Compared to the method based on light-active functional groups, the wavelength-selective SME based on the photo-thermal effect is more commonly used due to its higher efficiency and more suitability for biological applications.<sup>[14,282]</sup>

A multi-wavelength selective response of SMPs has been developed to enable on multiple shape changes and sequential actuation through the combination of two or more materials responsive to different wavelengths. This innovation allows on demand control and manipulation of shape-recovery, broadening their scope of applications in soft robotics and biomedicine with adaptive and responsive structures. For example, Fang, et al. has reported the integration of two fillers based on rare earth organic complexes, Yb(TTA)<sub>3</sub>Phen, and Nd(TTA)<sub>3</sub>Phen, into SMP poly[ethylene-ran-(vinyl acetate)] to achieve the selectively shape-recovery under NIR light of 980 or 808 nm as shown in **Figure 19I**.<sup>[33]</sup> An assembly of five photo-responsive polymers





was successfully prepared by Fang, et al. using EVA based composites containing AuNPs, Nd(TTA)<sub>3</sub>Phen, Yb(TTA)<sub>3</sub>Phen, and Sm(TTA)<sub>3</sub>Phen as photothermal fillers, respectively, and a UV light responsive PU elastomer, where shape-recovery can be triggered by UV, visible, and NIR light with different wavelengths as shown in Figure 19II.<sup>[43]</sup> The assembly of these five prepared photo-responsive blocks in three distinct configurations resulted in enhanced spatiotemporal control over complex shape deformations in response to diverse sequences of light illumination. Furthermore, wavelength-selective photothermal triggering of shape recovery was also reported to be easily achieved by embedding Au nanospheres and nanorods in thermoplastic PU SMPs, which were sensitive to light with wavelengths of 530 and 860 nm, respectively, enabling the sequential actuation as shown in Figure 19III.<sup>[283]</sup>

The implementation of shape-memory poly(aryl ether ketone) with two light-active groups, for instance, azobenzene, and cinnamic acid, was also reported to exhibit excellent wavelength-selective SME responsive to the irradiation with wavelength of 365 and 254 nm (Figure 19IV).<sup>[44]</sup> Furthermore, multi-wavelength selective responsive SMPs can also be realized by combining photothermal and photochemical effects. Wang et al. reported a UV-vis-NIR light-deformable SMP composite film via incorporating a LC mixture and GO into a shape-memory PU matrix. Three light-triggered mechanisms existed in these SMPs: a) photochemically induced LC phase transition upon UV exposure, b) photochemically and photothermally induced LC phase transition upon visible light irradiation, c) photothermally triggered LC phase transition and partial stress relaxation upon low-intensity NIR exposure, producing the wavelength-selective responsive structure capable of reversible, programmable, and controllable shape-memory actuations.<sup>[219]</sup>

The assembly of SMP blocks that are sensitive to light with different wavelengths is typically arranged in a horizontal manner. Otherwise, vertical binding can occur, when the bi-layer structures cannot achieve uniform expansion or contraction due to the weak penetration of light. Recently, Shan, et al. reported a NIR light (1064, 980, and 808 nm) induced SMP tri-layer film with the aid of vertical distribution of Sm<sub>2</sub>O<sub>3</sub>, Yb<sub>2</sub>O<sub>3</sub>, and Nd<sub>2</sub>O<sub>3</sub> as photothermal fillers along film thickness > 2 mm as shown in Figure 19V. It showed that the tri-layer films can present uniform contraction and lift a weight of 101.44 g by 8 mm under simultaneous irradiations of three NIR light beams.<sup>[45]</sup> This finding provides a new strategy to improve the output force of light induced soft actuators.

3D and 4D printing techniques as advanced manufacturing methods are intended for fast and precise fabrication of complex structures according to a pre-designed computer model. The personalized 4D printing together with multi-stimulus selective control have enabled diverse and effective utilization of

SMPs in various intelligent structures and systems.<sup>[128,284]</sup> For example, Jeong, et al. demonstrate the method to fabricate multi-wavelength selective responsive SMP samples using 4D printing after experimental evaluation and theoretical calculation of the relations between light absorption and temperature variation, and the bending-angle dependence on the programming strain. The multicolor 4D printing of SMPs with complex and multi-color geometries realized the remotely controlled shape changes according to its pre-designed responses to light.<sup>[273]</sup> Further, as reported by Wang, et al., 3D printed objects exhibiting selective photo-responsive SME were based on thermo-responsive SMP with AuNPs as photothermal converter. The transition temperature of acrylated-based SMPs can be easily tuned by adjusting its composition in the printing position. Therefore, multi-materials' printing was utilized to fabricate a light-activated 3D structure with two different T<sub>g</sub>s, enabling remotely controlled shape actuation.<sup>[285]</sup>

## 5. Functions

### 5.1. SMEs

Shape-memory material is capable of deforming into a desired temporary form or structure under the external stimulus, such as heat, stress, or light, and fixing the shape after the stimulus is removed. The recovery process can be activated by the corresponding stimulus and makes the material great potential as an intelligent tunable device for a wide range of applications. In the optical field, a thermo-responsive SMP-based color-changing system can identify the temperature or other fields in a remote control manner by exhibiting the corresponding visual color, representing the physical quantity of temperature or other energy. Because of its outstanding unique properties, extensive research has been carried out on SMPs for optical property control.

#### 5.1.1. One-Way SME

The programming can introduce diverse possibilities for creating micro/nanophotonic structures that can perform optical wave-front shaping, which can dynamically switch between different optical effects, such as altering beam-power distribution, transmittance, and color. Most SMPs employed have a one-way SME and can be triggered once after programming, thus only satisfying the need for single-use purposes. Though shape change cannot be reversibly returned by altering the stimulus, the effect can be reactivated by re-programming. Different micro/nanophotonic structures can be programmed in a subsequent cycle, leading to diverse effects and rewritable properties. To achieve feasible re-programming, materials that can deform

**Figure 19.** I) Photograph series of selective shape recovery demonstration experiment. The NIR light of 980 nm was irradiated onto EVA/Nd(TTA)<sub>3</sub>Phen first before it was moved to trigger the shape recovery of EVA/Yb(TTA)<sub>3</sub>Phen. The EVA/Nd(TTA)<sub>3</sub>Phen was finally exposed to the NIR light of 808 nm. Reproduced with permission.<sup>[33]</sup> Copyright 2017, Elsevier. II) Shape deformations of a conjoined specimen consisting of five photo-responsive polymers upon different irradiation sequences. Reproduced with permission.<sup>[43]</sup> Copyright 2018, Elsevier. III) Photographs of a wavelength-controlled stage constructed from accordion legs of GNR-TPU (left leg) and GNS-TPU (right leg). Reproduced with permission.<sup>[283]</sup> Copyright 2023, American Chemical Society. IV) Assembled PAEK-ABZ, PAEK, and PAEK/CA components into a whole construction. Reproduced with permission.<sup>[44]</sup> Copyright 2022, Elsevier. V) Preparations of tri-layer light responsive films composed of EVA and rare earth oxides. Reproduced with permission.<sup>[45]</sup> Copyright 2022, Wiley-VCH.

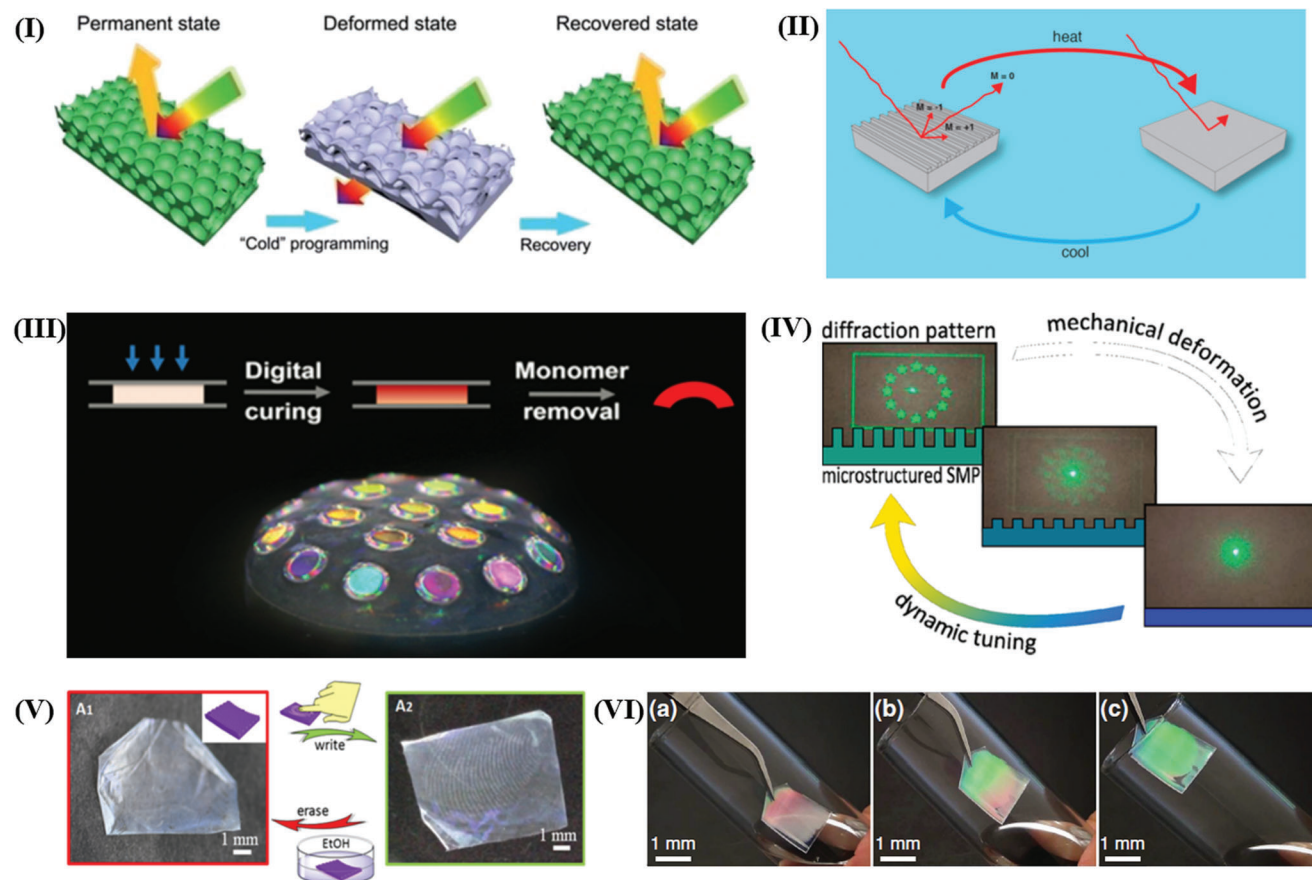


**Figure 20.** I) Schematic illustration of “cold” programming and recovery procedure of one-way SMP-based 3D ordered inverse opal photonic crystal membrane. Reproduced with permission.<sup>[46]</sup> Copyright 2017, RSC Publishing. II) Schematic presentation of dynamic intensity modulation of optical gratings utilizing two-way reversible shape changes. Reproduced with permission.<sup>[286]</sup> Copyright 2015, American Chemical Society. III) Demonstration of potential device applications of the digital SMP that combine multi-SME within a single material construct. Reproduced with permission.<sup>[47]</sup> Copyright 2019, American Chemical Society. IV) Schematic and demonstration of tunable diffractive optical elements fabricated from SMPs. Reproduced with permission.<sup>[48]</sup> Copyright 2016, American Chemical Society. V) Photographs of the sample taken in situ after undergoing the fingerprint process (A2) and its subsequent recovery to the original state (A1) after drying out EtOH. Reproduced with permission.<sup>[288]</sup> Copyright 2018, American Chemical Society. VI) Photos presenting a microporous SMP membrane placed to acetone vapor over liquid acetone at various positions. Reproduced with permission.<sup>[289]</sup> Copyright 2015, Wiley-VCH.

and be fixed at low temperature is favorable for applications. For example, Ji et al reported a novel type of shape-memory retroreflective structural color film that is reusable and rewritable based on its one-way SME and reprogrammability.<sup>[57]</sup> The film can be constructed with any customized patterns during each writing cycle and presented no change in performance after programmed and recovered 20 times, indicating excellent reusability. As another example, established on capillary “cold” programming induced by capillary pressure, Niu et al. reported reconfigurable 3D photonic crystal membranes using heat-triggered recoverable SMPs, which have optical bistability that presents two reversibly tunable stable equilibrium states (Figure 20I).<sup>[46]</sup>

### 5.1.2. Two-Way SME

Although reprogrammability of one-way SME can support the reusability of the material, it often requires external intervention or specific conditions to reset the material, making recon-

figuration more complex and time-consuming. The irreversibility of the conventional shape-memory process needs to be overcome to broaden the functionality of SMP-based optical devices. Recently revealed two-way shape-memory materials that can perform reversible shape reconfiguration between two certain conditions are of great interest to this concern. It has been reported that the intensity modulation of a diffraction grating has been accomplished by two-way reversible shape-memory actuation (Figure 20II). The reversible change in the diffraction intensity attained a maximum value of 36% and can be repeated over several cycles.<sup>[286]</sup> In such cases, reversible SMP normally contains a highly crystallizable component that prompts reversible shape changes by crystallization-induced elongation and melting-induced contraction. The shape reconfiguration is highly rely on the crystallization process, limiting the reversibility (up to  $\approx 20\%$  of strain) and the dynamics, where actuation takes at least several seconds. Unlike the shape change in one-way SME that can remain even after removing certain stimuli, the two shapes in reversible SME may only remain at certain condition (e.g., high



or low temperatures). It should be also noted that crystallization may interfere with the confinement of a grating at the nanoscale, resulting in a rough surface structure of semicrystalline polymers. The relationships between crystallite size and scattering effects should be considered and further studied.

### 5.1.3. Multi-Shape SME

Multi-shape SMP is favorable in the creation of 3D nano-phonic and electronic devices capable of unconventional shape-shifting. Besides creating structures that rely on traditional molding and machining techniques, complex shapes can be created by combination of SMPs with 3D printing. Zhang et al. developed a digital 4D printing strategy that allows the fabrication of complex 3D SMP with a tunable shape-memory response by controlling the printing constraints. The technique benefits from its ability to print designable 3D shapes in a fast manner, as well as its flexibility to incorporate multi-SME within an identical material structure using a single precursor (Figure 20III).<sup>[47]</sup> The digital SMP was demonstrated to provide unique advances for nano-photonics by replicating nanostructured 2D silicon wafers and transforming them into 3D photonic devices. It is a versatile approach to manipulate the nanostructure into a more complex conformation through a simple manipulation of the digital light pattern, without requiring any alteration to the template. The digital multi-SMP offers distinctive advantages in the fields of nano-photonics and the development of shrinkable electronics for the next generation.

### 5.1.4. Tunable SME

The programmability of SMP provides an additional valuable processing aspect in producing optical devices by actively controlling the structure of the devices. For example, diffractive optical elements (DOEs) with a wide range of optical applications can be manufactured by several different techniques from various materials with nanometer precision. However, their geometrical shape is fixed after production and a new required structure needs to be fabricated starting from the mold, normally with successive steps. To maximize the applicability of designed DOEs, SMP can be used to resolve the abovementioned issue, because programmable and recoverable shape changes can be utilized to actively regulate the diffractive structure of devices, enabling precise manipulation. Schauer et al. employed transparent, biocompatible, thermoplastic polyether urethane to create DOEs with varied diffractive microstructures using hot embossing. The ability to tune the diffractive optical element was achieved by introducing a second, temporary shape that is programmed through mechanical deformation at low temperatures. Accurate temperature control enables precise manipulation of both the switching speed and recovery ratio, resulting in a height tunable and a period tunable structure that can be used as tunable beam splitters and shapers, waveguide grating couplers where rapid actuation and wavelength regulating on the smallest areas are required (Figure 20IV).<sup>[48]</sup> As another example, Moirangthem et al. reported a photonic SMP film that exhibits a broad range of structural colors, ranging from blue to orange. This was achieved by

gradually recovering from mechanically embossed photonic film to its original shape upon heating through a broad thermal transition, resulting in a large color response of  $\approx 155$  nm over a wide temperature range.<sup>[287]</sup>

### 5.1.5. Multi-Stimuli-Responsive SME

Besides thermos-responsive SMPs, materials that can be triggered by multi-stimuli may enable sensitive colorimetric and/or spectroscopic detection of a wide range of biological and chemical analytes, such as proteins, glucose, metal ions, alcohols, and water. For example, the above-mentioned work from Quan et al. also observed that the shape-memory function of their material can be triggered by ethanol other than temperature (Figure 20V).<sup>[288]</sup> A similar principle has been also applied to other solvents to achieve novel acetone vapor-responsive shape-memory photonic crystals (Figure 20VI).<sup>[289]</sup> Later on, a novel type of chromogenic photonic crystal sensor based on SMPs has been reported, which allows for the selective detection of various swelling analytes (such as ethanol, acetone, and dichloromethane) in non-swelling solvents like gasoline and water.<sup>[56]</sup> Such multi-stimuli-responsive SMP are of great technological importance in creating sensors with a wide spectrum of applications ranging from environmental monitoring to process/product control in chemical, petroleum, and pharmaceutical industries.

## 5.2. Shape Reconfiguration Categories

In nature, many animals exhibit structural colors that result from specific optical processes of photonic crystals, including diffraction, interference, scattering, and others. With the rapid development of fabrication techniques, a wide variety of structural color materials are now available. Here, diverse structures of SMP color-changing materials and their synthetic/fabrication strategies are reviewed.

### 5.2.1. Photonic Crystal Geometries

Photonic crystals are engineered nanostructures with a periodic arrangement of matters on the scale corresponding roughly to the wavelength of visible light.<sup>[290]</sup> They either permit or prohibit the propagation of electromagnetic waves of specific frequency ranges, giving them interesting optical properties and enabling them to confine, control, and direct the light in a photonic chip. The use of diverse photonic crystal structures, including mesoporous 1D Bragg stacks, 2D photonic crystal fibers, 3D inverted photonic crystals, and porous silicon membranes, have facilitated sensitive colorimetric and/or spectroscopic recognitions.<sup>[291]</sup> Due to their exceptional properties, photonic crystals have great potential for a wide range of applications, including gas sensing, optical filters, inkless printing, photonic papers, and reflective flat displays. Through the slow-light effect, photonic crystals can significantly enhance the interaction between light and matter, providing reinforced interaction in terms of duration and intensity. This indicates that photonic crystals are suitable candidates for applications as chemical and biological sensors. The optically

bistable states of currently available tunable photonic crystals offer a unique opportunity to create rewritable and reconfigurable optical devices.

The photonic band gap, and thus the corresponding color in photonic crystals can be adjusted and tuned by changing the diameter, distance, and/or arrangement of the constituent spheres.<sup>[292,293]</sup> Espinha et al. introduced innovative photonic nanostructures using thermos-responsive SMPs.<sup>[294]</sup> By imprinting a surface nanopattern on shape-memory polydiolcitrate elastomers, novel materials were synthesized with programmable optical properties that can be changed or temporarily eliminated by external stimuli (Figure 21I). The versatility of these materials increases their applications in a wide range, including sensing, regenerative medicine, and photonics. Besides surface nanopatterns, Li et al. proved remarkable color switching in SMP membranes with a hexagonal array of micron-sized circular holes utilizing mechanical instability and pattern reconfiguration (Figure 21II).<sup>[295]</sup> Specifically engineered core-interlayer-shell polymer microspheres have been used to assemble 3D-ordered elastomeric polymer opal films, which exhibit reversible and tunable photonic band gaps that can be triggered by heat, light, and mechanical strains. Fang et al. reported a versatile templating method for creating thermos-responsive 3D macroporous SMP photonic crystals with optically bistable states (Figure 21III).<sup>[296]</sup> The approach can be applied to a wide range of functional SMPs, as long as they can withstand the template removal process, which involves a short hydrofluoric acid wash to remove the templating silica colloidal crystals. Additionally, the 3D macroporous SMP photonic crystals present stronger diffractive effects than 2D surface gratings due to their larger surface area and higher crystalline qualities. Besides, the transition between a 3D-ordered permanent state and a disordered temporary state triggered by heat leads to a noticeable changes in color and significant variations in their optical responses. In addition, the 3D photonic crystal structure offers a straightforward and precise optical technique to quantitatively analyzing the fascinating SMEs at the nanoscale.

Further efforts were carried out to achieve SMP photonic structures that can be alternated by other stimuli other than temperature. Fang et al. reported a series of SMPs with unusual 'cold' programming and instantaneous shape recovery capabilities activated by a contact pressure at ambient conditions.<sup>[297]</sup> Besides, the combination of photonic crystal and SMP technologies allows for the creation of reconfigurable photonic crystals, while also providing a straightforward and sensitive optical method for studying the fascinating SMEs at the nanoscale. The principle was further developed with a single-step direct writing technique for making reconfigurable/rewritable optical devices at the nanoscale (Figure 21IV).<sup>[298]</sup> The original macroporous photonic crystal lattices can be recovered at ambient conditions through direct writing using either macroscopic or nanoscopic tools, such as a pencil or a nanoindenter. Besides pressure-responsive, a novel type of SMP that is responsive to vapor was developed, which allows unconventional "cold" programming and instantaneous shape recovery at the nanoscale.<sup>[289]</sup> The highly ordered photonic crystal structure can rapidly recover from its temporary disordered configuration when triggered by multiple stimuli, including various vapors and solvents, heat, and microwave radiation.<sup>[299]</sup> Hsieh et al. developed a method to

engineer free-standing and flexible macroporous shape-memory photonic crystals, which exhibit high extensionality of up to 70% (Figure 21V).<sup>[300]</sup> It is worth noting that the macroporous film can retain its stretched structure as a temporary state without requiring any external contact force. Its original configuration and appearance can be instantaneously recovered under ambient conditions by inducing capillary pressures through the evaporation of ethanol. Ni et al. describe a novel type of polymer shape-memory photonic crystal (PSMPC) that exhibits autonomous programming of its microstructure through Laplace pressure as well as elastic modulus-dependent behavior, and shape-memory recovery triggered by solvent swelling, all of which occur at room temperature. The PSMPCs' elastic moduli could be systematically modulated by varying the compositions of their constituent polymers, resulting in different photonic bandgaps (i.e., diffractive colors) in response to various solvents, such as water, ethanol, and acetonitrile.<sup>[301]</sup> Wang et al. presented a novel SMP-based photonic crystal paper with multiple stable states, which exhibited several colors that could be controlled by heat or NIR irradiation to manipulate the deformation and recovery of their periodic microstructures with varying degrees.<sup>[302]</sup> Besides the one-way effect, Quan et al. developed a smart film containing poly(vinylidene fluoride-co-hexafluoropropylene) (PVDF-HFP) inverse opals together with bulk PVDF-HFP and its microscopic structure characteristic of shape-memory was simultaneously studied by scanning electron microscopy (SEM).<sup>[288]</sup> The materials exhibit a thermo-sensitive micro-shape-memory property together with reversible and modulated optical properties. It triggers a promising way toward designing reversible micro-deformed actuators. Though the combination of photonic crystals and SMP have been successfully carried out in various research, large-scale fabrication remains a big challenge, making the practical application difficult. Wu et al. reported novel scalable SMP photonic crystal films with both mechanochromic and thermochromic properties, which are prepared by a simple hot-pressing technique and subsequent photocuring process, resulting in freestanding polymer films with large-area.<sup>[303]</sup> The films are highly flexible and mechanically strong, and possess an excellent structural color that can be altered by stretching, similar to the color change ability of chameleons in response to their surroundings.

## 5.2.2. Gratings

With the advancements in optical technology, smart optics or micro-optical devices such as smart diffraction gratings have become essential for the new generation of optical devices as they can be externally stimulated to achieve beam splitting of incident light.

According to Bragg's law, the comparable  $\lambda$  and  $d$  produce a small value of  $n$ , in which case the photonic crystals display an excellent structural color. The period of grating is tunable by altering the angle between double beams.

1D gratings exhibit higher reflectivity and color saturation compared to 2D and 3D photonic crystal structures due to the strong interference of reflected light. Most of the research in this area has focused on inorganic materials as metals, which are difficult to modify optical properties without changing their

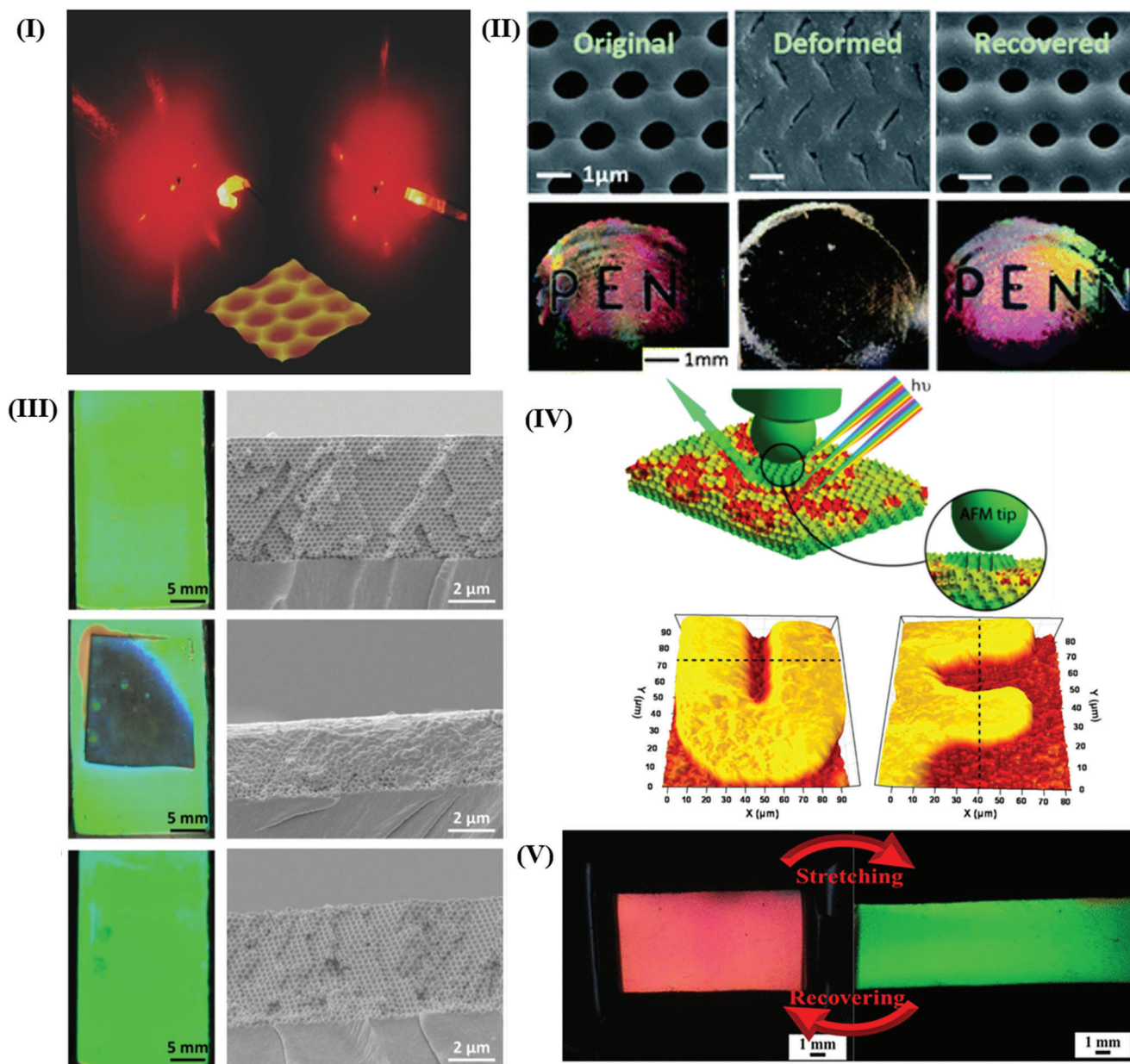


**Figure 21.** I) SMP membranes comprising a hexagonal arrangement of circular holes with micron-sized diameters showing different diffraction images between programmed and recovered states. Reproduced with permission.<sup>[294]</sup> Copyright 2014, Wiley-VCH. II) SEM and optical images presenting the display of “PENN” embedded in a 2D SMP membrane at the original, programmed, and recovered states. Reproduced with permission.<sup>[295]</sup> Copyright 2012, Royal Society of Chemistry. III) Photos and SEM images illustrating the noticeable changes in both the reflective colors (left) and nanostructures (right) during thermal-triggered programming and recovery steps of a microporous copolymer membrane with 300 nm macropores. Reproduced with permission.<sup>[296]</sup> Copyright 2015, Wiley-VCH. IV) Schematic illustration of the direct writing using AFM tip, showing the interaction on a macroporous SMP membrane with collapsed macropores. AFM height images of the resulted microscopic 3D photonic crystal patterns (letters “U” and “F”). Reproduced with permission.<sup>[298]</sup> Copyright 2015, American Chemical Society. V) Photographic images of the microporous SMP film prepared from 370 nm silica colloidal crystals as a template, changing between stretched state of 50% elongation, and a recovered state. Reproduced with permission.<sup>[300]</sup> Copyright 2020, American Chemical Society.

preparation process, but there is growing interest in developing smart diffraction gratings using organic and polymeric materials. LC materials can be used to prepare adjustable diffraction gratings, but their poor tensile properties typically limit the ability to modulate the period of the diffraction grating. More recently, SMPs have emerged as a promising material for prepar-

ing tunable diffraction gratings due to their unique properties such as SME, flexibility, and tenability. Several structural color materials and their thermo-responsive behaviors have been developed, though some open and important problems still exist in their efficient fabrication and application. The critical concern in preparing grating structures based on SMPs is achieving high



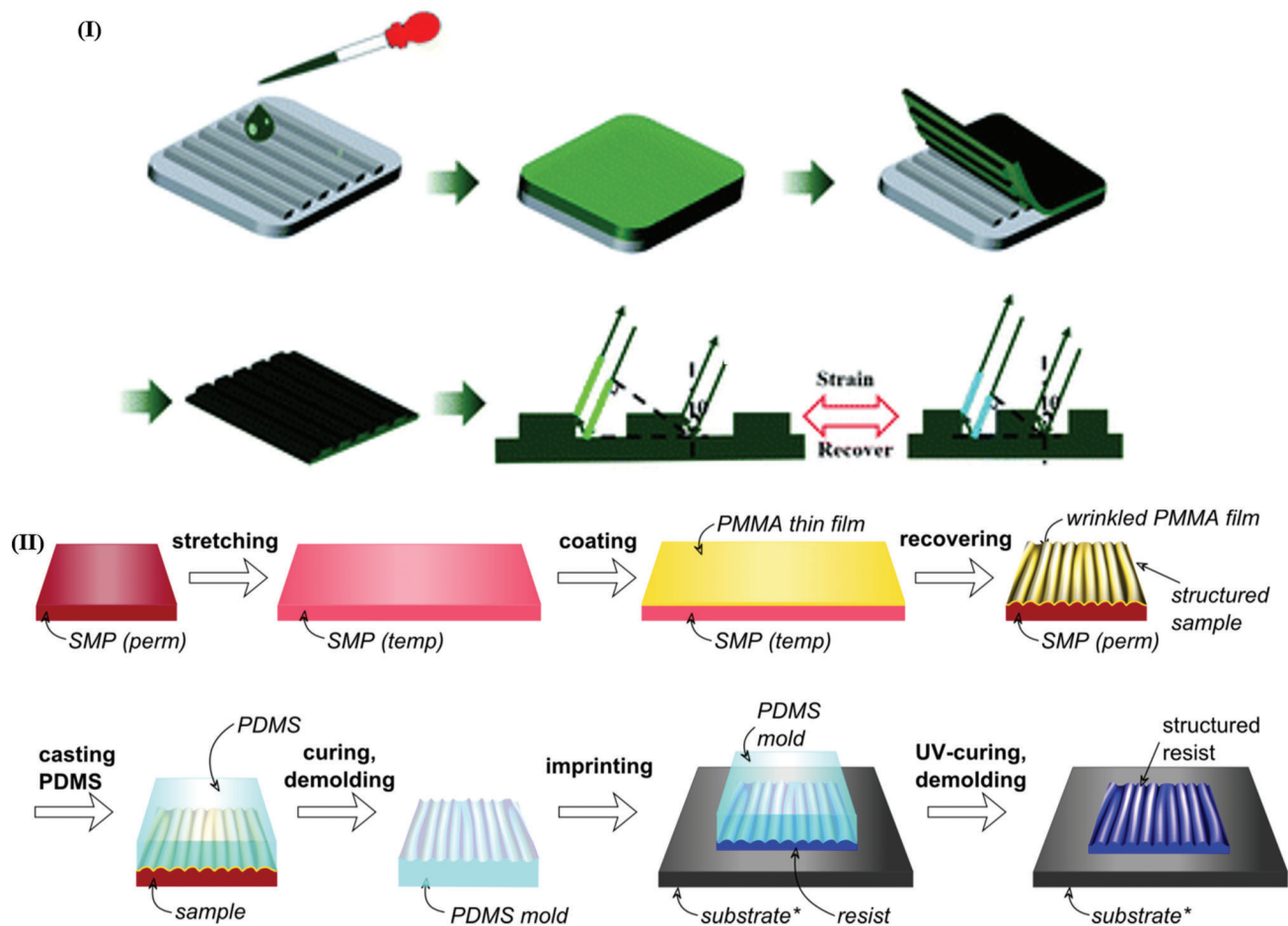


**Figure 22.** I) Fabrication of nano-patterned SMP, structural color exhibiting angle and deformation dependence. Reproduced with permission.<sup>[304]</sup> Copyright 2022, Royal Society of Chemistry. II) A schematic show of the process to fabricate and replicate disordered diffraction gratings. Reproduced under the terms of the OSA Open Access Publishing Agreement.<sup>[307]</sup> Copyright 2018, Optical Society of America.

precision (on micro/nanoscale) ordered structures on the surface of the SMPs. The continuous adjustment of structure color, especially across the entire visible wavelength range on a single sample, remains a significant challenge. The precise manipulation of micro- or nano-structure periods enables the achievement of the desired color covering the whole wavelength range. Besides, the brightness and saturation of structural color need to be further improved. Here, different strategies to prepare SMP-based smart diffraction grating are discussed.

**Soft Lithography Pattern:** Defined optical structures such as nano-strips,<sup>[304]</sup> 1D/2D grating micropatterns can be designed and fabricated as a hard template using photolithography methods.<sup>[49]</sup> The SMP films can then undergo a hot embossing process, which allows the diffraction grating patterns to be imprinted as nano-scale information onto their surface. (Figure 22I). For example, Li et al. developed a thermal-responsive optical beam-power splitter using a polystyrene film with programmable micropatterns based on SME. The smooth film demonstrates outstanding transparency with 95% transmittance in the visible spectrum and maintain optical stability during a continuous heating up to 90°C. Both sides of the shape-memory polystyrene film can be patterned into erasable

and switchable micro-groove gratings, enabling the transmission light to switch between different designed light divided directions and beam-power distributions based on the changing in optical diffraction effect and demonstrating its application as a beam-power splitter.<sup>[49]</sup>

**Two-Beam Interference:** Smart diffraction gratings based on SMP can be easily fabricated through two-beam interference, a technology that utilizes photopolymerizable materials to efficiently create regular grating on the surface at nanometer scale. It has been reported by Sun et al. that a UV-curable SMPs based smart diffraction grating was developed using two-beam interference method, demonstrating precision at nanometer scale, outstanding deformability and recovery capacity, as well as the tunable spectroscopic performance.<sup>[305]</sup> Because of the excellent stretching performance of the SMP, the structure can be adjusted to a broad range of grating period modifications (45%–380%) via temperature activation with extreme accuracy. Additionally, the fabricated grating displays bright structural colors when exposed to white light and has a long shelf-life. Besides stretching, the grating structure can also be interrupted to an intermediate state by compression against silicon wafer. The diffraction intensity of the intermediate stage can be changed by varying the

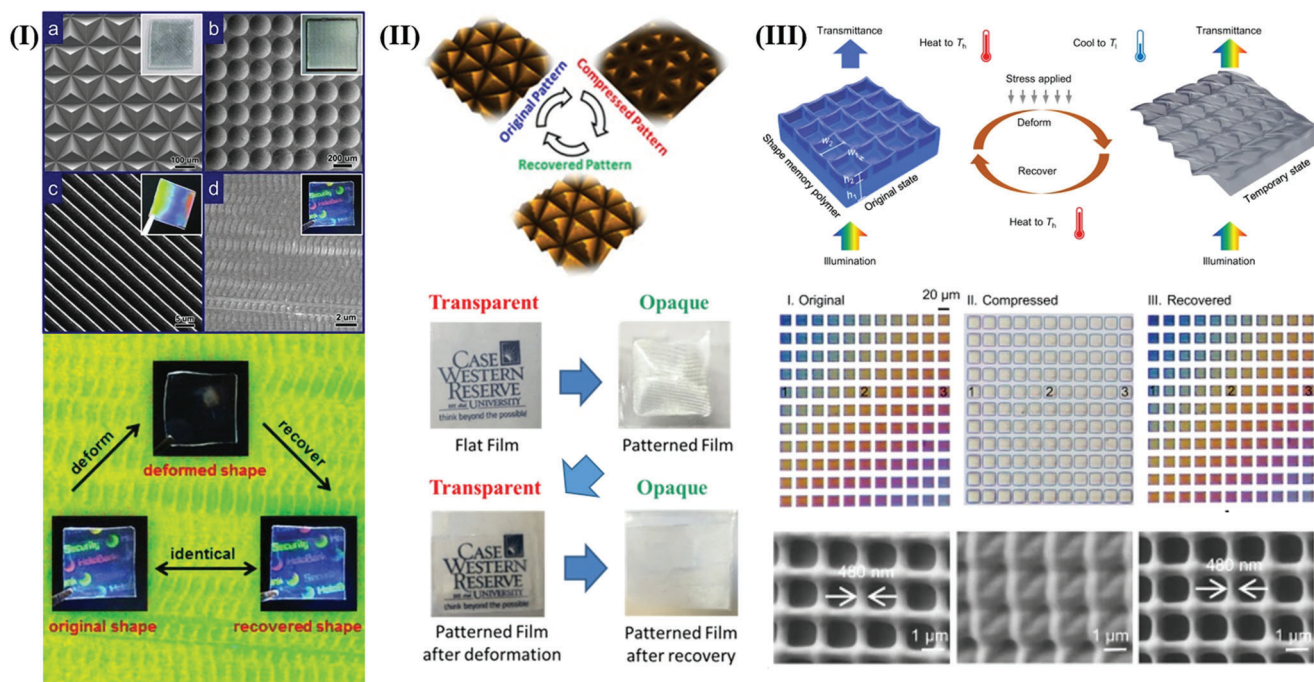


**Figure 23.** I) Top: SEM images and photographs of several micro-optic films, replicated from different microstructured mold: a) a microprism array, b) a microlens array, c) a transmission grating, and d) a white-light hologram. Bottom: photographs of shape deformation and recovery of an SMP hologram. Reproduced with permission.<sup>[51]</sup> Copyright 2013, Wiley-VCH. II) Switchable optical characteristics of PVAc film with micro-prismatic pattern. Top: surface profilometry of the structure memorizing cycle; Bottom: observation of the pattern programming and recovery process of three-step method (first cycle) with a visualizable change in transparency. Reproduced with permission.<sup>[309]</sup> Copyright 2017, Wiley Periodicals. III) Top: schematic showing the shape and color change of an integral nanostructured element of the “invisible ink” that is 3D printed in SMP; Middle: different colors as printed, compressed and recovered respectively, observed by the objective lens at the transmittance mode; Bottom: SEM images of the top surface structures at original, programmed and recovered state Reproduced under the terms of CC BY license.<sup>[52]</sup> Copyright 2021, the Author(s). Published by Springer Nature.

micro/nanograting height.<sup>[306]</sup> Such SMP smart grating has great potential applications in the fields that require high-precision structures.

**Winkle:** Lithography techniques necessitate a long exposure time to pattern designed structures over a limited area. Several groups demonstrate a more fast, highly scalable, and low-cost method to fabricate wrinkle structures using SMP to create localized structural color.<sup>[50]</sup> and disordered transmission grating.<sup>[307]</sup> Xie et al. created surface wrinkles on a SMP substrate-supported metallic film, with a wavelength approaching that of visible lights, thereby producing diffraction colors.<sup>[50]</sup> The control of geometric and spatial distribution of surface wrinkles can enable the capture of a 3D image on a macroscopically flat surface in an arbitrary fashion. It has been shown that more complex surface wrinkle patterns, such as quasi-periodic ones, can function as efficient broadband light extractors in both monochromatic and white organic light-emitting diodes (OLEDs). An all-polymer process can be utilized to introduce quasi-periodic surface wrinkles, which have been demonstrated to improve light harvesting. (Figure 22II). The scalable wrinkling process enables the tuning of the diffraction properties of the structures, making them suitable for various photovoltaic technologies. Disordered diffraction gratings are a type of optical element that has numerous applications. They exhibit controllable optical properties as quasi-periodic structures. At the same time, they are perturbed by structural irregularities, which makes them more effective over

a wider range of spectral and angular frequencies compared to periodic diffraction gratings. These irregularities can impact the grating height and/or period distribution, and can be tailored and introduced either deterministically or stochastically, depending on the intended application. Li et al. developed a versatile method for creating dynamic wrinkles that respond to NIR light by a bi-layer strategy, which use a poly(dimethylsiloxane) elastomer with CNT composite as the substrate and different functional polymeric stiff layers as the top surface.<sup>[308]</sup> Via NIR irradiation, the surface topography of the material can be switched between wrinkled and wrinkle-free states within tens of seconds.

### 5.2.3. 3D structures

Micropatterns can generate different optical properties, such as transparency and light refraction. Xu et al. utilized crosslinked EVA as a semi-crystalline SMP to create programmable, deformable, and shape-memorizing micro-optical devices.<sup>[51]</sup> Various micro-optic elements, such as microlens, holograms, diffraction gratings, and microprism arrays, can be precisely replicated as nano/micro-surface structures on the crosslinked SMP films in a single step via compression molding (Figure 23I). The structures can be further deformed in the programming process, resulting in distinct optical properties, which can be altered when recover to the initial structure. Such process is highly

repeatable and results in excellent reversibility in changing the optical properties. Furthermore, a selective trigger of the surface feature recovery can be achieved by controlling arrays of the transparent resistive microheaters. Similar approach has been also studied on polyvinyl acetate (PVAc) with two different test methodologies to explore the programmability of the patterns.<sup>[309]</sup> The ability to program patterns on the surface of the film, resulting in switchable optical properties between reflective and transparent, has potential applications in creating security information membranes capable of storing and recovering specific information (Figure 23II). Besides, 3D printing is also a powerful tool in creating complex structures with optical properties. Zhang et al. reported a novel type of SMP photoresist based on Vero Clear, which can achieve print features with a resolution of  $\approx 300$  nm half pitch using two-photon polymerization lithography.<sup>[52]</sup> SME can be used to obtain large visual shifts via nanoscale structure deformation on the prints that consists grids with size-tunable multi-colors. When the nanostructures are compressed, the printed information as well as the colors become invisible (Figure 23III). Wang et al. presented a SMP microarray, which is superhydrophobic and can control not only its wettability but also its optical performance. Inspired by the butterfly wings, such smart superhydrophobic SMP microarray is produced by combining methods of 3D printing, replica-molding, and a simple surface treatment.<sup>[310]</sup>

#### 5.2.4. Biomimetic Structure

In nature, there are numerous animals presenting structural color, such as tropical fish, longhorn beetles, gold bugs, butterflies, and chameleons.<sup>[311–315]</sup> Many inspiration came from nature, especially designing structure of functional materials, same in optical properties.<sup>[316]</sup> Nature has developed a wide range of strategies to adapt to survival encounters over millions of years of evolution. For example, cicada wings, glasswing butterfly wings, and hawk moth wings possess hexagonally ordered subwavelength structure arrays that enable them to evade detection by predators. These structure arrays create effective refractive index gradients that suppress optical reflectance and light scattering on transparent insect wings, allowing them to overcome the glare of light while in flight. Researchers have made many biomimetic structural color films by employing nanotechnology to create materials that mimic structural color in living things. The nature of the optical structures that are usually at micro/nanoscale promote the rapid response of SMP surface, which is beneficial for applications. Juhyuk Park et al. developed optical devices that can achieve a high transmittance of light energy based on the antireflection nanostructures mimicking a moth's eye.<sup>[317]</sup> The shape recovery ability can increase the sustainability of the antireflection nanopattern arrays that are mechanical vulnerable as well as induce the sustainable self-cleaning effect. The SMP was synthesized through a tri-copolymerization process, allowing for modulation of the transition temperature to be close to that of the human body, which is beneficial for biomedical applications. For another example, Tseng et al. employed a combination of a colloidal lithography technology and a shear-induced self-assembly approach to develop antireflective structures that are inspired by the dragonfly wings and exhibit omnidirectional

antireflection properties.<sup>[53]</sup> The nonclose-packed inclined conical structures composed of SMPs can be repeatedly deformed and recovered under physical stimuli at ambient conditions, and as a result, the corresponding broadband omnidirectional antireflection function can be erased and restored reversibly (Figure 24I). Recently, inspired by the leafhopper wings, Li et al. utilized self-assembly techniques and SMPs to create a novel reversible antireflection coating.<sup>[318]</sup> The resulting embroidered ball-like structure array creates a transition in refractive index transition on the surface, resulting in omnidirectional antireflective properties across a broadband visible light region (Figure 24II). The reversible omnidirectional antireflective characteristics provide a platform in developing various smart optical devices. Besides mimicking antireflective properties, some research work focused on simulate the tunable color change in nature. For example, Zhao et al. fabricated surface nano-strips and a reflective grating on SMPs to mimic the color-changing ability of chameleons.<sup>[304]</sup> Here, the structural color can be easily tailored by means of uniaxial tension and changed based on the combination of angle-dependency and SME (Figure 24III). As another approach to mimic chameleons, Schauer et al. developed a polymer opal with an embedded SMP in its matrix that can maintain a particular color fixed without continuous stretching or applying other stimuli or energy. The material can also be reprogrammed to other fixed color on demand (Figure 24IV).<sup>[54]</sup> Besides mimicking optical properties, multifunctions was also learned from nature. Wang et al. introduced a novel approach to create superhydrophobic surface by combining 3D printing, replica-molding and a simple surface treatment using SMPs. With the variation in the surface structure, such surface allows for vivid color conversion as well as switchable directional/anti-directional droplet sliding, similar to the wings of a butterfly (Figure 24V).<sup>[310]</sup>

### 5.3. Applications

#### 5.3.1. Sensor

Visualized color changes in structured materials can be widely applied to develop novel and low-cost sensors. Zhang et al. reported submicron 4D printing of SMP that can extend its application to nanophononics. By varying in both width and height of the grid structures at each pixel, an image can be printed and become invisible by compression programming.<sup>[52]</sup> The image can be recovered by heating, and this demonstrate a sensing function that can reveal whether a material has been exposed to high temperatures, which is crucial for transporting delicate products. Such versatile smart label is inexpensive and performs similarly to colorimetric pH papers commonly applied in industries and labs. As a result, it has significant potential for integrated cold chain monitoring, from manufacture to transport, storage, and final delivery to end-users as shown in Figure 25I).<sup>[303]</sup> Beside temperature sensors, Leo et al. reported a novel SMP-based chromogenic photonic crystal sensor that enables the selective detection of several swelling analytes (e.g., acetone, ethanol, and dichloromethane), as mentioned in multi-stimulus SME.<sup>[56,319]</sup> Their research suggests that this concept could be modified to detect a diverse range of other substances, including benzene, toluene, xylene and formaldehyde in both aqueous and



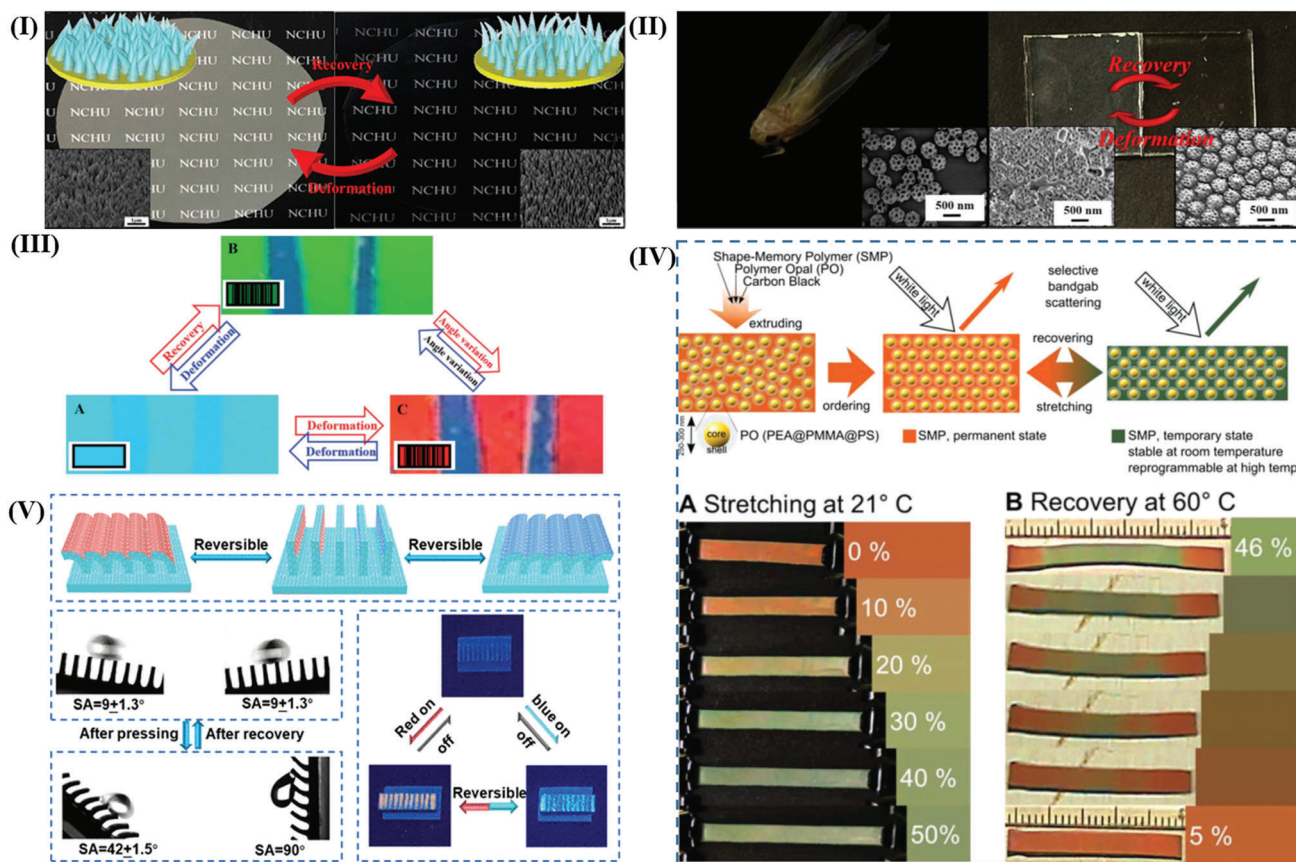


**Figure 24.** I) Schematic show of nonclose-packed inclined conical structures composed of SMPs and photographic images of structured film that can be repeatedly deformed and recovered to alter the corresponding broadband omnidirectional antireflection functionality. Reproduced with permission.<sup>[53]</sup> Copyright 2020, American Chemical Society. II) Left: photograph of a yellow leafhopper under natural lighting and its magnified SEM image; Right: SEM images and photograph of a polymer substrate top surface with close-packed embroidered ball-like textures at deformed and recovered states. Reproduced with permission.<sup>[318]</sup> Copyright 2021, Elsevier. III) A schematic presentation of the product code in hidden (A) readable (B) states, showing color evolution combining angle-dependent effect (B to C) and the SME (A to B). Reproduced with permission.<sup>[304]</sup> Copyright 2022, Royal Society of Chemistry. IV) Top: schematic representation of the manufacturing process used to create opal samples with different contents of SMP; Bottom: demonstration of the continuous color change of SMP opal sample with 15 wt% SMP. Reproduced with permission.<sup>[54]</sup> Copyright 2018, Wiley-VCH. V) Schematic illustration (top) and function demonstration (bottom left: changing in wettability, bottom right: activation and alteration in color) of the microstructure to mimic butterfly wings. Reproduced with permission.<sup>[310]</sup> Copyright 2020, American Chemical Society.

nonaqueous solutions. The work holds significant promise for a broad range of technological applications, such as environmental monitoring, process and product control in chemical, petroleum, and pharmaceutical industries (Figure 25II).

### 5.3.2. Smart Display

The SMPs are used in smart no-ink display application to enable the reversible tuning of the display in terms of shape and color in response to external stimuli. Li et al. developed a bilayer system consisting of a CNT-containing polydimethylsiloxane (PDMS) substrate and various responsive polymer layers, which exhibited a dynamic wrinkle pattern with excellent reversibility and sensitive response to NIR-light. The CNT-PDMS substrate enabled regulation of the applied strain through NIR-induced thermal expansion, facilitated by the efficient photon-to-thermal energy conversion of CNT. As an initial demonstration of its potential ap-

plications, this type of NIR-driven dynamic wrinkle pattern was used in dynamic smart no-ink displays and dynamic information record. As an example, the sample using photosensitive materials as the skin layer may present a positive letter “S” when exposed to 365nm UV light using a photomask. The information could be removed by converting the surface into fully wrinkled surface and write other information such a negative letter “T” by selectively dedimerization using 254nm UV light with another photomask (Figure 25III).<sup>[308]</sup> Besides photomask patterning, Zhang et al. reported a material and process concept that enables the digital fabrication of SMP with precise control over both its geometries and the shape-memory properties.<sup>[47]</sup> The use of digital light modulation introduces spatiotemporal tuning of the material characteristics, such as the shape-memory switching temperature, rubbery modulus, and the maximum elongation (up to 250%). The unique attribute of spatiotemporal tuning of material properties has been demonstrated to be beneficial in assembling unusual shape-shifting 3D nano-photonic and electronic devices.

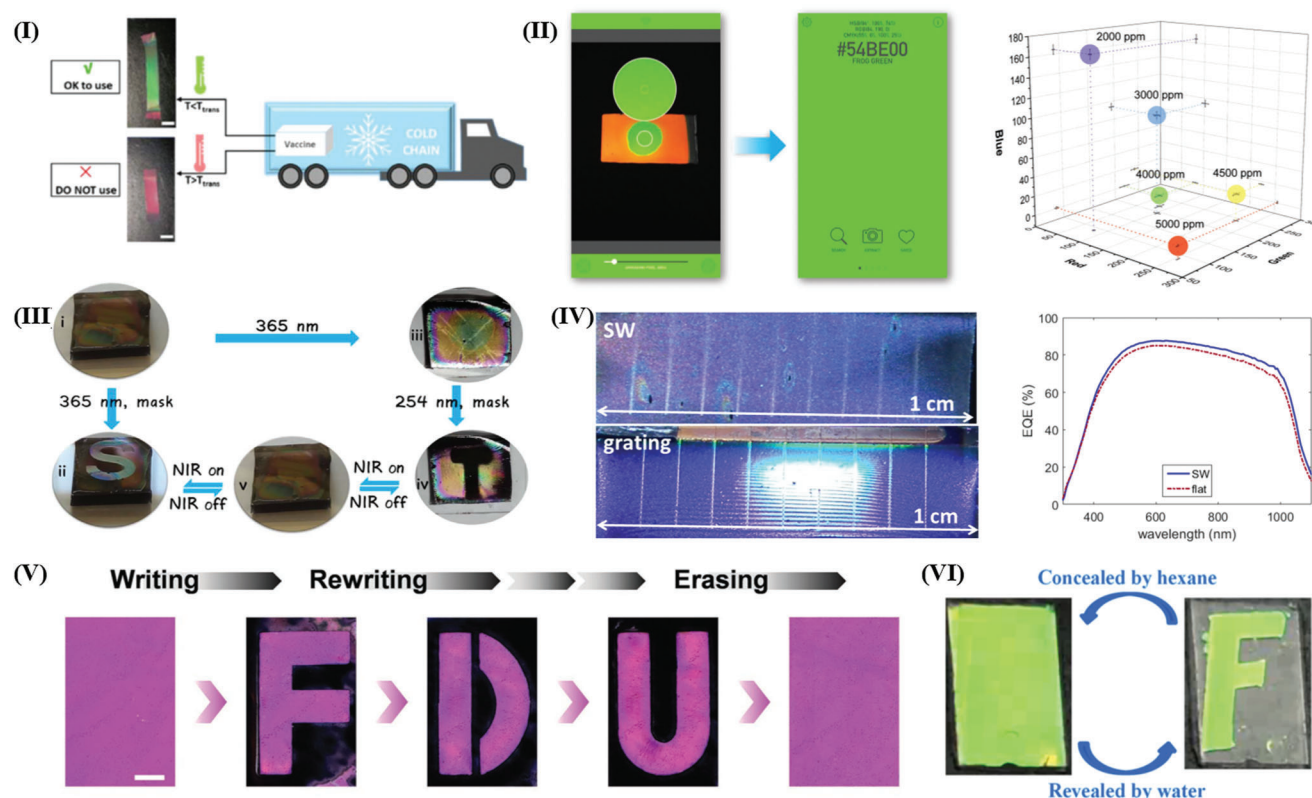


**Figure 25.** I) A schematic display of the color change in SMP film that can be applied as the smart label for checking cold chain storage. Reproduced with permission.<sup>[303]</sup> Copyright 2019, RSC Publishing. II) Left: screenshots of the Color Mate app interface displaying a macroporous SMP membrane with the central zone recovered into green color by 4000 ppm ethanol in TruFuel, and its corresponding Hex color code. Right: mean RGB values and the corresponding standard deviations projected on each plane obtained from a microporous SMP sample that was “cold”-programmed and subsequently recovered by ethanol-TruFuel solutions with varied concentrations. Reproduced with permission.<sup>[56]</sup> Copyright 2018, Wiley-VCH. III) Photographic illustration demonstrating dynamic information recording through controlled wrinkle formation using distinct photomasks. Reproduced under the terms of CC BY-NC 4.0.<sup>[308]</sup> Copyright 2018, the Author(s). Published by AAAS. IV) Left: the photographs show that the cells covered by wrinkles (with a pitch of 1:30  $\mu\text{m}$ ) have a low disability glare potential, compared to periodic diffraction gratings (with same pitch) observed under the same conditions (viewing angle  $\approx 50^\circ$ ). Right: the corresponding external quantum efficiency is shown. Reproduced under the OSA Open Access Publishing Agreement.<sup>[307]</sup> Copyright 2018, Optical Society of America. V) Rewriting different patterns on the 14  $\mu\text{m}$ -shape-memory retroreflective structural color film. Scale bar: 5 mm. Reproduced with permission.<sup>[57]</sup> Copyright 2021, Wiley-VCH. VI) Photographs displaying noticeable variations in structural colors observed from a macroporous SMP photonic crystal membrane while conducting anticounterfeiting procedures. Reproduced with permission.<sup>[58]</sup> Copyright 2019, American Chemical Society.

### 5.3.3. Energy Storage

The optical structures can be applied to achieve energy storage by creating photovoltaic light harvesting coatings. Schauer et al. developed an all-polymer process to introduce quasi-periodic surface wrinkles, which can improve light harvesting.<sup>[307]</sup> The quasi-periodic surface wrinkles demonstrate superior light-harvesting properties compared to periodic gratings produced via laser interference lithography. The planar heterojunction c-Si solar cells with wrinkle-based transmission gratings were tested and it was found that the short-circuit current density increased by up to 4.8% under normal incidence (Figure 25IV).<sup>[56]</sup>

### 5.3.4. Information Rewriting

Rewritable papers offer a promising environmentally friendly alternatives for information delivery, with the potential to re-

duce the excessive use of conventional papers that cause major environmental problems. Photonic crystals, in particular, have been shown to be a promising technology for developing such rewritable papers.<sup>[320]</sup> For example, Ji et al. created a novel retroreflective structural color SMP film capable of displaying excellent monochromatic, polychromatic, complex, and stitched patterns, depending on the customized templates.<sup>[57]</sup> The “two-template” method was employed to fabricate the film, utilizing the mechanisms of retroreflection and interference in combination with total internal reflection. The excellent reusability and rewritability were demonstrated up to 20 cycles with stable performance and making the film promising in practical application as rewritable photonic papers (Figure 25V). Besides regular mechanical deformation, Wang et al. reported a new rewritable photonic crystals paper based on laser-programmable SMP that can be facily written on using NIR light, without requiring any additional inks.<sup>[302]</sup> Diverse nanoscale stable configurations can be induced and thus create multiple colors. These images that are written/copied onto

the paper not only have the capability to be erased/rewritten over 50 times but also can be stably stored for more than six months. Niu et al. developed highly stable rewritable photonic patterns using PSMPC made of PEGDA and PU acrylate.<sup>[321]</sup> The patterns were programmed through direct pressure and could be rewritten multiple times. The material exhibits high optical reversibility, high spatial resolution, outstanding stability, and room temperature programmability via direct pressure. Xie et al. developed a nanocomposite-based ink-free rewritable paper that combines the latest advances in photonic crystals, SMPs, and electroactive polymers. This novel technology offers the benefits of paper as a long-term data storage medium that requires zero-energy, while also providing the additional benefit of rewritability.<sup>[322]</sup> Such nanocomposite can store high-fidelity color images without inks, which can be rewritten over 500 times without any degradation and remain stable over a year of storage in ambient conditions. The authors also demonstrated a seven-segment numerical display using the ink-free rewritable nanocomposite paper. In future studies, the polymer matrix should be improved, enabling photonic paper with full-color range.

### 5.3.5. Anti-Counterfeiting

The use of structural colors for anticounterfeiting is a well-established and reliable market-proven technology.<sup>[323]</sup> Structural color materials have been crucial for manipulating photons on the nanoscale and have played a significant role in enhancing security measures in the information era. The involvement of SMP enhances the ability to conceal and reveal more complex information, making them an excellent candidate for anti-counterfeiting applications. The desired color can be easily tailored by changing the deformation during the programming step. The precise control and manipulation of structural color is essential for the successful implementation of anti-counterfeiting measures. For example, Leverant et al. presented a novel reconfigurable coating for anticounterfeiting purposes by combining the working principles of SMPs and photonic crystal.<sup>[58]</sup> In this case, other than thermal activation, the iridescent pattern can be hidden and displayed by immersing in common household liquids (e.g., water and ethanol), thanks to the use of a shape-memory copolymer consisting of PEGDA and ethoxylated trimethylolpropane triacrylate (Figure 25VI). As another example, Li et al. produced multi-layer films with alternating layers of PVAc and PU having micro-scale patterned surfaces, including a sharp micro prismatic pattern and a smooth microlens pattern.<sup>[324]</sup> The changeable surface microstructures, programmed by compression and recovered by temperature, enable the corresponding optical property of the film to be switched, which can be utilized as an effective anti-counterfeiting feature in packaging.

## 6. Conclusion

Light plays a crucial role in the development and application of SMPs. With its unique properties and abilities to interact with polymers, light can be used for structural characterization, precise preparation of original shapes, non-contact stimuli sources, and tuning of SMPs' optical properties. The integration of light

into SMP research has greatly expanded the scope of these materials, allowing for their use in a wide range of applications.

In the first section of this paper, we discussed the various optical and spectroscopic approaches used to gain insights into the structure-property relationships of SMPs. Techniques such as X-ray scattering, reflection and absorption, UV-vis spectroscopy, fluorescence spectroscopy, IR and Raman scattering spectroscopies, and Brillouin spectroscopy provide valuable information about the molecular structures and orientations of SMPs. These techniques are essential for understanding the behavior of SMPs during the shape-memory process, and for developing new SMP materials with tailored properties.

In the second section, we explored how light can be used to build SMPs. Different photochemical reactions were discussed, including irreversible and reversible photo-crosslinking reactions, which can be used to create permanent and temporary shape networks. Various 3D photocuring technologies were also introduced, along with their characteristics and applications. By using advanced processing technology combined with SMPs, 4D printing has been made possible, enabling the digital design and manufacturing of smart materials.

In the third section, we examined how light can be used to trigger the shape change of SMPs. Photothermal fillers at the micro-/nanoscale can be used to create SMPCs that can present wide spectrum absorption. The dispersion of fillers in SMPCs is critical to ensure good thermal conductivity and mechanical property reinforcement. Organic functional groups and inorganic fillers can present selective absorption toward light with unique wavelengths, and the assembly of SMPs and SMPCs with such absorption units can realize the control of multiple shape changes upon light irradiations.

Finally, in the fourth section, we discussed how SME can be used to tune the optical properties of SMPs. Different types of SMEs were introduced, along with their unique functions for controlling optical properties. Various structures of SMP color-changing materials and their synthetic strategies were discussed, based on different working principles, including photonic structures, wrinkles, 3D structures, and biomimetic structures. The deformation-induced alteration in optical properties was also discussed for each structure. The precise control of optical properties using SMPs can be applied in various fields, such as sensors, rewritable paper, energy harvesters, and anti-counterfeiting.

In summary, light has become an indispensable tool in SMP research, enabling the precise control of SMP properties, structures, and functions. The integration of light-based techniques and stimuli into SMP design and application has opened up new avenues for SMP development, making them highly versatile and adaptable materials with wide-ranging applications.

In the future, there is a lot of potential for further research and development in the field of light and SMPs: (1) The developing equipment for in situ characterization of polymer aggregate structures, including orientation, crystallization, deorientation, melting, etc., under various stimulating environments can further accurately capture the structural evolution during the SMP deformation process; (2) Starting from an application-oriented perspective, design and synthesize irreversible/reversible photo-crosslinked network structures that meet application requirements, develop more advanced processing equipment, and achieve more precise preparation of the initial structure, enabling



optical manufacturing at the micro and nano scales; (3) There is a need to Design and develop photo-thermal fillers with stronger photo-thermal response to achieve shape changes of SMP under lower light conditions, as well as develop photo-thermal fillers with shorter absorption bands to enable the assembly of more characteristic wavelength units and achieve more complex shape changes; (4) It is also necessary to further achieve precise control of reversible structural changes at the micro-nanoscale to achieve precise adjustment of optical properties, and clarify the relationship between SME and surface tension for developing the next generation of intelligent optical devices.

## Acknowledgements

L.F. and Y.L. contributed equally to this work. This work was sponsored by the Jiangsu Agricultural Science and Technology Innovation Fund (CX(2021)3103 and CX(2022)2024). This work received financial support from the Priority Academic Program Development of the Jiangsu Higher Education Institutions (PAPD) was gratefully acknowledged. This work was financially supported by the Helmholtz Association through program-oriented funding.

## Conflict of Interest

The authors declare no conflict of interest.

## Keywords

characterization, light, optical properties, shape-memory polymers, stimulus, synthesis

Received: April 27, 2023

Revised: July 10, 2023

Published online: August 25, 2023

- [1] N. Liu, G. Sun, S. Gaan, P. Rupper, *J. Appl. Polym. Sci.* **2010**, *116*, 3629.
- [2] R. Razeghi, F. Kazemi, N. Nikfarjam, Y. Shariati, B. Kaboudin, *Eur. Polym. J.* **2021**, *144*, 110195.
- [3] B. Wenn, A. C. Martens, Y. M. Chuang, J. Gruber, T. Junkers, *Polym. Chem.* **2016**, *7*, 2720.
- [4] Y. Li, S. Wu, Q. Liu, J. Xie, H. Li, Y. Dai, C. Li, S. Nie, W. Song, *Polym. Test.* **2019**, *75*, 64.
- [5] A. K. Rodriguez, B. Mansoor, G. Ayoub, X. Colin, A. A. Benzerga, *Polym. Degrad. Stab.* **2020**, *180*, 109185.
- [6] T. Sai, S. Ran, Z. Guo, H. Yan, Y. Zhang, H. Wang, P. Song, Z. Fang, *Chem. Eng. J.* **2021**, *409*, 128223.
- [7] J. Jelken, C. Henkel, S. Santer, *Appl. Phys. B* **2020**, *126*, 1.
- [8] T. Ullsperger, Y. L. Wencke, B. Yuerekli, G. Matthaues, M. Rettenmayr, G. A. Luinstra, S. Nolte, *Mater. Des.* **2021**, *210*, 110048.
- [9] Y. Yamauchi, T. Kigure, K. Isoda, T. Niino, *Addit. Manuf.* **2021**, *46*, 102219.
- [10] P. T. Mather, X. Luo, I. A. Rousseau, *Annu. Rev. Mater. Res.* **2009**, *39*, 445.
- [11] C. Liu, H. Qin, P. Mather, *J. Mater. Chem.* **2007**, *17*, 1543.
- [12] K. K. Julich-Gruner, C. Löwenberg, A. T. Neffe, M. Behl, A. Lendlein, *Macromol. Chem. Phys.* **2013**, *214*, 527.
- [13] J. Delaey, P. Dubruel, S. Van Vlierberghe, *Adv. Funct. Mater.* **2020**, *30*, 1909047.
- [14] M. Herath, J. Epaarachchi, M. Islam, L. Fang, J. Leng, *Eur. Polym. J.* **2020**, *136*, 109912.
- [15] Y. Xia, Y. He, F. Zhang, Y. Liu, J. Leng, *Adv. Mater.* **2021**, *33*, 2000713.
- [16] X. Wang, X. Guo, J. Ye, N. Zheng, P. Kohli, D. Choi, Y. Zhang, Z. Xie, Q. Zhang, H. Luan, *Adv. Mater.* **2019**, *31*, 1805615.
- [17] M. R. Pfau, M. A. Grunlan, *J. Mater. Chem. B* **2021**, *9*, 4287.
- [18] L. Hou, Y. Wu, J. Xiao, B. Guo, Y. Zong, *Polym. Degrad. Stab.* **2019**, *166*, 8.
- [19] L. Fang, W. Yan, U. Nöchel, K. Kratz, A. Lendlein, *Polymer* **2016**, *102*, 54.
- [20] S. Y. Leo, W. Zhang, Y. Zhang, Y. Ni, H. Jiang, C. Jones, P. Jiang, V. Basile, C. Taylor, *Small* **2018**, *14*, 1703515.
- [21] J. Kim, H. Yun, Y. J. Lee, J. Lee, S.-H. Kim, K. H. Ku, B. Kim, *J. Am. Chem. Soc.* **2021**, *143*, 13333.
- [22] W. Lu, C. Ma, D. Zhang, X. Le, J. Zhang, Y. Huang, C.-F. Huang, T. Chen, *J. Phys. Chem. C* **2018**, *122*, 9499.
- [23] J. Kunzelman, T. Chung, P. T. Mather, C. Weder, *J. Mater. Chem.* **2008**, *18*, 1082.
- [24] T. Defize, J.-M. Thomassin, H. Ottevaere, C. d Malherbe, G. Eppe, R. Jellali, M. I. Alexandre, C. Jérôme, R. I. Riva, *Macromolecules* **2018**, *52*, 444.
- [25] H. Luo, Z. Li, G. Yi, Y. Wang, X. Zu, H. Wang, H. Huang, Z. Liang, *Mater. Lett.* **2015**, *140*, 71.
- [26] K. Holland-Moritz, I. Holland-Moritz, K. Van Werden, *Colloid Polym. Sci.* **1981**, *259*, 156.
- [27] M. Pezolet, C. Pellerin, R. E. Prud'homme, T. Buffeteau, *Vib. Spectrosc.* **1998**, *18*, 103.
- [28] Z. A. Steelman, A. C. Weems, A. J. Traverso, J. M. Szafron, D. J. Maitland, V. V. Yakovlev, *Appl. Phys. Lett.* **2017**, *111*, 241904.
- [29] P. R. Yadav, M. H. Rizvi, B. r. Kuttich, S. R. Mishra, B. S. Chapman, B. B. Lynch, T. Kraus, A. L. Oldenburg, J. B. Tracy, *ACS Appl. Nano Mater.* **2021**, *4*, 3911.
- [30] M. Nagata, Y. Yamamoto, *J. Polym. Sci., Part A: Polym. Chem.* **2009**, *47*, 2422.
- [31] A. Subash, B. Kandasubramanian, *Eur. Polym. J.* **2020**, *134*, 109771.
- [32] X. Kuang, D. J. Roach, J. Wu, C. M. Hamel, Z. Ding, T. Wang, M. L. Dunn, H. J. Qi, *Adv. Funct. Mater.* **2019**, *29*, 1805290.
- [33] L. Fang, S. Chen, T. Fang, J. Fang, C. Lu, Z. Xu, *Compos. Sci. Technol.* **2017**, *138*, 106.
- [34] J. Wang, Z. Xia, J. Liu, N. Zhang, W. Zhou, Z. Zhong, Z. Luo, W. Li, Z. Yang, Y. Hu, *J. Appl. Polym. Sci.* **2021**, *138*, 50938.
- [35] T. Wang, J. Zhao, C. Weng, T. Wang, Y. Liu, Z. Han, Z. Zhang, *Composites, Part A* **2021**, *144*, 106322.
- [36] Y.-M. Ha, Y.-O. Kim, Y.-N. Kim, J. Kim, J.-S. Lee, J. W. Cho, M. Endo, H. Muramatsu, Y. A. Kim, Y. C. Jung, *Composites, Part B* **2019**, *175*, 107065.
- [37] H. Lu, Y. Yao, W. M. Huang, J. Leng, D. Hui, *Composites, Part B* **2014**, *62*, 256.
- [38] Y. Liu, Z. Zhang, K. Yang, D. Chen, Z. Li, *Polymer* **2022**, *247*, 106928.
- [39] Y. Bai, J. Zhang, X. Chen, *ACS Appl. Mater. Interfaces* **2018**, *10*, 14017.
- [40] L. Yang, R. Tong, Z. Wang, H. Xia, *ChemPhysChem* **2018**, *19*, 2052.
- [41] H. Lu, Y. Wu, X. Qi, Z. Chi, Z. Li, L. Xu, Y. Fu, Y. Dong, *J. Appl. Polym. Sci.* **2021**, *138*, 50526.
- [42] A. Lendlein, H. Jiang, O. Jünger, R. Langer, *Nature* **2005**, *434*, 879.
- [43] T. Fang, L. Cao, S. Chen, J. Fang, J. Zhou, L. Fang, C. Lu, Z. Xu, *Mater. Des.* **2018**, *144*, 129.
- [44] S. Yang, Y. He, Y. Liu, J. Leng, *Eur. Polym. J.* **2022**, *164*, 110955.
- [45] P. Shan, X. Chen, B. Tan, D. Cao, L. Fang, C. Lu, Z. Xu, *Macromol. Mater. Eng.* **2022**, *307*, 2100683.
- [46] W. B. Niu, L. C. Qu, R. W. Lyv, S. F. Zhang, *RSC Adv.* **2017**, *7*, 22461.
- [47] Y. Zhang, L. M. Huang, H. J. Song, C. J. Ni, J. J. Wu, Q. Zhao, T. Xie, *ACS Appl. Mater. Interfaces* **2019**, *11*, 32408.
- [48] S. Schauer, T. Meier, M. Reinhard, M. Röhrig, M. Schneider, M. Heilig, A. Kolew, M. Worgull, H. Hölscher, *ACS Appl. Mater. Interfaces* **2016**, *8*, 9423.

- [49] P. Li, Y. Han, W. Wang, Y. Liu, P. Jin, J. Leng, *Sci. Rep.* **2017**, *7*, 44333.
- [50] T. Xie, X. Xiao, J. Li, R. Wang, *Adv. Mater.* **2010**, *22*, 4390.
- [51] H. X. Xu, C. J. Yu, S. D. Wang, V. Malyarchuk, T. Xie, J. A. Rogers, *Adv. Funct. Mater.* **2013**, *23*, 3299.
- [52] W. Zhang, H. Wang, H. Wang, J. Y. E. Chan, H. Liu, B. Zhang, Y.-F. Zhang, K. Agarwal, X. Yang, A. S. Ranganath, H. Y. Low, Q. Ge, J. K. W. Yang, *Nat. Commun.* **2021**, *12*, 112.
- [53] H.-Y. Tseng, Y.-H. Chen, R.-Y. Chen, H. Yang, *ACS Appl. Mater. Interfaces* **2020**, *12*, 10883.
- [54] S. Schauer, J. J. Baumberg, H. Hölscher, S. K. Smoukov, *Macromol. Rapid Commun.* **2018**, *39*, 1800518.
- [55] P. Zhang, B. Wu, S. Huang, F. Cai, G. Wang, H. Yu, *Polymer* **2019**, *178*, 121644.
- [56] S. Y. Leo, W. Zhang, Y. Zhang, Y. Ni, H. Jiang, C. Jones, P. Jiang, V. Basile, C. Taylor, *Small* **2018**, *14*, 1703515.
- [57] C. Ji, M. Chen, L. Wu, *Adv. Opt. Mater.* **2021**, *9*, 2100739.
- [58] C. J. Leverant, S.-Y. Leo, M. A. Cordoba, Y. Zhang, N. Charpota, C. Taylor, P. Jiang, *ACS Appl. Polym. Mater.* **2019**, *1*, 36.
- [59] L. O. Björn, in *Photobiology: The Science of Life and Light*, Springer, New York, NY, USA **2008**.
- [60] I. Pérez-Juste, O. Nieto Faza, in *Structure Elucidation in Organic Chemistry*, Wiley, Hoboken, NJ, USA, **2015**.
- [61] M. Blanco, J. Coello, H. Iturriga, S. MasPOCH, C. De La Pezuela, *Analyst* **1998**, *123*, 135R.
- [62] V. Barone, S. Alessandrini, M. Biczysko, J. R. Cheeseman, D. C. Clary, A. B. McCoy, R. J. DiRisio, F. Neese, M. Melosso, C. Pizzarini, *Nat. Rev. Methods Primers* **2021**, *1*, 1.
- [63] V. P. Ananikov, *Chem. Rev.* **2011**, *111*, 418.
- [64] C. Bressler, M. Chergui, *Annu. Rev. Phys. Chem.* **2010**, *61*, 263.
- [65] G. Fortunato, V. Marroccoli, F. Corsini, S. Turri, G. Griffini, *Prog. Org. Coat.* **2020**, *147*, 105840.
- [66] K. Wang, Y.-G. Jia, X. Zhu, *Macromolecules* **2017**, *50*, 8570.
- [67] C. B. Cooper, S. Nikzad, H. Yan, Y. Ochiai, J.-C. Lai, Z. Yu, G. Chen, J. Kang, Z. Bao, *ACS Cent. Sci.* **2021**, *7*, 1657.
- [68] Y.-C. Chien, W.-T. Chuang, U.-S. Jeng, S.-H. Hsu, *ACS Appl. Mater. Interfaces* **2017**, *9*, 5419.
- [69] G. Li, S. Wang, Z. Liu, Z. Liu, H. Xia, C. Zhang, X. Lu, J. Jiang, Y. Zhao, *ACS Appl. Mater. Interfaces* **2018**, *10*, 40189.
- [70] H. Zhang, J. Zhang, X. Tong, D. Ma, Y. Zhao, *Macromol. Rapid Commun.* **2013**, *34*, 1575.
- [71] H. Lv, J. Leng, Y. Liu, S. Du, *Adv. Eng. Mater.* **2008**, *10*, 592.
- [72] R. Hoehner, T. Raidt, N. Novak, F. Katzenberg, J. C. Tiller, *Macromol. Rapid Commun.* **2015**, *36*, 2042.
- [73] M. Tanaka, R. Young, *J. Mater. Sci.* **2006**, *41*, 963.
- [74] W. Liu, R. Zhang, M. Huang, X. Dong, W. Xu, N. Ray, J. Zhu, *Polymer* **2016**, *104*, 115.
- [75] G. Yang, X. Wan, Y. Liu, R. Li, Y. Su, X. Zeng, J. Tang, *ACS Appl. Mater. Interfaces* **2016**, *8*, 34744.
- [76] S. Sarabiyani Nejad, A. Babaie, M. Bagheri, M. Rezaei, F. Abbasi, A. Shomali, *Polym. Adv. Technol.* **2020**, *31*, 2279.
- [77] Z. Denchev, J. Viana, in *Handbook of Multiphase Polymer Systems*, Wiley, Hoboken, NJ, USA **2011**.
- [78] N. Stribeck, in *X-Ray Scattering of Soft Matter*, Springer, Berlin, **2007**.
- [79] W. Yan, T. Rudolph, U. Noechel, O. Gould, M. Behl, K. Kratz, A. Lendlein, *Macromolecules* **2018**, *51*, 4624.
- [80] Y. Wong, S. Venkatraman, *Acta Mater.* **2010**, *58*, 49.
- [81] I. A. Rousseau, P. T. Mather, *J. Am. Chem. Soc.* **2003**, *125*, 15300.
- [82] N. Choudhary, D. Kaur, *Sens. Actuators, A* **2016**, *242*, 162.
- [83] H. Chung, D. Dudenko, F. Zhang, G. D'Avino, C. Ruzié, A. Richard, G. Schweicher, J. Cornil, D. Beljonne, Y. Geerts, *Nat. Commun.* **2018**, *9*, 1.
- [84] B. A. Collins, E. Gann, *J. Polym. Sci.* **2022**, *60*, 1199.
- [85] K. Kago, H. Endo, H. Matsuoka, H. Yamaoka, N. Hamaya, M. Tanaka, T. Mori, *J. Synchrotron Radiat.* **1998**, *5*, 1304.
- [86] R. Machatschek, S. Saretia, A. Lendlein, *Adv. Mater. Interfaces* **2021**, *8*, 2001926.
- [87] J. Stöhr, in *NEXAFS Spectroscopy*, Springer, Berlin, **1992**.
- [88] D. Son, S. Cho, J. Nam, H. Lee, M. Kim, *Polymers* **2020**, *12*, 1053.
- [89] J. Fan, G. Li, *Nat. Commun.* **2018**, *9*, 1.
- [90] H.-H. Perkampus, in *UV-VIS Spectroscopy and its Applications*, Springer, Berlin, **2013**.
- [91] Y. Wu, Z. Hu, H. Huang, Y. Chen, *Polym. Chem.* **2019**, *10*, 1537.
- [92] W.-F. Su, in *Principles of Polymer Design and Synthesis*, Springer, Berlin, p. 89.
- [93] T. Liu, T. Zhou, Y. Yao, F. Zhang, L. Liu, Y. Liu, J. Leng, *Composites, Part A* **2017**, *100*, 20.
- [94] Y. Chen, H. Yu, M. Quan, L. Zhang, H. Yang, Y. Lu, *RSC Adv.* **2015**, *5*, 4675.
- [95] J. Ban, L. Mu, J. Yang, S. Chen, H. Zhuo, *J. Mater. Chem. A* **2017**, *5*, 14514.
- [96] P. Larkin, in *Infrared and Raman Spectroscopy: Principles and Spectral Interpretation*, Elsevier, Amsterdam, **2017**.
- [97] K. I. Hadjiivanov, D. A. Panayotov, M. Y. Mihaylov, E. Z. Ivanova, K. K. Chakarova, S. M. Andonova, N. L. Drenchev, *Chem. Rev.* **2020**, *121*, 1286.
- [98] G. S. Bumbrah, R. M. Sharma, *Egypt. J. Forensic Sci.* **2016**, *6*, 209.
- [99] D. Gerrard, W. Maddam, *Appl. Spectrosc. Rev.* **1986**, *22*, 251.
- [100] H. Liem, L. Yeung, *J. Appl. Polym. Sci.* **2007**, *105*, 765.
- [101] Y. Zhu, J. Hu, H. Luo, R. J. Young, L. Deng, S. Zhang, Y. Fan, G. Ye, *Soft Matter* **2012**, *8*, 2509.
- [102] J. R. Lombardi, R. L. Birke, *J. Phys. Chem. C* **2008**, *112*, 5605.
- [103] X. X. Han, R. S. Rodriguez, C. L. Haynes, Y. Ozaki, B. Zhao, *Nat. Rev. Methods Primers* **2022**, *1*, 1.
- [104] Z. T. Mengesha, J. Yang, *Anal. Chem.* **2016**, *88*, 10908.
- [105] C. M. Gabardo, J. Yang, N. J. Smith, R. C. Adams-McGavin, L. Soleymani, *ACS Nano* **2016**, *10*, 8829.
- [106] L. Bokobza, *Polymers* **2017**, *10*, 7.
- [107] N. Kumar, S. Mignuzzi, W. Su, D. Roy, *EPJ Tech. Instrum.* **2015**, *2*, 9.
- [108] S.-W. Weng, W.-H. Lin, W.-B. Su, E.-T. Hwu, P. Chen, T.-R. Tsai, C.-S. Chang, *Nanotechnology* **2014**, *25*, 255703.
- [109] A. A. Ismail, F. R. van de Voort, J. Sedman, in *Techniques and Instrumentation in Analytical Chemistry*, Elsevier, Amsterdam, **1997**, p. 93.
- [110] H. Lu, Y. Liu, J. Leng, S. Du, *Eur. Polym. J.* **2010**, *46*, 1908.
- [111] A. Salimi, A. Yousefi, *Polym. Test.* **2003**, *22*, 699.
- [112] X. Cai, T. Lei, D. Sun, L. Lin, *RSC Adv.* **2017**, *7*, 15382.
- [113] X. Ji, D. Chen, Y. Zheng, J. Shen, S. Guo, E. Harkin-Jones, *Chem. Eng. J.* **2019**, *362*, 190.
- [114] Z. Wen, M. K. McBride, X. Zhang, X. Han, A. M. Martinez, R. Shao, C. Zhu, R. Visvanathan, N. A. Clark, Y. Wang, *Macromolecules* **2018**, *51*, 5812.
- [115] C. Pellerin, R. E. Prud'Homme, M. Pezolet, B. A. Weinstock, P. R. Griffiths, *Macromolecules* **2003**, *36*, 4838.
- [116] D. Korouski, A. Dazzi, R. Zenobi, A. Centrone, *Chem. Soc. Rev.* **2020**, *49*, 3315.
- [117] A. Dazzi, C. B. Prater, *Chem. Rev.* **2017**, *117*, 5146.
- [118] Y. Tian, Q. Wang, Y. Hu, H. Sun, Z. Cui, L. Kou, J. Cheng, J. Zhang, *Polymer* **2019**, *178*, 121592.
- [119] B. Huang, L. Dai, W. Yang, Y. Yu, Y. Zhao, X. Zhang, Z. Xie, Z. Zhang, *Composites, Part B* **2020**, *200*, 108292.
- [120] F. Xie, L. Huang, J. Leng, Y. Liu, *Journal of Intelligent Material Systems and Structures* **2016**, *27*, 2433.
- [121] C. L. Lewis, E. M. Dell, *J. Polym. Sci., Part B: Polym. Phys.* **2016**, *54*, 1340.
- [122] T. Xie, *Polymer* **2011**, *52*, 4985.
- [123] J. Xu, J. Song, in *Shape Memory Polymers for Biomedical Applications*, Woodhead Publisher, Sawston, UK **2015**.
- [124] R. Xiao, J. Choi, N. Lakhera, C. M. Yakacki, C. P. Frick, T. D. Nguyen, *J. Mech. Phys. Solids* **2013**, *61*, 1612.

- [125] T. Chen, L. Fang, C. Lu, Z. Xu, *Macromol. Mater. Eng.* **2020**, *305*, 1900578.
- [126] E. Havens, E. A. Snyder, T. H. Tong, in *Smart Structures and Materials*, Vol. 5762, SPIE, San Diego, CA, USA, **2005**.
- [127] W. Guo, C. H. Lu, R. Orbach, F. Wang, X. J. Qi, A. Ceconello, D. Seliktar, I. Willner, *Adv. Mater.* **2015**, *27*, 73.
- [128] J. Zhang, Z. Yin, L. Ren, Q. Liu, L. Ren, X. Yang, X. Zhou, *Adv. Mater. Technol.* **2022**, *7*, 2101568.
- [129] A. Cosola, M. Sangermano, D. Terenziani, R. Conti, M. Messori, H. Grützmacher, C. F. Pirri, A. Chiappone, *Appl. Mater. Today* **2021**, *23*, 101060.
- [130] A. Kotikian, R. L. Truby, J. W. Boley, T. J. White, J. A. Lewis, *Adv. Mater.* **2018**, *30*, 1706164.
- [131] S. Wang, J. M. Lee, W. Y. Yeong, *Int. J. Bioprint.* **2015**, *1*, 3.
- [132] P. Imrie, J. Jin, *J. Polym. Sci.* **2022**, *60*, 149.
- [133] G. Capiel, N. E. Marcovich, M. A. Mosiewicki, *Eur. Polym. J.* **2019**, *116*, 321.
- [134] A. B. Lowe, *Polym. Chem.* **2014**, *5*, 4820.
- [135] Z.-C. Liu, B. Zuo, H.-F. Lu, M. Wang, S. Huang, X.-M. Chen, B.-P. Lin, H. Yang, *Polym. Chem.* **2020**, *11*, 3747.
- [136] K. S. Lim, J. H. Galarraga, X. Cui, G. C. Lindberg, J. A. Burdick, T. B. Woodfield, *Chem. Rev.* **2020**, *120*, 10662.
- [137] T. Hughes, G. Simon, K. Saito, *Mater. Horiz.* **2019**, *6*, 1762.
- [138] C. A. Spiegel, M. Hackner, V. P. Bothe, J. P. Spatz, E. Blasco, *Adv. Funct. Mater.* **2022**, *32*, 2110580.
- [139] D. I. Pattison, A. S. Rahmanto, M. J. Davies, *Photochem. Photobiol. Sci.* **2012**, *11*, 38.
- [140] A. K. Sinha, D. Equbal, *Asian J. Org. Chem.* **2019**, *8*, 32.
- [141] S. K. Rajaraman, W. A. Mowers, J. V. Crivello, *J. Polym. Sci., Part A: Polym. Chem.* **1999**, *37*, 4007.
- [142] E. Lallana, R. Riguera, E. Fernandez-Megia, *Angew. Chem., Int. Ed.* **2011**, *50*, 8794.
- [143] V. M. Lechner, M. Nappi, P. J. Deneny, S. Folliet, J. C. K. Chu, M. J. Gaunt, *Chem. Rev.* **2022**, *122*, 1752.
- [144] D. L. Safranski, K. Gall, *Polymer* **2008**, *49*, 4446.
- [145] M. Zarek, M. Layani, I. Cooperstein, E. Sacyani, D. Cohn, S. Magdassi, *Adv. Mater.* **2016**, *28*, 4449.
- [146] J. Zhou, S. A. Turner, S. M. Brosnan, Q. Li, J.-M. Y. Carrillo, D. Nykpanchuk, O. Gang, V. S. Ashby, A. V. Dobrynin, S. S. Sheiko, *Macromolecules* **2014**, *47*, 1768.
- [147] G. Godeau, L. Navailles, F. d r Nallet, X. Lin, T. J. McIntosh, M. W. Grinstaff, *Macromolecules* **2012**, *45*, 2509.
- [148] D. P. Nair, N. B. Cramer, T. F. Scott, C. N. Bowman, R. Shandas, *Polymer* **2010**, *51*, 4383.
- [149] W. D. Cook, F. Chen, D. W. Pattison, P. Hopson, M. Beaujon, *Polym. Int.* **2007**, *56*, 1572.
- [150] M. A. Cole, K. C. Jankousky, C. N. Bowman, *Polym. Chem.* **2013**, *4*, 1167.
- [151] S. K. Reddy, R. P. Sebra, K. S. Anseth, C. N. Bowman, *J. Polym. Sci., Part A: Polym. Chem.* **2005**, *43*, 2134.
- [152] C. E. Hoyle, C. N. Bowman, *Angew. Chem., Int. Ed.* **2010**, *49*, 1540.
- [153] C. E. Hoyle, A. B. Lowe, C. N. Bowman, *Chem. Soc. Rev.* **2010**, *39*, 1355.
- [154] X. Li, Y. Pan, J. Lai, R. Wu, Z. Zheng, X. Ding, *Polym. Chem.* **2017**, *8*, 3867.
- [155] C. L. Lewis, Y. Meng, M. Anthamatten, *Macromolecules* **2015**, *48*, 4918.
- [156] Y. Meng, J. Jiang, M. Anthamatten, *J. Polym. Sci., Part B: Polym. Phys.* **2016**, *54*, 1397.
- [157] A. Mautner, X. Qin, H. Wutzel, S. C. Ligon, B. Kapeller, D. Moser, G. Russmueller, J. Stampfl, R. Liska, *J. Polym. Sci., Part A: Polym. Chem.* **2013**, *51*, 203.
- [158] G. Zhang, Q. Zhao, L. Yang, W. Zou, X. Xi, T. Xie, *ACS Macro Lett.* **2016**, *5*, 805.
- [159] Q. Zhao, W. Zou, Y. Luo, T. Xie, *Sci. Adv.* **2016**, *2*, e1501297.
- [160] M. I. Lawton, K. R. Tillman, H. S. Mohammed, W. Kuang, D. A. Shipp, P. T. Mather, *ACS Macro Lett.* **2016**, *5*, 203.
- [161] Y. Meng, J. Jiang, M. Anthamatten, *ACS Macro Lett.* **2015**, *4*, 115.
- [162] J. V. Crivello, *J. Polym. Sci., Part A: Polym. Chem.* **1999**, *37*, 4241.
- [163] G. Griffini, M. Invernizzi, M. Levi, G. Natale, G. Postiglione, S. Turri, *Polymer* **2016**, *91*, 174.
- [164] J. V. Crivello, R. A. Ortiz, *J. Polym. Sci., Part A: Polym. Chem.* **2001**, *39*, 2385.
- [165] D. C. Hoekstra, M. G. Debye, A. P. Schenning, *Macromolecules* **2021**, *54*, 5410.
- [166] R. Yu, X. Yang, Y. Zhang, X. Zhao, X. Wu, T. Zhao, Y. Zhao, W. Huang, *ACS Appl. Mater. Interfaces* **2017**, *9*, 1820.
- [167] M. R. Ramdas, K. Vijayalakshmi, L. Munirathamma, H. Ravikumar, K. S. Kumar, *Mater. Today Commun.* **2018**, *17*, 180.
- [168] M. K. McBride, T. Gong, D. P. Nair, C. N. Bowman, *Polymer* **2014**, *55*, 5880.
- [169] J. Xu, J. Song, *Proc. Natl. Acad. Sci. USA* **2010**, *107*, 7652.
- [170] E. Y. Jeon, B. H. Hwang, Y. J. Yang, B. J. Kim, B.-H. Choi, G. Y. Jung, H. J. Cha, *Biomaterials* **2015**, *67*, 11.
- [171] X. Zhao, Y. Dang, J. Deng, J. Zhang, *Colloid Polym. Sci.* **2014**, *292*, 85.
- [172] B. T. Benkhaled, K. Belkhir, T. Brossier, C. Chatard, A. Graillet, B. Lonetti, A.-F. Mingotaud, S. Catrouillet, S. Blanquer, V. Lapinte, *Eur. Polym. J.* **2022**, *179*, 111570.
- [173] A. Garle, S. Kong, U. Ojha, B. M. Budhlall, *ACS Appl. Mater. Interfaces* **2012**, *4*, 645.
- [174] L. Wang, X. Yang, H. Chen, T. Gong, W. Li, G. Yang, S. Zhou, *ACS Appl. Mater. Interfaces* **2013**, *5*, 10520.
- [175] M. Klinger, L. P. Tolbod, K. V. Gothelf, P. R. Ogilby, *ACS Appl. Mater. Interfaces* **2009**, *1*, 661.
- [176] Z. Wang, K. Randazzo, X. Hou, J. Simpson, J. Struppe, A. Ugrinov, B. Kastern, E. Wysocki, Q. R. Chu, *Macromolecules* **2015**, *48*, 2894.
- [177] X. Liu, J. Wu, Z. Tang, J. Wu, Z. Huang, X. Yin, J. Du, X. Lin, W. Lin, G. Yi, *ACS Appl. Mater. Interfaces* **2022**, *14*, 33829.
- [178] T. Doi, H. Kashida, H. Asanuma, *Org. Biomol. Chem.* **2015**, *13*, 4430.
- [179] V. X. Truong, F. Li, F. Ercole, J. S. Forsythe, *ACS Macro Lett.* **2018**, *7*, 464.
- [180] C. García-Astrain, C. Peña-Rodríguez, A. Retegi, A. Eceiza, M. Corcuera, N. Gabilondo, *Mater. Lett.* **2015**, *160*, 142.
- [181] H. Xie, X. Y. Deng, C. Y. Cheng, K. K. Yang, Y. Z. Wang, *Macromol. Rapid Commun.* **2017**, *38*, 1600664.
- [182] Y. Li, M. Goswami, Y. Zhang, T. Liu, J. Zhang, M. R. Kessler, L. Wang, O. Rios, *Sci. Rep.* **2020**, *10*, 1.
- [183] Y. Gu, C. Ru, Z. Zhao, D. Chao, X. Liu, *Eur. Polym. J.* **2020**, *123*, 109413.
- [184] J. Hu, Z. Feng, X. Xu, W. Gao, N. Ning, B. Yu, L. Zhang, M. Tian, *Ind. Eng. Chem. Res.* **2021**, *60*, 2144.
- [185] C. W. Hull, Patent Number US4575330A **1984**.
- [186] S. Sharifi, S. Blanquer, D. W. Grijpma, *J. Appl. Biomater. Funct. Mater.* **2012**, *10*, 280.
- [187] A. D. Lantada, A. de Blas Romero, E. C. Tanarro, *Smart Mater. Struct.* **2016**, *25*, 065018.
- [188] T. Zhao, R. Yu, X. Li, B. Cheng, Y. Zhang, X. Yang, X. Zhao, Y. Zhao, W. Huang, *Eur. Polym. J.* **2018**, *101*, 120.
- [189] C. Sun, N. Fang, D. M. Wu, X. Zhang, *Sens. Actuators, A* **2005**, *121*, 113.
- [190] Q. Ge, Z. Li, Z. Wang, K. Kowsari, W. Zhang, X. He, J. Zhou, N. X. Fang, *Int. J. Extreme Manuf.* **2020**, *2*, 022004.
- [191] Y. Shi, G. Fang, Z. Cao, F. Shi, Q. Zhao, Z. Fang, T. Xie, *Chem. Eng. J.* **2021**, *426*, 131306.
- [192] W. Zhang, J. Chen, X. Li, Y. Lu, *Small* **2020**, *16*, 2004190.
- [193] W. Du, Y. Jin, L. Shi, Y. Shen, S. Lai, Y. Zhou, *Composites, Part B* **2020**, *195*, 108092.



- [194] Y. Mao, Z. Ding, C. Yuan, S. Ai, M. Isakov, J. Wu, T. Wang, M. L. Dunn, H. J. Qi, *Sci. Rep.* **2016**, *6*, 24761.
- [195] X. Zhang, Y. Zhang, R. Ma, Y. Yang, Y. Zhou, Authorea **2022**. <https://www.authorea.com/doi/full/10.22541/au.165354674.43292092>
- [196] J. K. Wilt, D. Gilmer, S. Kim, B. G. Compton, T. Saito, *MRS Commun.* **2021**, *11*, 106.
- [197] M. Diba, G. L. Koons, M. L. Bedell, A. G. Mikos, *Biomaterials* **2021**, *274*, 120871.
- [198] V. Harinarayana, Y. Shin, *Opt. Laser Technol.* **2021**, *142*, 107180.
- [199] W. Zhang, H. Wang, A. T. Tan, A. Sargur Ranganath, B. Zhang, H. Wang, J. Y. E. Chan, Q. Ruan, H. Liu, S. T. Ha, *Nano Lett.* **2022**, *22*, 8917.
- [200] H. Quan, T. Zhang, H. Xu, S. Luo, J. Nie, X. Zhu, *Bioactive Mater.* **2020**, *5*, 110.
- [201] Q. Ge, B. Jian, H. Li, *Forces Mech.* **2022**, 100074.
- [202] J. Qi, C. Sun, D. Li, H. Zhang, W. Yu, A. Zebibula, J. W. Lam, W. Xi, L. Zhu, F. Cai, *ACS Nano* **2018**, *12*, 7936.
- [203] X. Xu, P. Robles-Martinez, C. M. Madla, F. Joubert, A. Goyanes, A. W. Basit, S. Gaisford, *Addit. Manuf.* **2020**, *33*, 101071.
- [204] B. Huang, Z. Du, T. Yong, W. Han, *J. Wuhan Univ. Technol., Mater. Sci. Ed.* **2017**, *32*, 726.
- [205] R. Januszewicz, J. R. Tumbleston, A. L. Quintanilla, S. J. Mecham, J. M. DeSimone, *Proc. Natl. Acad. Sci. USA* **2016**, *113*, 11703.
- [206] P. Wei, H. Leng, Q. Chen, R. C. Advincula, E. B. Pentzer, *ACS Appl. Polym. Mater.* **2019**, *1*, 885.
- [207] G. Witzgall, R. Vrijen, E. Yablonovitch, V. Doan, B. J. Schwartz, *Opt. Lett.* **1998**, *23*, 1745.
- [208] W. Sun, in *Tissue Engineering*, Mary Ann Liebert, Inc., New Rochelle, NY, USA, **2006**.
- [209] R. Ketchum, P. Alcaraz, P.-A. Blanche, *Opt. Mater. Express* **2022**, *12*, 3152.
- [210] Y. Bai, J. Zhang, D. Wen, P. Gong, J. Liu, J. Ju, X. Chen, *Compos. Sci. Technol.* **2020**, *187*, 107940.
- [211] W. Du, Y. Jin, S. Lai, L. Shi, Y. Shen, H. Yang, *Composites, Part A* **2020**, *128*.
- [212] W. Du, Y. Jin, S. Lai, L. Shi, W. Fan, J. Pan, *Polymer* **2018**, *158*, 120.
- [213] V. D. Punetha, Y.-M. Ha, Y.-O. Kim, Y. C. Jung, J. W. Cho, *Sens. Actuators, B* **2020**, *321*, 128468.
- [214] Y. Bai, J. Zhang, D. Wen, P. Gong, X. Chen, *Compos. Sci. Technol.* **2019**, *170*, 101.
- [215] S.-T. Li, X.-Z. Jin, Y.-W. Shao, X.-D. Qi, J.-H. Yang, Y. Wang, *Eur. Polym. J.* **2019**, *116*, 302.
- [216] T. Li, Y. Li, X. Wang, X. Li, J. Sun, *ACS Appl. Mater. Interfaces* **2019**, *11*, 9470.
- [217] E. Wang, Y. Wu, M. Z. Islam, Y. Dong, Y. Zhu, F. Liu, Y. Fu, Z. Xu, N. Hu, *Mater. Lett.* **2019**, *238*, 54.
- [218] J. H. Park, B. K. Kim, *Smart Mater. Struct.* **2014**, *23*, 025038.
- [219] P. Zhang, F. Cai, G.-J. Wang, H.-F. Yu, *Chin. J. Polym. Sci.* **2022**, *40*, 166.
- [220] H. Yang, W. R. Leow, T. Wang, J. Wang, J. Yu, K. He, D. Qi, C. Wan, X. Chen, *Adv. Mater.* **2017**, *29*, 1701627.
- [221] Y. Liu, G. Zhu, W. Liu, H. Liu, Y. Huo, T. Ren, X. Hou, *Smart Mater. Struct.* **2018**, *27*, 095008.
- [222] F. Wang, W. Wang, C. Zhang, J. Tang, X. Zeng, X. Wan, *Composites, Part B* **2021**, *219*, 108927.
- [223] F. Wang, C. Zhang, X. Wan, *Ind. Eng. Chem. Res.* **2021**, *60*, 2954.
- [224] Q. Wanyan, Y. Qiu, J. Xi, S. Yin, W. Zhang, D. Wu, *ACS Appl. Polym. Mater.* **2020**, *2*, 5889.
- [225] J. Bai, Z. Shi, *ACS Appl. Mater. Interfaces* **2017**, *9*, 27213.
- [226] Z. Xu, C. Ding, D. W. Wei, R. Y. Bao, K. Ke, Z. Liu, M. B. Yang, W. Yang, *ACS Appl. Mater. Interfaces* **2019**, *11*, 30332.
- [227] H. Bi, G. Ye, H. Yang, H. Sun, Z. Ren, R. Guo, M. Xu, L. Cai, Z. Huang, *Eur. Polym. J.* **2020**, *136*, 109920.
- [228] L. Du, Z.-Y. Xu, C.-L. Huang, F.-Y. Zhao, C.-J. Fan, J. Dai, K.-K. Yang, Y.-Z. Wang, *Appl. Mater. Today* **2020**, *18*, 100463.
- [229] J. Huang, L. Cao, D. Yuan, Y. Chen, *ACS Appl. Mater. Interfaces* **2018**, *10*, 40996.
- [230] L. Du, Z.-Y. Xu, C.-J. Fan, G. Xiang, K.-K. Yang, Y.-Z. Wang, *Macromolecules* **2018**, *51*, 705.
- [231] Y. Bai, J. Liu, J. Ju, X. Chen, *ACS Appl. Mater. Interfaces* **2021**, *13*, 23011.
- [232] Y. Bai, J. Zhang, D. Wen, B. Yuan, P. Gong, J. Liu, X. Chen, *J. Mater. Chem. A* **2019**, *7*, 20723.
- [233] K. Wang, X. X. Zhu, *ACS Biomater. Sci. Eng.* **2018**, *4*, 3099.
- [234] Y. Chen, X. Zhao, C. Luo, Y. Shao, M.-B. Yang, B. Yin, *Composites, Part A* **2020**, *135*, 105931.
- [235] Y. Wei, X. Qi, S. He, S. Deng, D. Liu, Q. Fu, *ACS Appl. Mater. Interfaces* **2018**, *10*, 32922.
- [236] Y. Chen, M. Zhang, Z. Lin, X. Shi, *Polymer* **2020**, *206*, 122898.
- [237] G. Tian, G. Zhu, S. Xu, L. Pan, *Smart Mater. Struct.* **2020**, *29*, 105019.
- [238] Y. Dong, C. Geng, C. Liu, J. Gao, Q. Zhou, *Synth. Met.* **2020**, *266*, 116417.
- [239] M. S. Heo, T. H. Kim, Y. W. Chang, K. S. Jang, *Polymers* **2021**, *13*, 3984.
- [240] H. Xie, J. Shao, Y. Ma, J. Wang, H. Huang, N. Yang, H. Wang, C. Ruan, Y. Luo, Q. Q. Wang, P. K. Chu, X. F. Yu, *Biomaterials* **2018**, *164*, 11.
- [241] S. Ishii, K. Uto, E. Niiyama, M. Ebara, T. Nagao, *ACS Appl. Mater. Interfaces* **2016**, *8*, 5634.
- [242] C. Yang, R. Zheng, M. R. Younis, J. Shao, L.-H. Fu, D.-Y. Zhang, J. Lin, Z. Li, P. Huang, *Chem. Eng. J.* **2021**, *419*, 129437.
- [243] Z. Feng, J. Hu, H. Zuo, N. Ning, L. Zhang, B. Yu, M. Tian, *ACS Appl. Mater. Interfaces* **2019**, *11*, 1469.
- [244] L. Fang, T. Fang, X. Liu, S. Chen, C. Lu, Z. Xu, *Macromol. Mater. Eng.* **2016**, *301*, 1111.
- [245] J. Chen, D.-X. Sun, T. Gu, X.-D. Qi, J.-H. Yang, Y.-Z. Lei, Y. Wang, *Compos. Sci. Technol.* **2022**, *217*, 109123.
- [246] Y. Dong, M. Gong, D. Huang, J. Gao, Q. Zhou, *Prog. Org. Coat.* **2019**, *136*, 105232.
- [247] Y. Li, O. Rios, J. K. Keum, J. Chen, M. R. Kessler, *ACS Appl. Mater. Interfaces* **2016**, *8*, 15750.
- [248] L. Yu, Q. Wang, J. Sun, C. Li, C. Zou, Z. He, Z. Wang, L. Zhou, L. Zhang, H. Yang, *J. Mater. Chem. A* **2015**, *3*, 13953.
- [249] W. Li, Y. Liu, J. Leng, *Composites, Part A* **2018**, *110*, 70.
- [250] L. Wu, C. Jin, X. Sun, *Biomacromolecules* **2011**, *12*, 235.
- [251] J. M. Rochette, V. S. Ashby, *Macromolecules* **2013**, *46*, 2134.
- [252] H. Du, J. Zhang, *Sens. Actuators, A* **2012**, *179*, 114.
- [253] K. Wang, Y.-G. Jia, X. X. Zhu, *ACS Biomater. Sci. Eng.* **2015**, *1*, 855.
- [254] H. Xie, C.-Y. Cheng, L. Du, C.-J. Fan, X.-Y. Deng, K.-K. Yang, Y.-Z. Wang, *Macromolecules* **2016**, *49*, 3845.
- [255] H. Xie, C.-Y. Cheng, X.-Y. Deng, C.-J. Fan, L. Du, K.-K. Yang, Y.-Z. Wang, *Macromolecules* **2017**, *50*, 5155.
- [256] H. Xie, C.-Y. Cheng, L. Li, X.-Y. Deng, K.-K. Yang, Y.-Z. Wang, *J. Mater. Chem. C* **2018**, *6*, 10422.
- [257] H. Xie, K.-K. Yang, Y.-Z. Wang, *Mater. Today: Proc.* **2019**, *16*, 1524.
- [258] J. Bai, Z. Shi, *ACS Macro Lett.* **2017**, *6*, 1025.
- [259] Y. Wu, J. Hu, C. Zhang, J. Han, Y. Wang, B. Kumar, *J. Mater. Chem. A* **2015**, *3*, 97.
- [260] M. Burnworth, L. Tang, J. R. Kumpfer, A. J. Duncan, F. L. Beyer, G. L. Fiore, S. J. Rowan, C. Weder, *Nature* **2011**, *472*, 334.
- [261] X. Zhang, Q. Zhou, H. Liu, H. Liu, *Soft Matter* **2014**, *10*, 3748.
- [262] X. Wang, Y. He, J. Leng, *Macromol. Mater. Eng.* **2022**, *307*, 2100778.
- [263] K. C. Hribar, R. B. Metter, J. L. Ifkovits, T. Troxler, J. A. Burdick, *Small* **2009**, *5*, 1830.
- [264] N. Yenpech, V. Intasanta, S. Chirachanchai, *Polymer* **2019**, *182*, 121792.
- [265] H. Zhang, H. Xia, Y. Zhao, *J. Mater. Chem.* **2012**, *22*, 845.

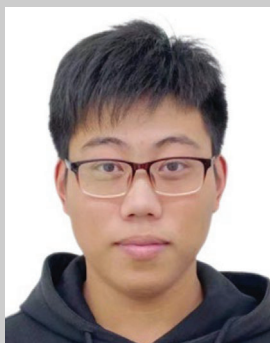
- [266] H. Zhang, Y. Zhao, *ACS Appl. Mater. Interfaces* **2013**, *5*, 13069.
- [267] A. B. Leonardi, J. Puig, J. Antonacci, G. F. Arenas, I. A. Zucchi, C. E. Hoppe, L. Reven, L. Zhu, V. Toader, R. J. J. Williams, *Eur. Polym. J.* **2015**, *71*, 451.
- [268] H. Zhang, H. Xia, Y. Zhao, *ACS Macro Lett.* **2014**, *3*, 940.
- [269] Y. Zheng, J. Li, E. Lee, S. Yang, *RSC Adv.* **2015**, *5*, 30495.
- [270] W. Wang, X. Liu, W. Xu, H. Wei, Y. Liu, Y. Han, P. Jin, H. Du, J. Leng, *Smart Mater. Struct.* **2018**, *27*, 105047.
- [271] Q. Guo, C. J. Bishop, R. A. Meyer, D. R. Wilson, L. Olasov, D. E. Schlesinger, P. T. Mather, J. B. Spicer, J. H. Elisseeff, J. J. Green, *ACS Appl. Mater. Interfaces* **2018**, *10*, 13333.
- [272] S. Ji, F. Fan, C. Sun, Y. Yu, H. Xu, *ACS Appl. Mater. Interfaces* **2017**, *9*, 33169.
- [273] H. Y. Jeong, B. H. Woo, N. Kim, Y. C. Jun, *Sci. Rep.* **2020**, *10*, 6258.
- [274] L. Yu, H. Yu, *ACS Appl. Mater. Interfaces* **2015**, *7*, 3834.
- [275] Z. Xiao, Q. Wu, S. Luo, C. Zhang, J. Baur, R. Justice, T. Liu, *Part. Part. Syst. Charact.* **2013**, *30*, 338.
- [276] Q. Shou, K. Uto, M. Iwanaga, M. Ebara, T. Aoyagi, *Polym. J.* **2014**, *46*, 492.
- [277] S. R. Mishra, J. B. Tracy, *ACS Appl. Nano Mater.* **2018**, *1*, 3063.
- [278] Y. Zhou, J. Tan, D. Chong, X. Wan, J. Zhang, *Adv. Funct. Mater.* **2019**, *29*, 1901202.
- [279] H. Wang, L. Fang, Z. Zhang, J. Epaarachchi, L. Li, X. Hu, C. Lu, Z. Xu, *Composites, Part A* **2019**, *125*, 105525.
- [280] K. M. Lee, H. Koerner, R. A. Vaia, T. J. Bunning, T. J. White, *Soft Matter* **2011**, *7*, 4318.
- [281] G. Davidson-Rozenfeld, L. Stricker, J. Simke, M. Fadeev, M. Vázquez-González, B. J. Ravoo, I. Willner, *Polym. Chem.* **2019**, *10*, 4106.
- [282] M. Herath, J. Epaarachchi, M. Islam, C. Yan, F. Zhang, J. Leng, *J. Intell. Mater. Syst. Struct.* **2019**, *30*, 3124.
- [283] X. Wang, Y. He, J. Leng, *ACS Appl. Polym. Mater.* **2023**, *5*, 1398.
- [284] X. Wang, Y. He, Y. Liu, J. Leng, *Mater. Sci. Eng., R* **2022**, *151*, 100702.
- [285] Y. Wang, E. Sachyani Keneth, A. Kamyshny, G. Scalet, F. Auricchio, S. Magdassi, *Adv. Mater. Technol.* **2022**, *7*, 2101058.
- [286] C. A. Tippets, Q. Li, Y. Fu, E. U. Donev, J. Zhou, S. A. Turner, A.-M. S. Jackson, V. S. Ashby, S. S. Sheiko, R. Lopez, *ACS Appl. Mater. Interfaces* **2015**, *7*, 14288.
- [287] M. Moirangthem, T. A. P. Engels, J. Murphy, C. W. M. Bastiaansen, A. Schenning, *ACS Appl. Mater. Interfaces* **2017**, *9*, 32161.
- [288] M. Quan, B. Yang, J. Wang, H. Yu, X. Cao, *ACS Appl. Mater. Interfaces* **2018**, *10*, 4243.
- [289] Y. Fang, Y. L. Ni, B. Choi, S. Y. Leo, J. Gao, B. Ge, C. Taylor, V. Basile, P. Jiang, *Adv. Mater.* **2015**, *27*, 3696.
- [290] J. D. Joannopoulos, P. R. Villeneuve, S. H. Fan, *Solid State Commun.* **1997**, *102*, 165.
- [291] S. Kinoshita, S. Yoshioka, J. Miyazaki, *Rep. Prog. Phys.* **2008**, *71*, 076401.
- [292] C. I. Aguirre, E. Reguera, A. Stein, *Adv. Funct. Mater.* **2010**, *20*, 2565.
- [293] Y. Gu, L. Zhang, J. K. W. Yang, S. P. Yeo, C.-W. Qiu, *Nanoscale* **2015**, *7*, 6409.
- [294] A. Espinha, M. C. Serrano, Á. Blanco, C. López, *Adv. Opt. Mater.* **2014**, *2*, 516.
- [295] J. Li, J. M. Shim, J. Deng, J. T. B. Overvelde, X. L. Zhu, K. Bertoldi, S. Yang, *Soft Matter* **2012**, *8*, 10322.
- [296] Y. Fang, S. Y. Leo, Y. L. Ni, L. Yu, P. X. Qi, B. C. Wang, V. Basile, C. Taylor, P. Jiang, *Adv. Opt. Mater.* **2015**, *3*, 1509.
- [297] Y. Fang, Y. Ni, S.-Y. Leo, C. Taylor, V. Basile, P. Jiang, *Nat. Commun.* **2015**, *6*, 7416.
- [298] Y. Fang, Y. L. Ni, S. Y. Leo, B. C. Wang, V. Basile, C. Taylor, P. Jiang, *ACS Appl. Mater. Interfaces* **2015**, *7*, 23650.
- [299] Y. Fang, S. Y. Leo, Y. L. Ni, J. Y. Wang, B. C. Wang, L. Yu, Z. Dong, Y. Q. Dai, V. Basile, C. Taylor, P. Jiang, *ACS Appl. Mater. Interfaces* **2017**, *9*, 5457.
- [300] C.-H. Hsieh, Y.-C. Lu, H. Yang, *ACS Appl. Mater. Interfaces* **2020**, *12*, 36478.
- [301] Y. Ni, Y. Zhang, S.-Y. Leo, Y. Fang, M. Zhao, L. Yu, K. D. Schulze, W. G. Sawyer, T. E. Angelini, P. Jiang, C. R. Taylor, *ACS Appl. Nano Mater.* **2018**, *1*, 6081.
- [302] Y. L. Wang, Q. L. Zhao, X. M. Du, *Mater. Horiz.* **2020**, *7*, 1341.
- [303] P. Wu, X. Q. Shen, C. G. Schafer, J. Pan, J. Guo, C. C. Wang, *Nanoscale* **2019**, *11*, 20015.
- [304] J. Q. Zhao, L. Zhang, X. Y. Du, J. Y. Xu, T. T. Lin, Y. J. Li, X. X. Yang, J. C. You, *Nanoscale Adv.* **2022**, *4*, 2942.
- [305] X. C. Sun, Z. P. Zhang, Z. J. Sun, J. X. Zheng, X. Q. Liu, H. Xia, *Macromol. Rapid Commun.* **2022**, *43*, 2100863.
- [306] Y. Luo, L. N. Fang, W. H. Wei, W. Guan, Y. Z. Dai, X. C. Sun, B. R. Gao, *Appl. Opt.* **2022**, *61*, 792.
- [307] S. Schauer, R. Schmagel, R. Hunig, K. N. Ding, U. W. Paetzold, U. Lemmer, M. Worgull, H. Holscher, G. Gomard, *Opt. Mater. Express* **2018**, *8*, 184.
- [308] F. Li, H. Hou, J. Yin, X. Jiang, *Sci. Adv.* **2018**, *4*, eaar5762.
- [309] Z. Li, M. A. Rahman, A. Olah, E. Baer, *J. Appl. Polym. Sci.* **2017**, *134*, 44659.
- [310] W. Wang, H. Lai, Z. J. Cheng, Z. M. Fan, D. J. Zhang, J. F. Wang, S. J. Yu, Z. M. Xie, Y. Y. Liu, *ACS Appl. Mater. Interfaces* **2020**, *12*, 49219.
- [311] V. J. Lloyd, N. J. Nadeau, *Curr. Opin. Genet. Dev.* **2021**, *69*, 28.
- [312] A. E. Seago, P. Brady, J. P. Vigneron, T. D. Schultz, *J. R. Soc., Interface* **2009**, *6*, S165.
- [313] O. D. Onelli, T. v. d. Kamp, J. N. Skepper, J. Powell, T. d S Rolo, T. Baumbach, S. Vignolini, *Sci. Rep.* **2017**, *7*, 1373.
- [314] D. Gur, B. A. Palmer, B. Leshem, D. Oron, P. Fratzl, S. Weiner, L. Addadi, *Angew. Chem., Int. Ed.* **2015**, *54*, 12426.
- [315] J. Teyssier, S. V. Saenko, D. van der Marel, M. C. Milinkovitch, *Nat. Commun.* **2015**, *6*, 6368.
- [316] A. G. Dumanli, T. Savin, *Chem. Soc. Rev.* **2016**, *45*, 6698.
- [317] J. Park, J. R. Youn, Y. S. Song, *J. Mater. Chem. C* **2017**, *5*, 10600.
- [318] P. C. Li, H. Y. Chen, K. T. Chiang, H. T. Yang, *J. Colloid Interface Sci.* **2021**, *599*, 119.
- [319] S. Y. Leo, W. Zhang, Y. F. Zhang, Y. L. Ni, H. Jiang, C. Jones, P. Jiang, V. Basile, C. Taylor, *Small* **2018**, *14*, 1703515.
- [320] J. J. Yang, W. D. Zhao, Z. Yang, W. L. He, J. X. Wang, T. Ikeda, L. Jiang, *ACS Appl. Mater. Interfaces* **2019**, *11*, 46124.
- [321] W. B. Niu, K. Zhao, L. C. Qu, S. F. Zhang, *J. Mater. Chem. C* **2018**, *6*, 8385.
- [322] Y. Xie, Y. Meng, W. X. Wang, E. Zhang, J. S. Leng, Q. B. Pei, *Adv. Funct. Mater.* **2018**, *28*.
- [323] W. Hong, Z. K. Yuan, X. D. Chen, *Small* **2020**, *16*, 1802430.
- [324] Z. P. Li, T. Black, M. A. Rahman, J. X. Feng, A. Olah, E. Baer, *Polymer* **2018**, *137*, 1907626.



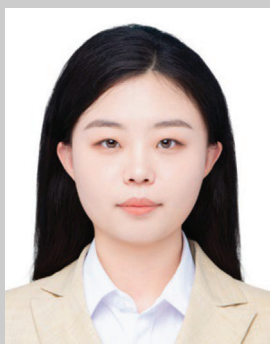
**Liang Fang** received his B.S. degree in polymer materials and engineering from the Beijing University of Chemical Technology (BUCT), Beijing, China in 2004 and the M.S. degree in materials processing engineering from BUCT as well in 2007. After obtaining Ph.D. degree in plastics engineering from the University of Massachusetts Lowell in 2011, he was working as a postdoc researcher in Helmholtz–Zentrum Geesthacht until October 2014. Now, he is a professor in Nanjing Tech University, Nanjing, China. His research focuses on polymer composites with abilities to absorb and adjust light spectrum and sound (S2A2).



**Wan Yan** has the master's degree from joint program in polymer science from the Free University Berlin, Humboldt University Berlin, Technical University Berlin, and University of Potsdam in 2013 and her doctoral degree in materials, science from University of Potsdam in 2022. Her research interests include multifunctional polymers based on biodegradable materials and micro-/nanostructural fabrication and analysis of intelligent polymers.



**Shunping Chen** is a Ph.D. student in the Department of Macromolecular Science at Fudan University, China. He received his B.Sc. in materials science and engineering (2017) and M.Sc. in polymeric chemistry and physics (2020) from the Nanjing Tech University, China. His current research focuses on the design and preparation of advanced biocompatible elastomers for human cardiovascular implantation, such as polymeric heart valve and small-diameter artificial vessel.



**Qiong Duan** is a master student in materials science and engineering of Nanjing Tech University, China. She received her B.Sc. degree in polymer materials and engineering from the Nanjing Tech University, Nanjing, China, in 2020. Her research interest is currently focus on shape memory polymers.





**Madhubhashitha Herath** is a senior lecturer at the Uva Wellassa University, Sri Lanka. He earned his Ph.D. in 2020 from the University of Southern Queensland, Australia. In 2013, he obtained his B.Sc. Eng. degree from the University of Ruhuna, Sri Lanka. In 2017, he obtained his M.Eng. degree from the University of Moratuwa, Sri Lanka. He is a member of the Institution of Mechanical Engineers, UK, and the Institution of Engineers Sri Lanka. His current research interests are light-activated shape memory polymer composites (LASMPCs), enhancement of structural performance and durability of smart materials, and photonic sensing technologies.



**Jayantha Epaarachchi** is an associate professor in the School of Mechanical and Electrical Engineering, University of Southern Queensland. He has obtained his Ph.D. from the University of Newcastle, Australia in 2003. To date, he has edited one book and published more than 120 book chapters, journals, and conference papers. He has completed ten Ph.D. projects and is currently supervising five Ph.D. projects. His major research areas are the structural health monitoring and development of smart composite materials, fatigue and fracture. He is an editorial member of *Structural Health Monitoring* (SHM) and has a patent for use of optical sensors for SHM.



**Yue Liu** is a postdoctoral researcher in the Department of Dynamic Materials Transformations at Helmholtz-Zentrum Hereon, Germany. She received her M.Sc. from joint program in polymer science from the Free University Berlin, Humboldt University Berlin in 2015, and her doctoral degree in materials science from University of Potsdam in 2021. Her current research interests focus on sustainable multifunctional materials, including micro-/nano-structural functional design, integrated system development and advanced surface analysis with atomic force microscopy.



**Chunhua Lu** is currently a professor at the College of Materials Science and Engineering, Nanjing Tech University (Nanjing Tech). He received his Ph.D. degree in 2002 from the Department of Materials, Nanjing Tech. Then he worked as a lecturer and associate professor at Nanjing Tech from 2002 to 2009. Prior to his appointment as a professor in 2010, he was a senior visiting scholar at the University of Arizona from June to December 2010. His research interests are mainly focused on nanomaterials for the selective absorption and energy conversion of optical electromagnetic waves.